AD-A059 028 SPERRY RAND CORP GREAT NECK N Y SPERRY GYROSCOPE F/G 17/7
SLIC-7 LASER GYRO INVESTIGATIONS.(U)
MAR 78 J ABDALE, W DREXEL
UNCLASSIFIED SG-4240-1027 AFAL-TR-78-32 F33615-77-C-1196 NL

| OF |
AD
A059028

END
DATE
FILMED
11-78
DDC

(2) LEVEL II

AFAL-TR-78-32

SLIC-7 LASER GYRO INVESTIGATIONS

John Abdale
Werner Drexel

Sperry Division
Sperry Rand Corporation
Great Neck, New York 11020

MARCH 1978

Final Report July 1977 - December 1977

AIR FORCE AVIONICS LABORATORY
AIR FORCE SYSTEMS COMMAND
UNITED STATES AIR FORCE
WRIGHT-PATTERSON AFB, OHIO 45433

NOTICE

When Government drawings, specifications, or other data are used for any purpose other than in connection with a definitely related Government procurement operation, the United States Government thereby incurs no responsibility nor any obligation whatsoever; and the fact that the government may have formulated, furnished, or in any way supplied the said drawings, specifications, or other data, is not to be regarded by implication or otherwise as in any manner licensing the holder or any other person or corporation, or conveying any rights or permission to manufacture, use, or sell any patented invention that may in any way be related thereto.

This report has been reviewed by the Information Office (OI) and is releasable to the National Technical Information Service (NTIS). At NTIS, it will be available to the general public, including foreign nations.

This technical report has been reviewed and is approved for publication.

Robert W. McAdory, Project Engr.
Reference System Technology Gp.

Ronald L. Ringo, Chief
Reference Systems Branch

FOR THE COMMANDER

Richard M. Roberds, Colonel, USAF
Chief, Reconnaissance and Weapon
Delivery Division

"If your address has changed, if you wish to be removed from our mailing list, or if the addressee is no longer employed by your organization please notify AFAL/RWA ,W-PAFB, OH 45433 to help us maintain a current mailing list".

Copies of this report should not be returned unless return is required by security considerations, contractual obligations, or notice on a specific document.

AIR FORCE/56780/14 July 1978 — 75

SECURITY CLASSIFICATION OF THIS PAGE *(When Data Entered)*

REPORT DOCUMENTATION PAGE

READ INSTRUCTIONS BEFORE COMPLETING FORM

1. REPORT NUMBER: AFAL-TR-78-32	2. GOVT ACCESSION NO.
3. RECIPIENT'S CATALOG NUMBER	
4. TITLE *(and Subtitle)*: SLIC-7 LASER GYRO INVESTIGATIONS	5. TYPE OF REPORT & PERIOD COVERED: Final Technical Report, July 1977 - December 1977
6. PERFORMING ORG. REPORT NUMBER: SG-4240-1027	
7. AUTHOR(s): John Abdale, Werner Drexel	8. CONTRACT OR GRANT NUMBER(s): F33615-77-C-1196
9. PERFORMING ORGANIZATION NAME AND ADDRESS: Sperry Gyroscope, an operating unit of Sperry Division, Sperry Rand Corporation, Great Neck, N.Y. 11020	10. PROGRAM ELEMENT, PROJECT, TASK AREA & WORK UNIT NUMBERS: 6095-11-05, 17 11
11. CONTROLLING OFFICE NAME AND ADDRESS: Air Force Avionics Laboratory (RWA), Air Force Systems Command, Wright-Patterson AFB, Ohio 45433	12. REPORT DATE: March 1978
	13. NUMBER OF PAGES: 84
14. MONITORING AGENCY NAME & ADDRESS *(if different from Controlling Office)*	15. SECURITY CLASS. *(of this report)*: Unclassified
	15a. DECLASSIFICATION/DOWNGRADING SCHEDULE

16. DISTRIBUTION STATEMENT *(of this Report)*

Approved for public release; distribution unlimited.

12 89 p.

17. DISTRIBUTION STATEMENT *(of the abstract entered in Block 20, if different from Report)*

18. SUPPLEMENTARY NOTES

DDC RECEIVED SEP 26 1978 B

19. KEY WORDS *(Continue on reverse side if necessary and identify by block number)*

Laser Gyro	Shelf Life
Missile Guidance	Discharge Tube
Thermal Analysis	Thermal Gradients

20. ABSTRACT *(Continue on reverse side if necessary and identify by block number)*

This program is the initial phase of an effort to develop laser gyro technology for application to low cost inertial missile guidance systems. As part of the research and development effort two investigations of SLIC-7 laser gyro were conducted:
(1) thermal analysis and
(2) storage and shelf life evaluation.

DD FORM 1 JAN 73 1473 EDITION OF 1 NOV 65 IS OBSOLETE S/N 0102-014-6601 |

UNCLASSIFIED

SECURITY CLASSIFICATION OF THIS PAGE *(When Data Entered)*

403 189

The key to quick reaction and performance stability is the design to minimize thermal gradients and, therefore, thermal sensitivities. Test results disclose that the thermal gradients across the discharge tubes are the key factors. Analyses indicate that the SLIC-7 gyro can meet the low thermal sensitivity goals and the storage and shelf life requirements postulated for the missile guidance systems.

PREFACE

This report, which describes investigations relative to evaluation of specific characteristics of the Sperry SLIC-7 laser gyro as they pertain to low cost missile guidance system requirements, is the latest in a series of reports on the development of the device for tactical missile applications.

TABLE OF CONTENTS

LIST OF ILLUSTRATIONS

LIST OF ILLUSTRATIONS - Continued

LIST OF ILLUSTRATIONS - Continued

LIST OF TABLES

SECTION I

INTRODUCTION AND SUMMARY

INTRODUCTION

This final technical report was prepared for the United States Air Force (USAF) Systems Command, Aeronautical Systems Division, Avionics Laboratory, Wright-Patterson Air Force Base, Dayton, Ohio, under contract number F33615-77-C-1196, by Sperry Gyroscope, an operating unit of the Sperry Division, Sperry Rand Corporation, Great Neck, New York. It documents the results of investigations relative to evaluating specific characteristics of the Sperry SLIC-7 laser gyro as they pertain to low cost missile guidance system requirements.

Specifically two investigations were conducted: a thermal analysis and a storage and shelf life evaluation. The thermal analysis is keyed to a particular sensitivity laser gyros possess, which is that discharge gas flow rate changes (output null shifts) are caused by temperature gradients. The lifetime analyses relate to the discharge tube size constraints imposed by the compact design of the SLIC-7 laser gyro.

SUMMARY OF RESULTS

Thermal Investigation

An extremely detailed thermal model of the SLIC-7 laser gyro was prepared. Thermal impedances were derived and simulated in this model where the three-axis gyro optical cavity and case was divided into over 200 nodes. (Temperature points). In terms of laser gyro operation the key to quick reaction and performance stability is thermal gradients, particularly across the discharge tubes.

The thermal model was converted into a digital computer program to facilitate the analysis of the thermal behavior of the laser gyro configuration for different ambient temperatures. The results of these analyses are documented herein. The key response area, temperature gradient across each discharge tube, shows that the use of a ceramic body discharge tube (nominal design for SLIC-7) effectively minimizes the tube gradient. In all cases tube 3 had the largest gradient which never exceeded $0.05^{o}F$. This translates into a maximum induced drift of 0.5 degrees per hour, uncompensated. This performance can be further improved by thermal compensation of the gyro output as a function of measured tube temperature gradients.

Life Investigation and Test

The SLIC-7 discharge tube is the key element relative to life and reliability of this sensor. The size constraints imposed by the small size of the sensor limited both the available gas volume and cold cathode area. The subject investigation was directed towards maximizing the life of the tube through design investigation and then measuring the result.

The design investigation centered around the selection of the most optimum cathode configuration that maximizes the cathode area (within the size constraints) and minimizes the current density.

The test consisted of two types: storage and operating life. Tubes of the selected design were made and put into storage with periodic test of key parameters. Three tubes were committed to the storage test. Two were stored at elevated temperature ($64^{o}C$) and one stored at room temperature. Approximately every other week the tubes were put into a linear laser for performance evaluation (4 hour test) and returned to storage. To date, all three samples are unchanged for a total accumulation of 1500 hours on each sample. These tests are continuing in a post-contract effort.

The operating life tests are also under way. The selected cathode configuration with a maximum operating current of 1.5 ma is projected to have a life expectancy in excess of 15,000 hours.

Therefore, it is projected on the basis of the life investigation that the SLIC-7 laser gyro will satisfy the requirements postulated for a missile system; that is, 10 years of shelf life with an 85% probability of operating 4 hours any time within the 10 years.

RECOMMENDATIONS

The subject investigations were made on a SLIC-7 laser gyro design that had not been built. Two of these sensors are being manufactured for the Air Force for performance evaluation relative to the Low Cost Inertial Guidance System program. The current USAF plan is to have Draper Laboratories test and evaluate these units.

It is strongly recommended that Sperry participate in the evaluation program. There is no argument against independent test and evaluation, where the sensor will be evaluated from a "black box" standpoint. However, the designer and manufacturer has insight into the design that could explain (and possibly compensate) performance anomalies. Therefore, in addition to the independent testing provided by the Draper Laboratories, Sperry should be funded to perform similar tests and evaluations. As part of the Sperry effort, the results of both the thermal and life investigations could be further validated. The SLIC-7 laser gyro could be implemented with thermal sensors to validate the analytic thermal model developed on the subject contract. This validation would be correlated to measured performance to validate the thermal modeling of the SLIC-7 design. Thermal changes and/or compensations could be developed, if required.

In the area of life, additional operational and storage times would be accumulated providing increased confidence in the capability of the SLIC-7 laser gyro.

SECTION II

TECHNICAL PROBLEM

BACKGROUND

There is an Air Force requirement for an adverse weather, standoff, launch and leave capability in both powered and unpowered tactical missiles. Key to attaining this capability is the successful development of a Low Cost Inertial Guidance System that will satisfy the tactical missile guidance requirements.

Laser gyro technology development has progressed to the stage where 0.1^{o}/hr accuracy can be achieved routinely. This 0.1^{o}/hr accuracy coupled with the low cost potential of the laser gyro makes it an ideal candidate for tactical missile guidance. This effort is the initial phase of a planned multi-phase program, the objective of which is to develop laser gyro technology for low cost guidance. Specifically, the SLIC-7 (Sperry Laser Inertial Cluster - 7 inch perimeter) is investigated under this effort. The SLIC-7 was selected because it has the lowest cost potential of the laser gyro designs that have been independently tested.

The SLIC-7 is a follow on design to the SLIC-15 (Sperry Laser Inertial Cluster - 15 inch perimeter gyro). The SLIC-15 was developed by Sperry under subcontract to Lockheed for use on the RACG (Radiometric Area Correlation Guidance) system. The SLIC-15 has been flight tested at CIGTF, Holloman AFB in a pure inertial mode with in-air-transfer alignment and was being flight tested by Lockheed in a RACG mid-course guidance mode. Performance data from these flight tests indicated that the SLIC-15 accuracy is sufficient to satisfy most anticipated tactical missile guidance requirements; however, the size of SLIC-15 is marginal for many applications. The

SLIC-7 size is such that it will fit practically any anticipated size requirements; however, its performance is unproven. A SLIC-7 rate package was being tested by Martin - Orlando for the U. S. Army AIMS (Advanced Intercept Missile System). The accuracy requirements for the AIMS application were crude (30^{o}/hr drift) relative to LCIGS requirements. This effort will investigate the performance-cost potential of SLIC-7 for application to LCIGS.

The SLIC-7, a new laser gyro, differs from the SLIC-15 design mainly in cluster size and discharge tube design and size. Since there is little experience with this design, these potential problem areas were to be investigated under this effort. Areas of concern included thermal response of the cluster and reliability of the discharge tube.

Low thermal sensitivity was a goal. Thermal sensitivity should be such that the system can operate over a specified range (-55^{o}C to $+71^{o}$C) with <1 minute reaction time and $<0.5^{o}$/hr drift stability and repeatability.

The reliability goal to be achieved was a 10-year shelf life and a 85% probability that the system will turn on anytime within the 10 year period and remain operating for 4 hours.

THERMAL PROBLEM

The current design approach to laser gyros is to use a helium - neon gas discharge laser to generate the light beams used to sense angular rotation. This gas is contained within a ceramic envelope. When the discharge is excited via a high dc voltage, it generates heat. This heat diffuses along the total discharge path, establishing a temperature gradient that sets up a gas flow profile. The laser gyro responds to gas flow rates in the same way it responds to input rotation rate. Therefore, changes in flow rate produce errors in the gyro output normally referred to as drift rate errors.

The objective of the subject thermal investigation is to analyze the SLIC-7 design from a thermal gradient standpoint in order to evolve a design that minimizes all gradients and, therefore, all thermal sensitivities.

LIFE PROBLEM

The laser gyro, a solid-state inertial angular rate sensor, has the potential for high reliability and long life. It consists of optical components that are inactive elements and a gas discharge tube, an active element. The life limiting element for the laser gyro ultimately is the gas discharge tube. The discharge tube must exihibit stable characteristics for various periods of operation and storage under changing ambient conditions.

There are essentially only three discharge tube failure mechanisms: gas impurity, gas diffusion and cathode sputter. Gas impurity results from inability to purge and seal the gas container. In the SLIC-7 design, the all glass-metal or eventually ceramic-metal construction makes a container that can be purged and sealed effectively so that gas impurity is not a potential failure mechanism. In addition, this tube construction minimizes gas diffusion due to the nature of the materials employed. However, because of its extremely compact design, cathode area is limited with a potential failure resulting from cathode sputter.

The primary objective of the subject life investigation is to evaluate the small SLIC-7 discharge tube relative to its capability of satisfying tactical missile guidance system requirements for operating and storage life.

SECTION III

DESCRIPTION OF INVESTIGATIONS AND RESULTS

This section of the report presents the details of the thermal and life investigations.

THERMAL INVESTIGATION

The three-axis SLIC-7 laser gyro sensor assembly was thermally modeled in order to investigate its transient and steady-state thermal behavior. The following discussion describes the four-step process associated with this investigation. The specific tasks included:

- Define the SLIC-7 laser gyro sensor design configuration
- Refine method of analysis
- Prepare thermal model program on digital computer
- Analyze transient and steady-state responses
- Recommend design changes, if any.

Design Configuration

The laser gyro cluster assembly is designed symmetrically to prevent non-uniform temperature gradients. The cervit block is mounted to both top and bottom of the case in such a manner as to allow heat flow to occur equally in both directions. Heat conduction paths are provided by way of narrow gaps and joint interfaces to keep conduction of heat balanced between the top and bottom. With the internal gas pressure at 0.5 torr, all air gaps over 0.0025 inch conduct heat as if at atmospheric pressures; joint interfaces, however, conduct heat as if under full vacuum conditions.

The laser tube is made of beryllium oxide, a material with high thermal conductivity. Thermal conductances from end to end in the tube are large due to a combination of large material cross-section and high material thermal conductivity.

Figure 1 shows a cross-section of the SLIC 7/2 platform unit. The view shows a front view of the laser tube mounted on the cervit block as well as the supporting hardware, shields and case.

Figure 2 is a slightly different cross-sectional view showing the mounting pads of the base which are shown further on figure 3. Note that the mounting pad on the right combines the pad and the locating pin. The three shields with their aluminum spacer disks are screw mounted directly to the base. A more detailed view of the base is seen on figure 4. If there are any circumferentialy asymmetrical aspects affecting heat conduction, they would be associated with the base and bottom cervit block mounting hardware.

Figure 5 shows the laser tube, mu-metal shield and mounting configuration. The laser tube contacts the cervit block only at the two mounting tabs where heat is transferred across the joint contact. In the area of the windows and lower body the tube thermally communicates with the cervit block by radiation and air gap conduction.

Heat generation in the laser gyro platform originates primarily in the three laser tubes. The heat from the tubes is transferred to the central portion of the cervit block from where it flows to the upper and lower block mounting hardware. The objective is to allow the heat to flow equally in both directions. A certain amount of heat also flows radially outward through the three shields into the case.

Any vertical temperature gradient set up in the cervit block due to unequal heat conduction at the top and bottom mounting is reflected into the laser tubes through the radiative and gas conductive links with the block in the area of the tube windows. The gradients in the tube as a result of these effects are smaller than in the block as a result of attenuation. The tube temperature gradient objective of $0.05^{o}F$ is satisfied with the present design.

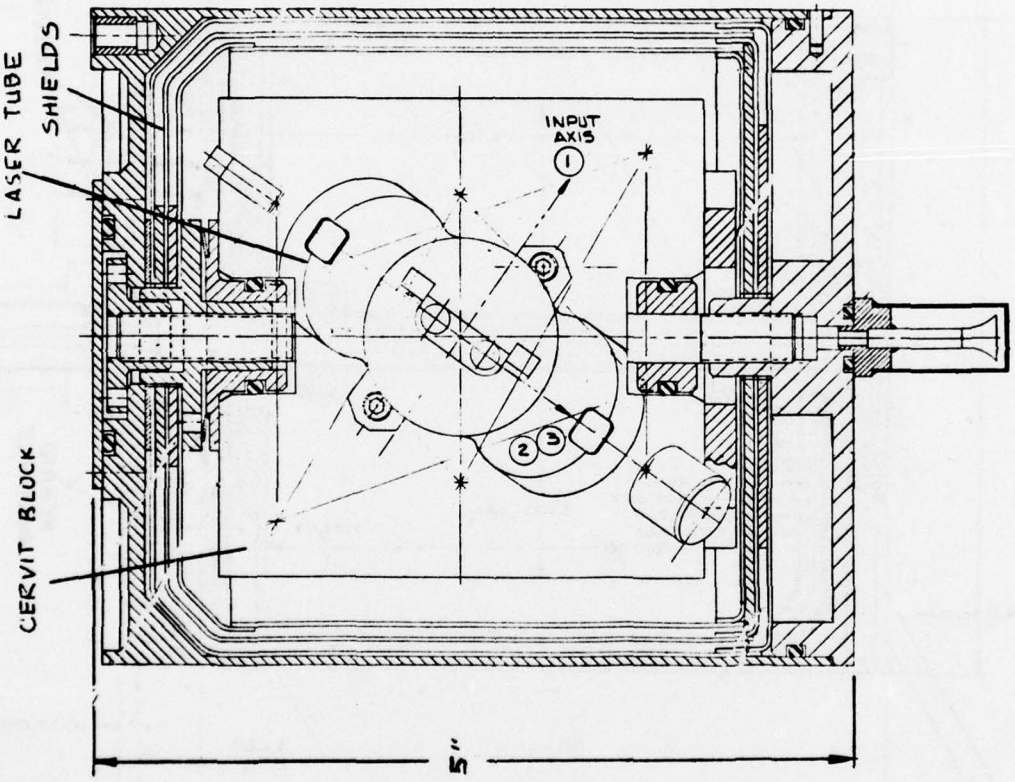

Figure 1. Cross-section of SLIC 7/2 Platform Showing Front View of Laser Tube

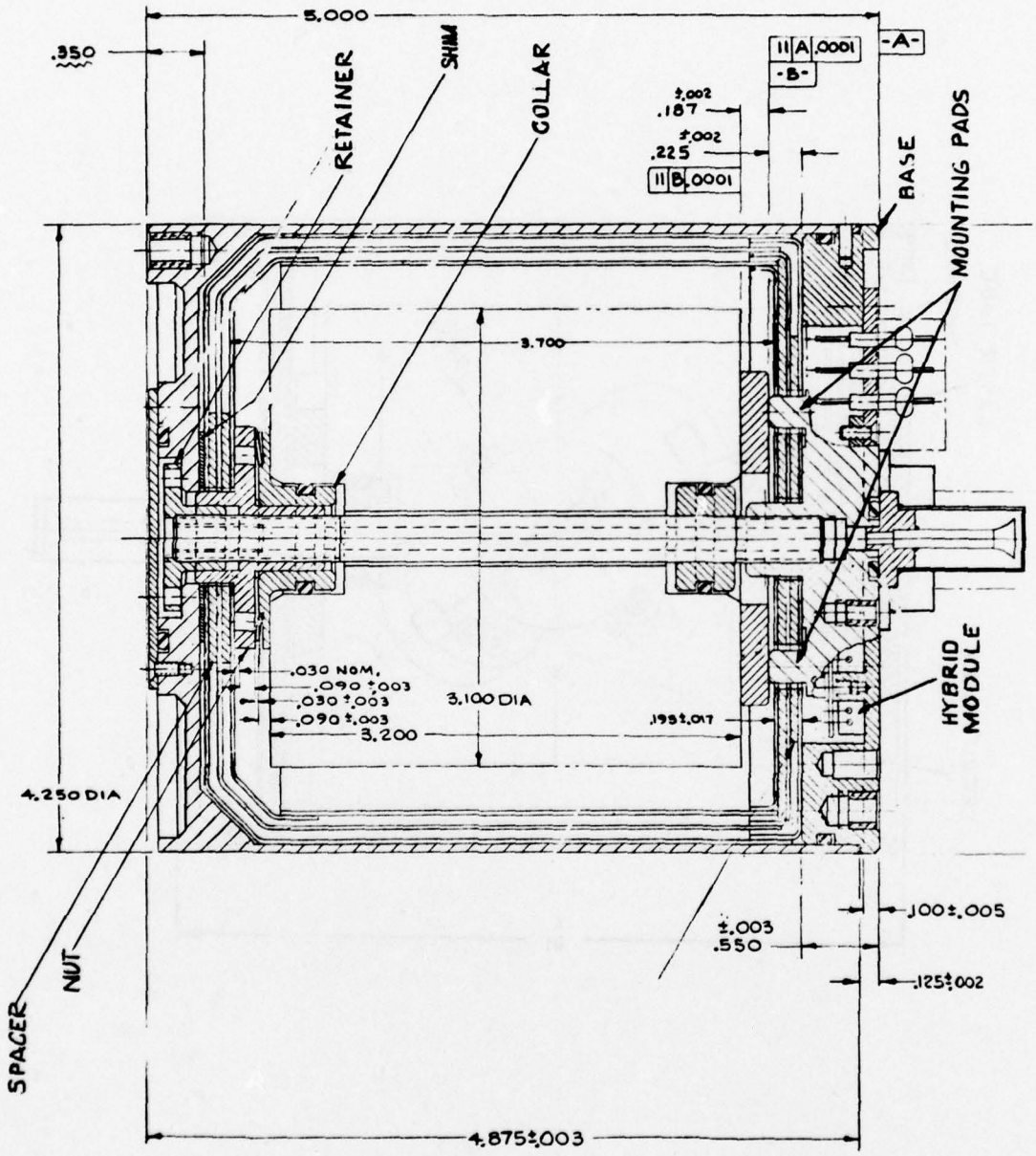

Figure 2. Cross-section of SLIC 7/2 Platform Showing Mounting Pads of Base

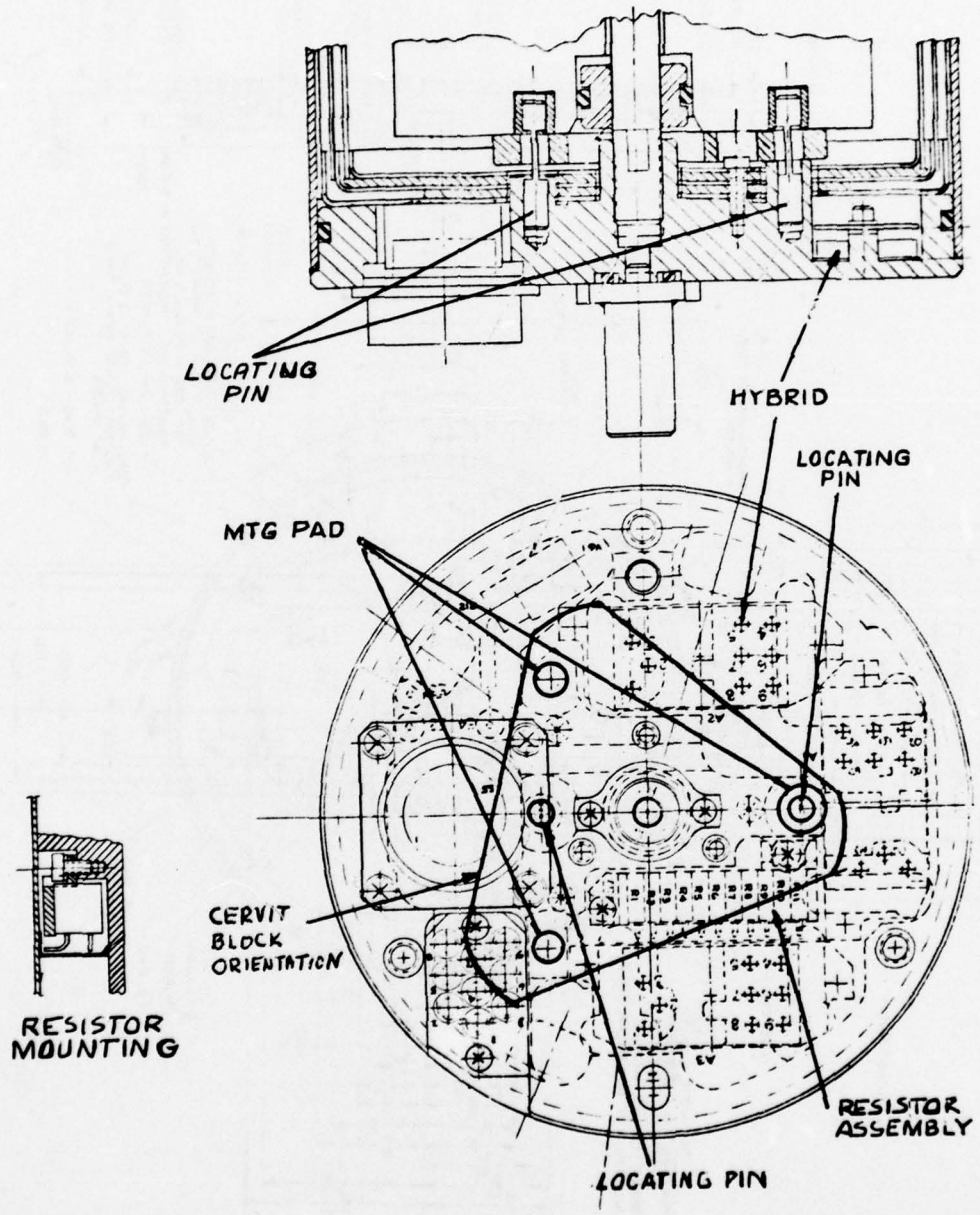

Figure 3. Cervit Block Bottom Mounting Configuration

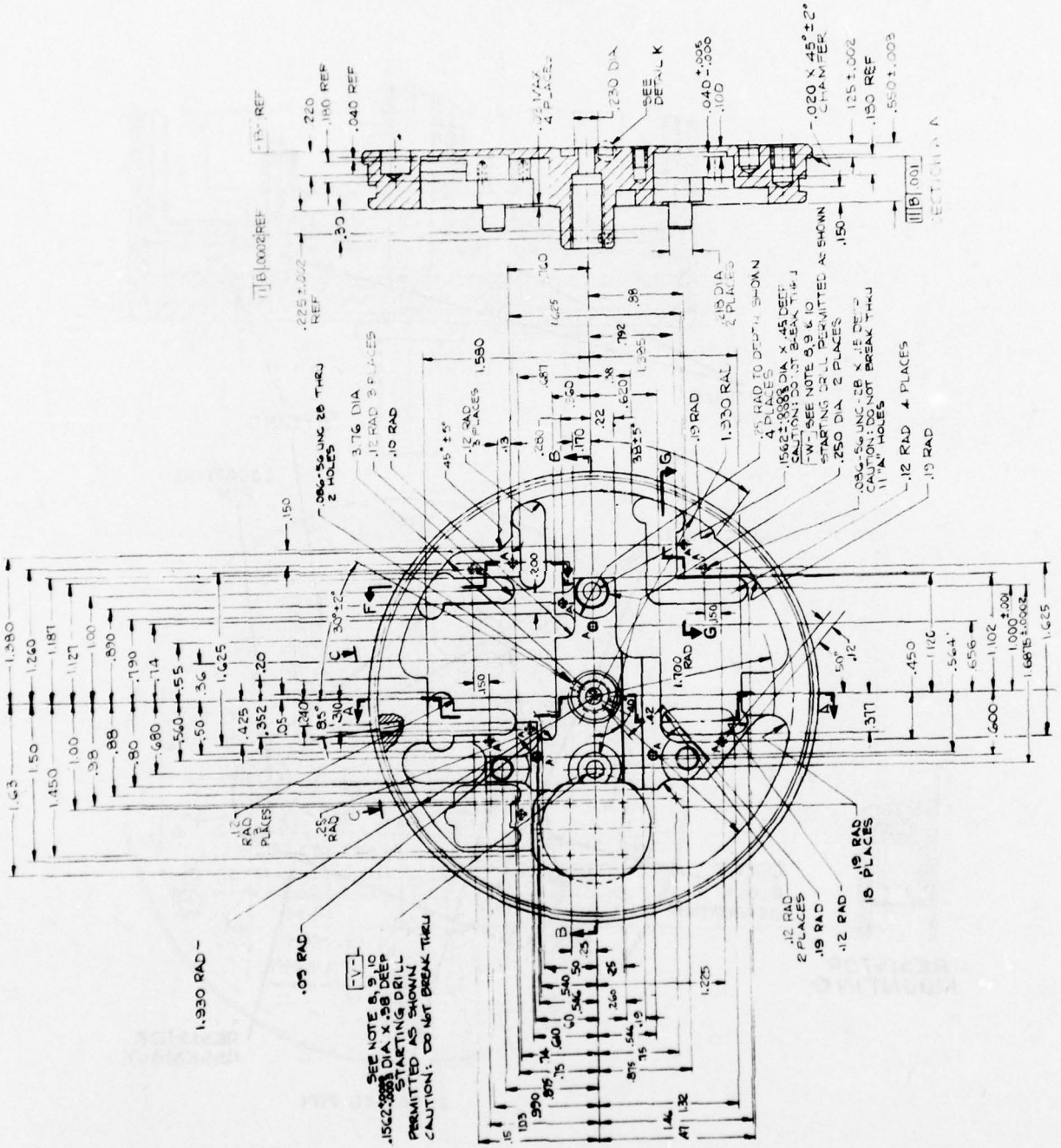

Figure 4. Platform Base

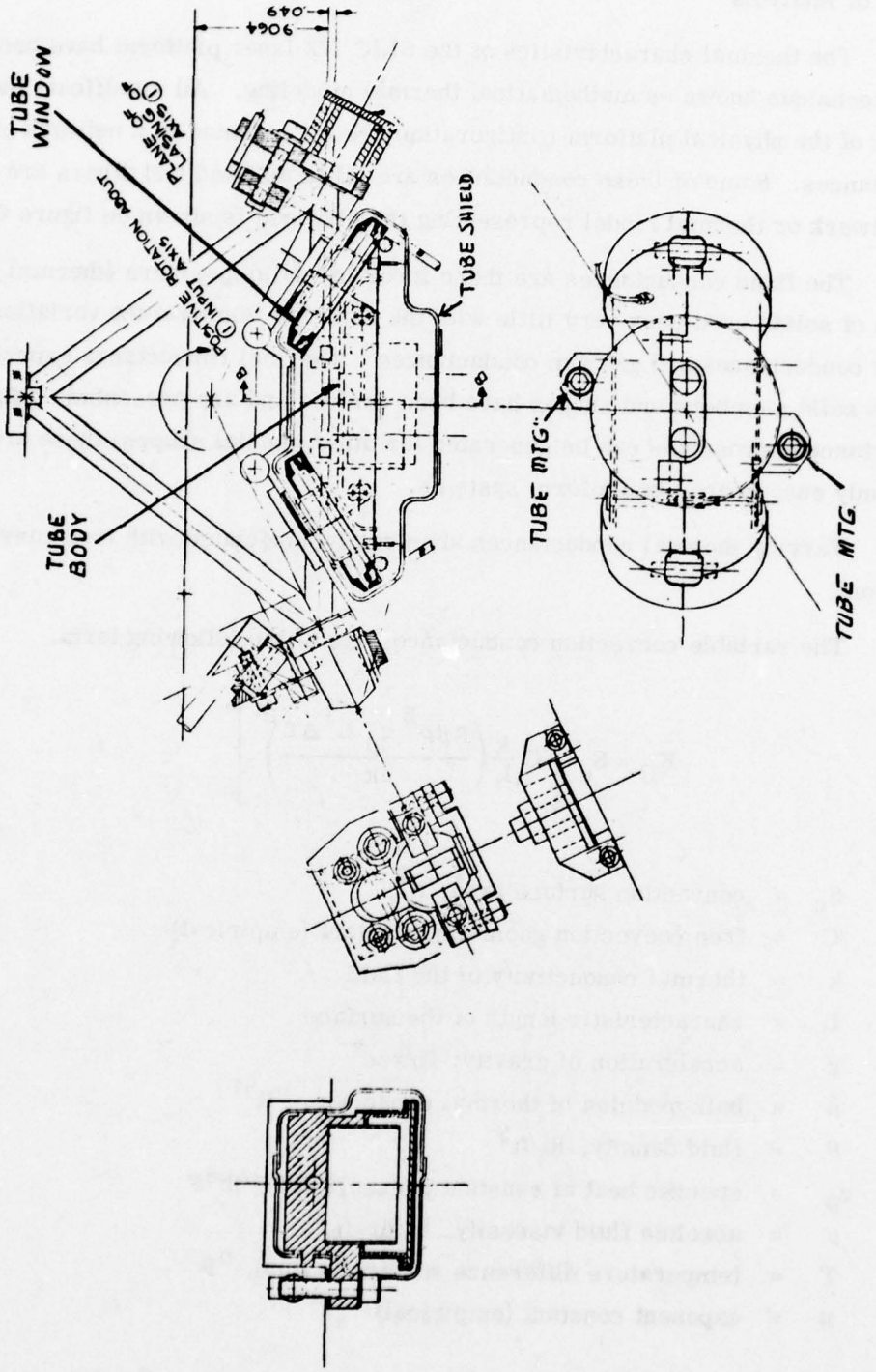

Figure 5. Laser Tube and Shield Configuration

Method of Analysis

The thermal characteristics of the SLIC 7/2 laser platform have been analyzed by the technique known as mathematical thermal modeling. All significant thermal aspects of the physical platform configuration are represented in a network of thermal conductances. Some of these conductances are taken as fixed and others are variable. The network or thermal model representing the platform is shown on figure 6.

The fixed conductances are those involving solid members (thermal conductivities of solids used vary very little with the expected temperature variations), joint contact conductances and gas gap conductances. Thermal conductance expressions of various solid members and shapes have been derived and are presented on figure 7. Conductance expressions can be generated for other special shapes; these are most commonly encountered in platform systems.

Varying thermal conductances are usually associated with free convection and radiation.

The variable convection conductances are of the following form.

$$K_C = S_c \left[C \frac{k}{L} \left(\frac{g \beta \rho^2 c_p L^3 \Delta T}{\mu k} \right)^n \right]$$

where

S_c = convection surface area, ft^2

C = free convection geometry constant (empirical)

k = thermal conductivity of the fluid

L = characteristic length of the surface

g = acceleration of gravity, ft/sec^2

β = bulk modulus of thermal expansion, $^oR^{-1}$

ρ = fluid density, lb/ft^3

c_p = specific heat at constant pressure BTU/lb^oF

μ = absolute fluid viscosity, lb/hr-ft

T = temperature difference surface to fluid, ^oF

n = exponent constant (empirical)

The radiation conductance is of the following form.

$$K_R = S_R \left(F_\epsilon \; F_a \; \frac{0.172 \times 10^{-8} \; (T_2^{\,4} - T_1^{\,4})}{T_2 - T_1} \right)$$

S_R = radiation surface area, ft^2

F_ϵ = surface emissivity factor

F_a = surface configuration shape factor

Stefan - Boltzmann constant is 0.172×10^{-8}

T_2 = temperature of radiating surface, ^oR

T_1 = temperature of receiving surface, ^oR

To generate the mathematical thermal model for the computer assembly, each geometric element is represented by a node point. The nodes are interconnected by thermal conductances representing the ability to transfer heat between elements or nodes. The inputs for the computer program also include heat generation and location data, and element boundary characteristics such as air or sink temperatures. In addition, the thermal capacitance of each node must be computed based on the specific heat and weight of each node or element. All this data is punched on computer cards which form the data portion of the computer program. Utilizing the computer program and the data of the particular thermal model under consideration, the Univac 1108 computer exercises the node equations by stepwise iteration (also known as marching solution) and computes the desired node temperatures.

The general form of the node equation is

$$\dot{q}_1 = K_{2-1} (T_2 - T_1) + K_{3-1} (T_3 - T_1) \; .... \; K_{n-1} (T_n - T_1) + q_1$$

$$\frac{C_1 (T_1' - T_1)}{\Delta \theta} = K_{2-1} (T_2 - T_1) + K_{3-1} (T_3 - T_1) \; ... \; K_{n-1} (T_n - T_1) + q_1$$

$$T_1' - T_1 = \frac{K_{2-1} \, \Delta \theta}{C_1} \; T_2 + \frac{K_{3-1} \, \Delta \theta}{C_1} \; T_3 \; .... \frac{K_{n-1} \, \Delta \theta}{C_1} \; T_n + \frac{q_1 \, \Delta \theta}{C_1}$$

$$T_1' = F_{2-1} \, T_2 + F_{3-1} \, T_3 + F_{n-1} \, T_n + (1 - \Sigma_n \, F_{n-1}) \, T_1 + Q_1$$

where

$\dot{q}_1$ = energy stored at node over finite time $\Delta\theta$, BTU/hr

q_{n-1} = heat conducted BTU/hr

T_1 = temperature at node "1" ^{O}F

T_n = temperature at node "n" ^{O}F

T_1' = temperature at node "1" after iteration, ^{O}F

K_{n-1} = conductance between nodes, BTU/hr^{O}F

C_1 = capacitance of node "1" = Wc_p, BTU/^{O}F

W = mass of node, lbs

c_p = specific heat of material, BTU/lb^{O}F

$\Delta\theta$ = time step or iteration interval, hrs.

$F = \frac{\Delta\theta}{C}$

The computer program contains the general form of the node equation. When it receives input data such as specific node-to-node conductances, node capacitances, convection and radiation properties, and heat generation characteristics, the computer program can construct the entire array of node equations which in this case is 205 equations. It solves each of the 205 node equations for every time-step iteration, resulting in a node temperature. Since initial and surrounding node temperatures are known - assuming all heat is being conducted into the node in question - the node equation becomes a linear equation with a single unknown T_1'. This is the future node temperature after time $\Delta\theta$ has elapsed.

In terms of platform warm-up time, the computer takes approximately 1/30th of a second to solve a complete iteration for all 205 nodes. The new set of node temperatures calculated for time interval $\Delta\theta$ now forms the initial condition for the second iteration of node temperatures. For the platform warm-up time of approximately 3 hours 30,000 complete iterations are required.

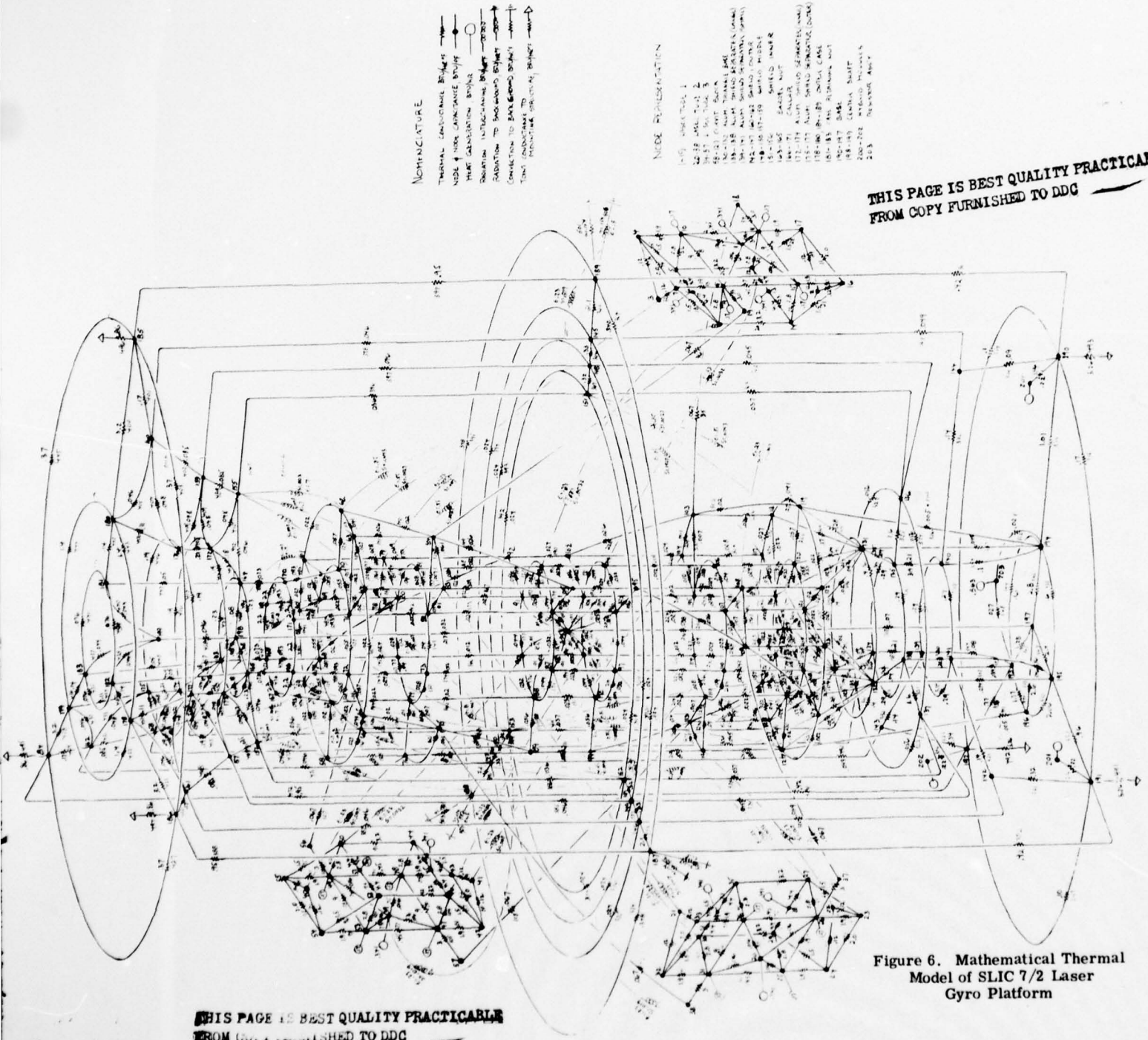

Figure 6. Mathematical Thermal Model of SLIC 7/2 Laser Gyro Platform

CONDUCTANCE OF CUBE ELEMENTS

$A = a^2$ (CONSTANT)

$K = \frac{kA}{L}$

$K = ka$

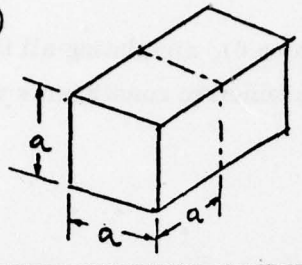

CONDUCTANCE OF DISK ELEMENT IN CIRCUMFERENTIAL HEAT FLOW

$A = dr\,\ell$

$L = \int_0^{\theta r} dx$

$K = \frac{kA}{L}$

$K = \frac{k\ell \ln \frac{r_2}{r_1}}{\theta}$

NOTE: FOR ONE QUADRANT $\theta = \frac{\pi}{2}$

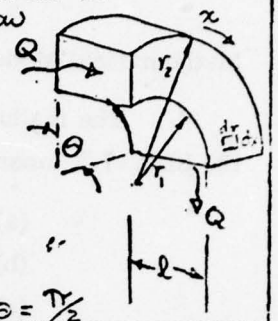

CONDUCTANCE OF RECTANGULAR ELEMENTS

$A = bc$ (CONSTANT).

$K = \frac{kA}{L}$

$K = \frac{kbc}{a}$

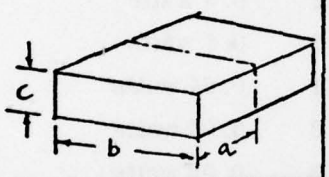

CONDUCTANCE OF TRUNCATED PYRAMID

$A(r) = \left[b + \frac{r}{h}(B-b)\right]^2$

$\frac{A}{L} = \int_0^h \frac{\left[b + \frac{r}{h}(B-b)\right]^2}{dr}$

$K = \frac{kbB}{h}$

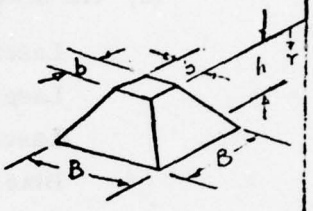

CONDUCTANCE OF CYLINDRICAL ELEMENTS

$A = \pi r^2$ (CONSTANT)

$K = \frac{kA}{L}$

$K = \frac{k\pi r^2}{\ell}$

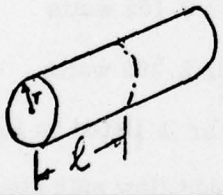

CONDUCTANCE OF TRUNCATED CONE

$\frac{A}{L} = \frac{\pi r_1 r_2}{h}$

$K = \frac{kA}{L}$

$K = \frac{k\pi r_1 r_2}{h}$

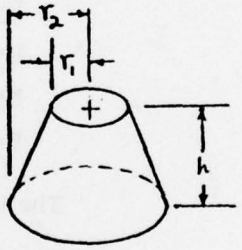

CONDUCTANCE OF DISK IN RADIAL DIRECTION

$\frac{A}{L} = \theta\ell \int_{r_1}^{r_2} \frac{dr}{r}$

$K = \frac{k\theta\ell}{\ln\left(\frac{r_2}{r_1}\right)}$

NOTE: FOR ENTIRE DISK $\theta = 2\pi$

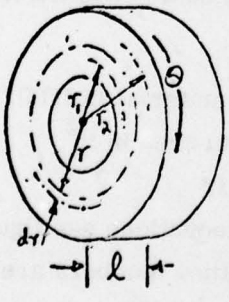

CONDUCTANCE OF HEMISPHERE IN RADIAL DIRECTION

$\frac{A}{L} = \int_{r_1}^{r_2} \frac{2\pi r^2}{dr}$

$K = \frac{kA}{L}$

$K = \frac{k2\pi r_1 r_2}{r_2 - r_1}$

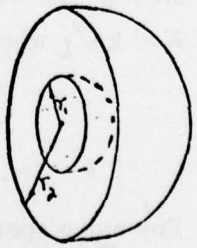

Figure 7. Thermal Conductance Expressions of Building Blocks

Mathematical Model and Its Parameters

The mathematical thermal model (figure 6), simulating all thermal aspects of the SLIC-7/2 laser gyro platform, has four parametric constituents which are

(a) heat generation
(b) thermal conductance
(c) thermal capacitance
(d) boundary conditions

(a) The heat sources in the platform are

Laser tube	No. 1	0.5 watts
Laser tube	No. 2	0.5 watts
Laser tube	No. 3	0.5 watts
Bias coil	No. 1	0.04 watts
Bias coil	No. 2	0.04 watts
Bias coil	No. 3	0.04 watts
Hybrid module	No. 1	0.21 watts
Hybrid module	No. 2	0.21 watts
Hybrid module	No. 3	0.21 watts
Resistor assembly		0.165 watts

The total platform heat generation is 2.265 watts.

The individual node dissipation in BTU/hr is listed on figure 8.

(b) The thermal conductances are the heat flow path connecting node or element points with the units in BTU/hr^{o}F. The basic equation for conductance is $K = kA/_{L}$ where

k = thermal conductivity of material in BTU/hr^{o}F ft^{2}/ft
A = heat flow cross-sectional area in ft^{2}
L = heat flow path length in ft

For more specific information on conduction equations see figure 7. A complete listing of all conductances identified by their designation numbers are presented on figure 9.

(c) The thermal capacitance as associated with every node is the heat storage capacity of each particular element. A complete list of node capacitance is given on figure 10.

(d) The boundary values are the thermal interface conditions tieing the external platform case to its surrounding environment. The external ambient temperature was taken at 120°F (approximately 50°C). Free convection and radiation ($\epsilon = 0.5$) was taken to exist at the cylindrical portion of the platform case. Both end surfaces of the case are conduction mounted with a joint pressure of at least 15 psi.

Q(1)= 3.4100-01	Q(2)= 0.0000	Q(3)= 0.0000	Q(4)= 0.0000	Q(5)= 0.0000
Q(6)= 3.4100-01	Q(7)= 0.0000	Q(8)= 0.0000	Q(9)= 1.7000-01	Q(10)= 1.7000-01
Q(11)= 1.7000-01	Q(12)= 0.0000	Q(13)= 3.4100-01	Q(14)= 0.0000	Q(15)= 1.7000-01
Q(16)= 0.0000	Q(17)= 0.0000	Q(18)= 0.0000	Q(19)= 0.0000	Q(20)= 3.4100-01
Q(21)= 0.0000	Q(22)= 0.0000	Q(23)= 0.0000	Q(24)= 0.0000	Q(25)= 1.7000-01
Q(26)= 1.7000-01	Q(27)= 0.0000	Q(28)= 3.4100-01	Q(29)= 0.0000	Q(30)= 0.0000
Q(31)= 1.7000-01	Q(32)= 0.0000	Q(33)= 0.0000	Q(34)= 3.4100-01	Q(35)= 0.0000
Q(36)= 1.7000-01	Q(37)= 0.0000	Q(38)= 0.0000	Q(39)= 3.4100-01	Q(40)= 0.0000
Q(41)= 0.0000	Q(42)= 0.0000	Q(43)= 0.0000	Q(44)= 0.0000	Q(45)= 3.4100-01
Q(46)= 0.0000	Q(47)= 1.7000-01	Q(48)= 1.7000-01	Q(49)= 1.7000-01	Q(50)= 0.0000
Q(51)= 3.4100-01	Q(52)= 0.0000	Q(53)= 1.7000-01	Q(54)= 0.0000	Q(55)= 0.0000
Q(56)= 0.0000	Q(57)= 0.0000	Q(58)= 0.0000	Q(59)= 0.0000	Q(60)= 0.0000
Q(61)= 0.0000	Q(62)= 0.0000	Q(63)= 0.0000	Q(64)= 0.0000	Q(65)= 0.0000
Q(66)= 0.0000	Q(67)= 0.0000	Q(68)= 0.0000	Q(69)= 0.0000	Q(70)= 0.0000
Q(71)= 0.0000	Q(72)= 0.0000	Q(73)= 0.0000	Q(74)= 0.0000	Q(75)= 0.0000
Q(76)= 0.0000	Q(77)= 0.0000	Q(78)= 0.0000	Q(79)= 0.0000	Q(80)= 0.0000
Q(81)= 0.0000	Q(82)= 0.0000	Q(83)= 0.0000	Q(84)= 0.0000	Q(85)= 7.0000-02
Q(86)= 0.0000	Q(87)= 0.0000	Q(88)= 0.0000	Q(89)= 7.0000-02	Q(90)= 0.0000
Q(91)= 0.0000	Q(92)= 7.0000-02	Q(93)= 0.0000	Q(94)= 0.0000	Q(95)= 7.0000-02
Q(96)= 0.0000	Q(97)= 0.0000	Q(98)= 0.0000	Q(99)= 7.0000-02	Q(100)= 0.0000
Q(101)= 0.0000	Q(102)= 7.0000-02	Q(103)= 0.0000	Q(104)= 0.0000	Q(105)= 0.0000
Q(106)= 0.0000	Q(107)= 0.0000	Q(108)= 0.0000	Q(109)= 0.0000	Q(110)= 0.0000
Q(111)= 0.0000	Q(112)= 0.0000	Q(113)= 0.0000	Q(114)= 0.0000	Q(115)= 0.0000

DISSIPATION IN BTU/HR
ie 7×10^{-2} BTU/HR

NODE NO.

Q(116)= 0.0000	Q(117)= 0.0000	Q(118)= 0.0000	Q(119)= 0.0000	Q(120)= 0.0000
Q(121)= 0.0000	Q(122)= 0.0000	Q(123)= 0.0000	Q(124)= 0.0000	Q(125)= 0.0000
Q(126)= 0.0000	Q(127)= 0.0000	Q(128)= 0.0000	Q(129)= 0.0000	Q(130)= 0.0000
Q(131)= 0.0000	Q(132)= 0.0000	Q(133)= 0.0000	Q(134)= 0.0000	Q(135)= 0.0000
Q(136)= 0.0000	Q(137)= 0.0000	Q(138)= 0.0000	Q(139)= 0.0000	Q(140)= 0.0000
Q(141)= 0.0000	Q(142)= 0.0000	Q(143)= 0.0000	Q(144)= 0.0000	Q(145)= 0.0000
Q(146)= 0.0000	Q(147)= 0.0000	Q(148)= 0.0000	Q(149)= 0.0000	Q(150)= 0.0000
Q(151)= 0.0000	Q(152)= 0.0000	Q(153)= 0.0000	Q(154)= 0.0000	Q(155)= 0.0000
Q(156)= 0.0000	Q(157)= 0.0000	Q(158)= 0.0000	Q(159)= 0.0000	Q(160)= 0.0000
Q(161)= 0.0000	Q(162)= 0.0000	Q(163)= 0.0000	Q(164)= 0.0000	Q(165)= 0.0000
Q(166)= 0.0000	Q(167)= 0.0000	Q(168)= 0.0000	Q(169)= 0.0000	Q(170)= 0.0000
Q(171)= 0.0000	Q(172)= 0.0000	Q(173)= 0.0000	Q(174)= 0.0000	Q(175)= 0.0000
Q(176)= 0.0000	Q(177)= 0.0000	Q(178)= 0.0000	Q(179)= 0.0000	Q(180)= 0.0000
Q(181)= 0.0000	Q(182)= 0.0000	Q(183)= 0.0000	Q(184)= 0.0000	Q(185)= 0.0000
Q(186)= 0.0000	Q(187)= 0.0000	Q(188)= 0.0000	Q(189)= 0.0000	Q(190)= 0.0000
Q(191)= 0.0000	Q(192)= 0.0000	Q(193)= 0.0000	Q(194)= 0.0000	Q(195)= 0.0000
Q(196)= 0.0000	Q(197)= 0.0000	Q(198)= 0.0000	Q(199)= 0.0000	Q(200)= 7.2000-01
Q(201)= 7.2000-01	Q(202)= 7.2000-01	Q(203)= 5.6300-01	Q(204)= 0.0000	Q(205)= 0.0000

HEAT GENERATION VALUES ARE IN BTU/HR

Figure 8. Heat Generation Nodes

SLIC 7/2 LASER GYRO PLATFORM

K(1)= 1.6000-02	K(2)= 4.5000-01	K(3)= 1.6000-02	K(4)= 9.0000-01	K(5)= 1.6000-02
K(6)= 1.6000-02	K(7)= 4.5000-01	K(8)= 9.0000-01	K(9)= 1.9000+00	K(10)= 1.9000+00
K(11)= 2.0000+00	K(12)= 1.9000+00	K(13)= 1.9000+00	K(14)= 2.0000+00	K(15)= 1.5000+00
K(16)= 3.4000+00	K(17)= 3.4000+00	K(18)= 1.5000+00	K(19)= 2.8000+00	K(20)= 3.2000+00
K(21)= 1.5000+00	K(22)= 2.8000+00	K(23)= 3.4000+00	K(24)= 3.4000+00	K(25)= 3.2000+00
K(26)= 2.8000+00	K(27)= 2.8000+00	K(28)= 1.5000+00	K(29)= 1.2000-01	K(30)= 1.2000-01
K(31)= 1.2000-01	K(32)= 1.2000-01	K(33)= 3.0000+00	K(34)= 3.0000+00	K(35)= 6.7000-02
K(36)= 6.7000-02	K(37)= 1.6000-02	K(38)= 1.6000-02	K(39)= 1.6000-02	K(40)= 1.6000-02
K(41)= 9.0000-01	K(42)= 4.5000-01	K(43)= 9.0000-01	K(44)= 4.5000-01	K(45)= 1.9000+00
K(46)= 1.5000+00	K(47)= 2.0000+00	K(48)= 1.9000+00	K(49)= 1.5000+00	K(50)= 1.2000-01
K(51)= 1.2000-01	K(52)= 3.4000+00	K(53)= 3.4000+00	K(54)= 3.2000+00	K(55)= 3.4000+00
K(56)= 3.4000+00	K(57)= 3.2000+00	K(58)= 2.8000+00	K(59)= 2.8000+00	K(60)= 2.8000+00
K(61)= 2.8000+00	K(62)= 1.5000+00	K(63)= 1.9000+00	K(64)= 1.2000-01	K(65)= 1.2000-01
K(66)= 2.0000+00	K(67)= 1.5000+00	K(68)= 1.9000+00	K(69)= 3.0000+00	K(70)= 6.7000-02
K(71)= 3.0000+00	K(72)= 6.7000-02	K(73)= 1.6000-02	K(74)= 1.6000-02	K(75)= 1.6000-02
K(76)= 1.6000-02	K(77)= 4.5000-01	K(78)= 9.0000-01	K(79)= 4.5000-01	K(80)= 9.0000-01
K(81)= 1.9000+00	K(82)= 2.0000+00	K(83)= 1.9000+00	K(84)= 2.8000+00	K(85)= 3.4000+00
K(86)= 3.4000+00	K(87)= 1.5000+00	K(88)= 1.2000-01	K(89)= 1.2000-01	K(90)= 1.5000+00
K(91)= 3.2000+00	K(92)= 3.2000+00	K(93)= 3.4000+00	K(94)= 3.4000+00	K(95)= 1.5000+00
K(96)= 1.5000+00	K(97)= 1.9000+00	K(98)= 2.0000+00	K(99)= 1.2000-01	K(100)= 1.2000-01
K(101)= 1.9000+00	K(102)= 2.8000+00	K(103)= 2.8000+00	K(104)= 2.8000+00	K(105)= 3.0000+00
K(106)= 3.0000+00	K(107)= 6.7000-02	K(108)= 6.7000-02	K(109)= 2.2000-02	K(110)= 4.1000-02
K(111)= 2.7000-02	K(112)= 2.2000-02	K(113)= 4.1000-02	K(114)= 2.7000-02	K(115)= 2.2000-02
K(116)= 2.7000-02	K(117)= 4.1000-02	K(118)= 5.7000-02	K(119)= 2.2000-02	K(120)= 2.0000-02
K(121)= 5.7000-02	K(122)= 2.2000-02	K(123)= 2.0000-02	K(124)= 5.7000-02	K(125)= 2.2000-02
K(126)= 2.0000-02	K(127)= 5.5000-02	K(128)= 5.5000-02	K(129)= 5.5000-02	K(130)= 5.5000-02
K(131)= 5.5000-02	K(132)= 5.5000-02	K(133)= 2.8000-02	K(134)= 2.0000-02	K(135)= 2.8000-02
K(136)= 2.6000-02	K(137)= 2.0000-02	K(138)= 2.6000-02	K(139)= 2.8000-02	K(140)= 2.0000-02
K(141)= 2.6000-02	K(142)= 2.2000-02	K(143)= 2.4000-02	K(144)= 2.2000-02	K(145)= 2.4000-02
K(146)= 2.2000-02	K(147)= 2.4000-02	K(148)= 2.8000-02	K(149)= 4.1000-02	K(150)= 2.8000-02
K(151)= 4.0000-02	K(152)= 2.8000-02	K(153)= 4.0000-02	K(154)= 1.0000-02	K(155)= 6.1000-02
K(156)= 7.0000-03	K(157)= 7.0000-03	K(158)= 6.1000-02	K(159)= 1.0000-02	K(160)= 7.0000-03
K(161)= 1.0000-02	K(162)= 6.1000-02	K(163)= 2.6000-02	K(164)= 2.9000-02	K(165)= 2.0000-02
K(166)= 1.2000-02	K(167)= 2.0000-02	K(168)= 1.2000-02	K(169)= 2.6000-02	K(170)= 2.9000-02
K(171)= 2.6000-02	K(172)= 2.9000-02	K(173)= 2.0000-02	K(174)= 1.2000-02	K(175)= 4.4000-02
K(176)= 3.2000-02	K(177)= 4.4000-02	K(178)= 3.2000-02	K(179)= 4.4000-02	K(180)= 3.2000-02
K(181)= 1.0000-02	K(182)= 1.0000-02	K(183)= 1.0000-02	K(184)= 1.0000-02	K(185)= 1.0000-02
K(186)= 1.0000-02	K(187)= 5.6000-02	K(188)= 5.6000-02	K(189)= 5.6000-02	K(190)= 2.4000-02
K(191)= 2.3000-02	K(192)= 2.4000-02	K(193)= 2.5000-02	K(194)= 2.3000-02	K(195)= 2.5000-02
K(196)= 2.3000-02	K(197)= 2.5000-02	K(198)= 4.4000-02	K(199)= 3.2000-02	K(200)= 4.4000-02
K(201)= 3.2000-02	K(202)= 4.4000-02	K(203)= 3.2000-02	K(204)= 1.0000-02	K(205)= 1.0000-02
K(206)= 1.0000-02	K(207)= 1.0000-02	K(208)= 1.0000-02	K(209)= 1.0000-02	K(210)= 5.6000-02
K(211)= 2.4000-02	K(212)= 2.9000-02	K(213)= 2.6000-02	K(214)= 2.0000-02	K(215)= 1.2000-02
K(216)= 3.8000-02	K(217)= 3.2000-02	K(218)= 2.0000-02	K(219)= 1.2000-02	K(220)= 2.6000-02
K(221)= 2.9000-02	K(222)= 5.6000-02	K(223)= 5.6000-02	K(224)= 2.0000-02	K(225)= 1.2000-02
K(226)= 2.8000-02	K(227)= 4.0000-02	K(228)= 1.0000-02	K(229)= 6.1000-02	K(230)= 7.0000-03
K(231)= 2.8000-02	K(232)= 2.9000-02	K(233)= 2.6000-02	K(234)= 4.0000-02	K(235)= 1.0000-02
K(236)= 6.1000-02	K(237)= 7.0000-03	K(238)= 2.8000-02	K(239)= 4.0000-02	K(240)= 1.0000-02
K(241)= 6.1000-02	K(242)= 7.0000-03	K(243)= 2.8000-02	K(244)= 2.6000-02	K(245)= 2.2000-02
K(246)= 2.4000-02	K(247)= 2.2000-02	K(248)= 2.4000-02	K(249)= 2.2000-02	K(250)= 2.8000-02
K(251)= 2.6000-02	K(252)= 2.0000-02	K(253)= 2.4000-02	K(254)= 5.5000-02	K(255)= 5.5000-02
K(256)= 5.5000-02	K(257)= 5.5000-02	K(258)= 5.5000-02	K(259)= 5.5000-02	K(260)= 1.4000-02
K(261)= 1.4000-02	K(262)= 1.4000-02	K(263)= 1.4000-02	K(264)= 1.4000-02	K(265)= 1.4000-02
K(266)= 5.7000-02	K(267)= 2.0000-02	K(268)= 2.2000-02	K(269)= 5.7000-02	K(270)= 2.0000-02

Figure 9. Thermal Conductance Values (Sheet 1 of 2)

K(271)= 2.2000-02	K(272)= 5.7000-02	K(273)= 2.0000-02	K(274)= 2.2000-02	K(275)= 2.7000-02
K(276)= 4.1000-02	K(277)= 2.2000-02	K(278)= 2.7000-02	K(279)= 4.1000-02	K(280)= 2.2000-02
K(281)= 2.7000-02	K(282)= 4.1000-02	K(283)= 2.2000-02	K(284)= 5.0000-02	K(285)= 2.0000-02
K(286)= 4.0000-02	K(287)= 2.8000-01	K(288)= 2.0000-02	K(289)= 1.7000-01	K(290)= 5.0000-02
K(291)= 2.8000-01	K(292)= 2.0000-02	K(293)= 4.0000-02	K(294)= 1.7000-01	K(295)= 2.0000-02
K(296)= 2.0000-02	K(297)= 5.0000-02	K(298)= 2.0000-02	K(299)= 4.0000-02	K(300)= 1.7000-01
K(301)= 2.8000-01	K(302)= 2.0000-02	K(303)= 2.6000-02	K(304)= 2.8000-02	K(305)= 2.0000-02
K(306)= 4.5000-02	K(307)= 1.1600+01	K(308)= 4.0000-02	K(309)= 4.0000-01	K(310)= 4.0000-01
K(311)= 4.0000-01	K(312)= 4.0000-02	K(313)= 2.9000-01	K(314)= 2.9000-01	K(315)= 4.0000-02
K(316)= 2.9000-01	K(317)= 7.0000-02	K(318)= 2.1000-01	K(319)= 2.1000-01	K(320)= 2.1000-01
K(321)= 1.6000+00	K(322)= 5.6000-02	K(323)= 5.6000-02	K(324)= 5.6000-02	K(325)= 1.6000+00
K(326)= 5.0000-03	K(327)= 2.9000-01	K(328)= 2.9000-01	K(329)= 2.9000-01	K(330)= 1.4000-01
K(331)= 1.4000-01	K(332)= 1.4000-01	K(333)= 3.4000-01	K(334)= 9.0000-02	K(335)= 3.2000-01
K(336)= 2.2000-01	K(337)= 9.6000-01	K(338)= 2.0600+00	K(339)= 2.6000+00	K(340)= 1.3700+00
K(341)= 5.0000-03	K(342)= 3.4000-02	K(343)= 3.4000-02	K(344)= 8.0000-02	K(345)= 1.2800+00
K(346)= 1.6000-01	K(347)= 2.4000+00	K(348)= 2.7000-02	K(349)= 6.0000-01	K(350)= 2.8000+00
K(351)= 6.0000-01	K(352)= 2.7000-02	K(353)= 4.5000-02	K(354)= 1.0000-01	K(355)= 1.0100+00
K(356)= 1.7000-01	K(357)= 1.0000-01	K(358)= 7.7000-01	K(359)= 1.7000-01	K(360)= 4.2000-01
K(361)= 4.9000-02	K(362)= 4.5000-02	K(363)= 3.7000-02	K(364)= 3.4800-01	K(365)= 2.1000+00
K(366)= 3.3000-01	K(367)= 3.2000-01	K(368)= 2.4000-02	K(369)= 2.4000-02	K(370)= 2.4000-02
K(371)= 3.2000-01	K(372)= 3.3000-01	K(373)= 2.1000+00	K(374)= 3.4800-01	K(375)= 2.4000-02
K(376)= 2.4000-02	K(377)= 2.4000-02	K(378)= 3.7000-02	K(379)= 4.5000-02	K(380)= 4.9000-02
K(381)= 4.2000-01	K(382)= 4.2000-01	K(383)= 2.2000-01	K(384)= 2.2000-01	K(385)= 4.6000-02
K(386)= 3.6000-02	K(387)= 4.6000-02	K(388)= 9.5000-01	K(389)= 3.2000-01	K(390)= 3.3000-01
K(391)= 2.1000+00	K(392)= 2.4000-02	K(393)= 2.4000-02	K(394)= 2.4000-02	K(395)= 3.4800-01
K(396)= 3.6000-02	K(397)= 4.6000-02	K(398)= 4.6000-02	K(399)= 9.5000-01	K(400)= 3.2000+00
K(401)= 1.7000-01	K(402)= 8.5000-02	K(403)= 3.7000-01	K(404)= 4.8000-02	K(405)= 4.6000-02
K(406)= 1.1000-01	K(407)= 2.1000-01	K(408)= 4.8000-02	K(409)= 4.8000-02	K(410)= 4.8000-02
K(411)= 3.7000-02	K(412)= 4.6000-02	K(413)= 1.8000-01	K(414)= 1.9000-01	K(415)= 1.9000-01
K(416)= 1.9000-01	K(417)= 1.9000-01	K(418)= 1.9000-01	K(419)= 4.8000-02	K(420)= 4.8000-02
K(421)= 2.1000-01	K(422)= 4.8000-02	K(423)= 8.5000-02	K(424)= 4.6000-02	K(425)= 3.2000+00
K(426)= 1.7000-01	K(427)= 3.7000-01	K(428)= 3.2000+00	K(429)= 1.7000-01	K(430)= 4.6000-02
K(431)= 8.5000-02	K(432)= 1.4000+00	K(433)= 4.8000-02	K(434)= 1.1000-01	K(435)= 7.6000-02
K(436)= 1.4000-01	K(437)= 4.4000-02	K(438)= 4.4000-02	K(439)= 7.6000-02	K(440)= 4.4000-02
K(441)= 7.6000-02	K(442)= 1.4000-01	K(443)= 1.4000+00	K(444)= 1.4000+00	K(445)= 3.7000-01
K(446)= 1.9000-01	K(447)= 5.0000-02	K(448)= 5.0000-02	K(449)= 5.0000-02	K(450)= 1.4000-01
K(451)= 1.1000-01	K(452)= 4.8000-02	K(453)= 4.8000-02	K(454)= 4.8000-02	K(455)= 2.1000-01
K(456)= 4.6000-02	K(457)= 1.8000-01	K(458)= 9.6000-02	K(459)= 2.3000-01	K(460)= 8.0000-02
K(461)= 2.3000-01	K(462)= 8.0000-02	K(463)= 8.0000-02	K(464)= 1.8000-01	K(465)= 2.3000-01
K(466)= 4.6000-02	K(467)= 4.8000-02	K(468)= 8.5000-02	K(469)= 8.5000-02	K(470)= 4.6000-02
K(471)= 4.6000-02	K(472)= 9.5000-01	K(473)= 3.6000-02	K(474)= 9.3000-02	K(475)= 2.2000+00
K(476)= 2.2000+00	K(477)= 7.3000-02	K(478)= 7.3000-02	K(479)= 9.3000-02	K(480)= 2.2000+00
K(481)= 2.2000+00	K(482)= 2.2000+00	K(483)= 2.2000+00	K(484)= 9.3000-02	K(485)= 9.3000-02
K(486)= 7.3000-02	K(487)= 9.3000-02	K(488)= 9.3000-02	K(489)= 8.5000-02	K(490)= 4.9000-02
K(491)= 5.2600+00	K(492)= 5.2600+00	K(493)= 5.2600+00	K(494)= 8.6000-01	K(495)= 8.6000-01
K(496)= 8.6000-01	K(			

CONDUCTANCE UNITS ARE BTU/HR °F

Figure 9. Thermal Conductance Values (Sheet 2 of 2)

C(1)= 2.2000-03	C(2)= 2.8000-03	C(3)= 2.8000-03	C(4)= 1.6000-03	C(5)= 1.2000-03
C(6)= 9.0000-04	C(7)= 1.6000-03	C(8)= 9.0000-04	C(9)= 1.0000-03	C(10)= 1.0000-03
C(11)= 1.0000-03	C(12)= 1.2000-03	C(13)= 9.0000-04	C(14)= 1.2000-03	C(15)= 1.0000-03
C(16)= 1.6000-03	C(17)= 1.6000-03	C(18)= 1.0000-03	C(19)= 1.0000-03	C(20)= 2.2000-03
C(21)= 2.8000-03	C(22)= 2.8000-03	C(23)= 1.6000-03	C(24)= 1.6000-03	C(25)= 1.0000-03
C(26)= 1.0000-03	C(27)= 1.2000-03	C(28)= 9.0000-04	C(29)= 1.2000-03	C(30)= 1.2000-03
C(31)= 1.0000-03	C(32)= 1.6000-03	C(33)= 1.6000-03	C(34)= 9.0000-04	C(35)= 1.2000-03
C(36)= 1.0000-03	C(37)= 1.0000-03	C(38)= 1.0000-03	C(39)= 2.2000-03	C(40)= 2.8000-03
C(41)= 2.8000-03	C(42)= 1.6000-03	C(43)= 1.6000-03	C(44)= 1.2000-03	C(45)= 9.0000-04

C(46)= 1.2000-03	C(47)= 1.0000-03	C(48)= 1.0000-03	C(49)= 1.0000-03	C(50)= 1.2000-03
C(51)= 9.0000-04	C(52)= 1.2000-03	C(53)= 1.0000-03	C(54)= 1.6000-03	C(55)= 1.6000-03
C(56)= 1.0000-03	C(57)= 1.0000-03	C(58)= 3.8000-03	C(59)= 7.6000-03	C(60)= 3.8000-03
C(61)= 3.8000-03	C(62)= 7.6000-03	C(63)= 3.8000-03	C(64)= 3.8000-03	C(65)= 7.6000-03
C(66)= 3.8000-03	C(67)= 1.9000-03	C(68)= 1.9000-03	C(69)= 1.9000-03	C(70)= 1.9000-03
C(71)= 1.9000-03	C(72)= 1.9000-03	C(73)= 1.4000-03	C(74)= 1.4000-03	C(75)= 3.3000-03
C(76)= 3.3000-03	C(77)= 1.4000-03	C(78)= 3.3000-03	C(79)= 3.3000-03	C(80)= 1.4000-03
C(81)= 1.4000-03	C(82)= 1.4000-03	C(83)= 3.3000-03	C(84)= 3.3000-03	C(85)= 2.6000-03
C(86)= 1.6000-03	C(87)= 1.1000-03	C(88)= 1.6000-03	C(89)= 2.6000-03	C(90)= 1.1000-03
C(91)= 1.6000-03	C(92)= 2.6000-03	C(93)= 1.1000-03	C(94)= 1.1000-03	C(95)= 2.6000-03
C(96)= 1.6000-03	C(97)= 1.1000-03	C(98)= 1.6000-03	C(99)= 2.6000-03	C(100)= 1.1000-03
C(101)= 1.6000-03	C(102)= 2.6000-03	C(103)= 3.3000-03	C(104)= 3.3000-03	C(105)= 1.4000-03
C(106)= 1.4000-03	C(107)= 1.4000-03	C(108)= 3.3000-03	C(109)= 3.3000-03	C(110)= 1.4000-03
C(111)= 1.4000-03	C(112)= 3.3000-03	C(113)= 3.3000-03	C(114)= 1.4000-03	C(115)= 1.9000-03
C(116)= 1.9000-03	C(117)= 3.8000-03	C(118)= 3.8000-03	C(119)= 7.6000-03	C(120)= 1.9000-03
C(121)= 1.9000-03	C(122)= 3.8000-03	C(123)= 3.8000-03	C(124)= 7.6000-03	C(125)= 1.9000-03
C(126)= 1.9000-03	C(127)= 3.8000-03	C(128)= 3.8000-03	C(129)= 7.6000-03	C(130)= 3.8000-03
C(131)= 3.8000-03	C(132)= 3.8000-03	C(133)= 5.3000-03	C(134)= 4.7000-03	C(135)= 4.7000-03
C(136)= 5.3000-03	C(137)= 5.3000-03	C(138)= 4.7000-03	C(139)= 5.2000-03	C(140)= 5.2000-03
C(141)= 5.2000-03	C(142)= 2.0000-03	C(143)= 2.0000-03	C(144)= 2.0000-03	C(145)= 1.1200-02
C(146)= 1.1200-02	C(147)= 1.1200-02	C(148)= 1.0400-02	C(149)= 1.0400-02	C(150)= 1.0400-02
C(151)= 9.5000-03	C(152)= 9.5000-03	C(153)= 9.5000-03	C(154)= 2.2000-03	C(155)= 2.2000-03
C(156)= 2.2000-03	C(157)= 2.5000-03	C(158)= 2.5000-03	C(159)= 2.5000-03	C(160)= 3.0000-03
C(161)= 3.0000-03	C(162)= 3.0000-03	C(163)= 2.9000-03	C(164)= 2.9000-03	C(165)= 2.9000-03
C(166)= 8.0000-04	C(167)= 8.0000-04	C(168)= 8.0000-04	C(169)= 8.0000-04	C(170)= 8.0000-04
C(171)= 8.0000-04	C(172)= 1.9000-03	C(173)= 1.9000-03	C(174)= 1.9000-03	C(175)= 1.9000-03
C(176)= 1.9000-03	C(177)= 1.9000-03	C(178)= 5.7000-03	C(179)= 5.7000-03	C(180)= 5.7000-03
C(181)= 1.2000-03	C(182)= 1.2000-03	C(183)= 1.2000-03	C(184)= 1.5400-02	C(185)= 1.5400-02
C(186)= 1.5400-02	C(187)= 1.7800-02	C(188)= 1.7800-02	C(189)= 1.7800-02	C(190)= 1.3400-02
C(191)= 1.3400-02	C(192)= 1.3400-02	C(193)= 5.9000-03	C(194)= 8.9000-03	C(195)= 8.8000-03
C(196)= 2.3000-03	C(197)= 1.1000-03	C(198)= 1.1000-03	C(199)= 1.1000-03	C(200)= 3.3000-03
C(201)= 3.3000-03	C(202)= 3.3000-03	C(203)= 2.1000-03	C(204)= 3.9000-03	C(205)= 4.4000-03

CAPACITANCE VALUES ARE IN UNITS OF BTU/°F

Figure 10. Node Thermal Capacitance

Results of the Analysis

There are several major objectives which were expected to result from the mathematical thermal modeling of the SLIC 7/2 laser gyro platform analysis. These are:

- Steady-state temperature level of parts
- Warmup time required and thermal time constant
- Transient temperature response of parts
- Temperature gradients experienced along the laser tube especially window to window, both time varying and steady state
- Axial temperature gradient and direction of gradient in cervit block
- Symmetry of temperature distribution in the block circumferentially and axially
- Ability of the cervit block connecting hardware, top and bottom, to produce similar temperature levels top and bottom of the cervit block.

The application environment of the laser platform system was taken to be $120^{o}F$ which applies to both ambient and structure mounting.

The first information presented is the platform warmup response and consequently the steady state temperature levels. Figure 11 shows the warmup curve of the laser tube body/windows and tube cathode as well as various parts on the cervit block. This figure also shows the warmup of the resistor and hybrid module. The hottest area on the cervit block is the upper tube mounting point; the coldest is the bottom of the block. There exists a $12^{o}F$ gradient between these two points. The overall axial gradient of the cervit block is $5^{o}F$ with the center of the block hotter than either top or bottom.

The tube body steady-state temperature is $153^{o}F$ with the cathode $3^{o}F$ higher. This is a safe operating temperature level when at a maximum environment of $120^{o}F$.

The electronics operates at very safe temperature levels with the hybrids at $124^{o}F$ and the resistor assembly at $132^{o}F$.

The main concerns are the various time varying temperature gradients, primarily those associated with the laser tubes. The temperature distributions after 0.86 hour, 1.5 hours and 2.78 hours of operation are pictorially shown for:

(a) Cervit block and laser tubes on figures 12, 13, and 14

(b) Cervit block on side of tube No. 1 on figures 15, 16, and 17

(c) Shields and case on figures 18, 19, and 20

(d) Upper connecting hardware on figures 21, 22, and 23

(e) Lower connecting hardware on figures 24, 25, and 26

(f) Platform base on figures 27, 28, and 29

A graph showing how the cervit block gradient varies over its entire height and from the area of the upper and lower laser tube windows is shown on figure 30. The temperature gradient which most strongly influences the laser tube windows is the area on the cervit block near nodes 79 and 108.

Figure 31 shows the time varying temperature gradients of the three laser tubes. The largest gradient is found in tube No. 3 with almost $0.05^{o}F$. Tube No. 1 and No. 2 run very close with a final (steady-state) gradient of 0.03 and $0.035^{o}F$. The gradients plotted are those occurring from window to window. A detail temperature distribution and gradient picture of tube No. 1 is seen on figure 32.

The tube mounting tabs are lower in temperature than any other portion of the tube because they are in contact with the colder cervit block. Since the mounting tabs are offset, the upper left and lower right areas of the tube are dragged down in temperature. This can be seen on the diagram of figure 32. The lower mounting tab is $0.062^{o}F$ lower due to the generally lower temperatures at the lower end of the cervit block.

The temperature difference from tube No. 1 to tube No. 2 is only $0.018^{o}F$.

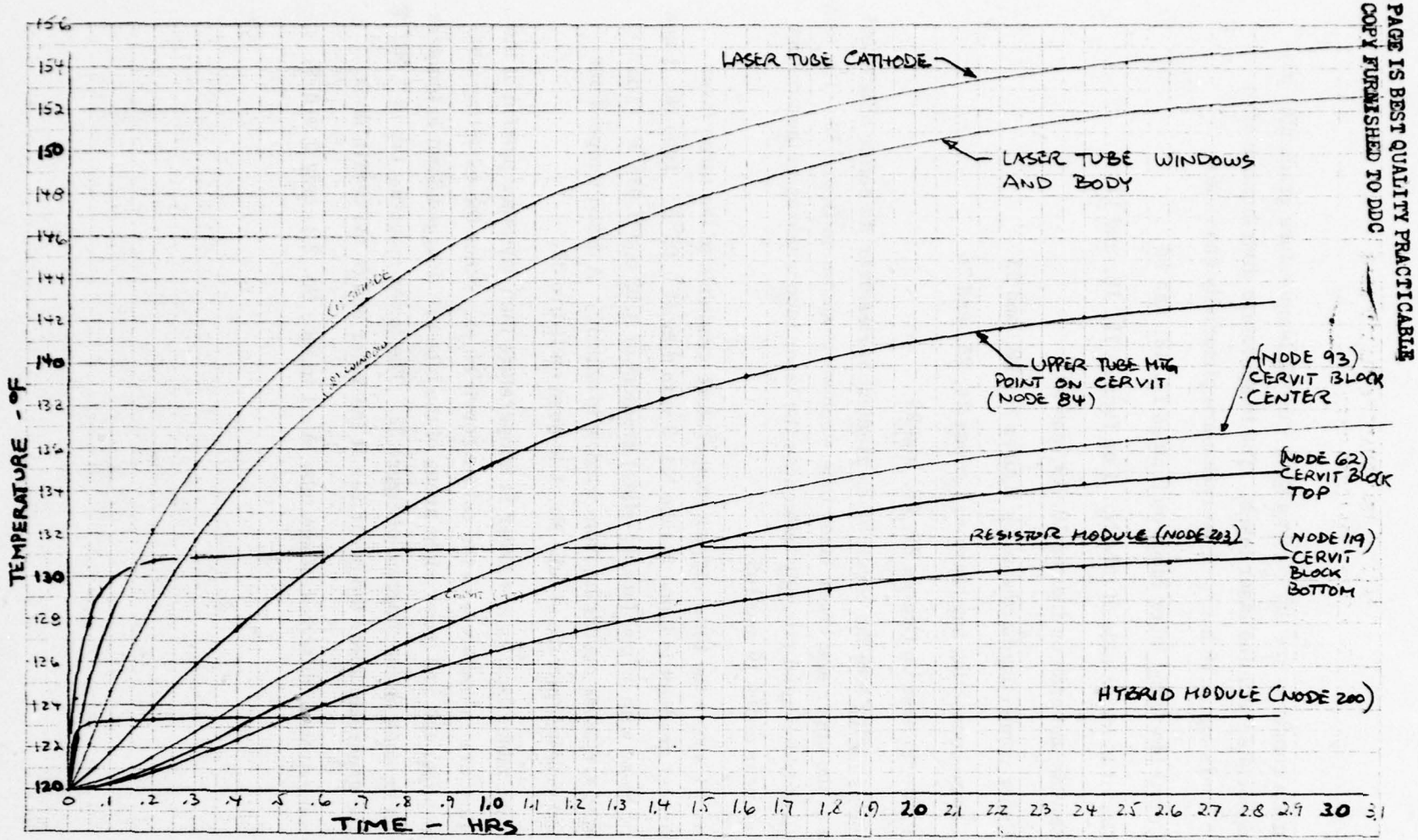

Figure 11. Tube and Cervit Block Warmup Curve

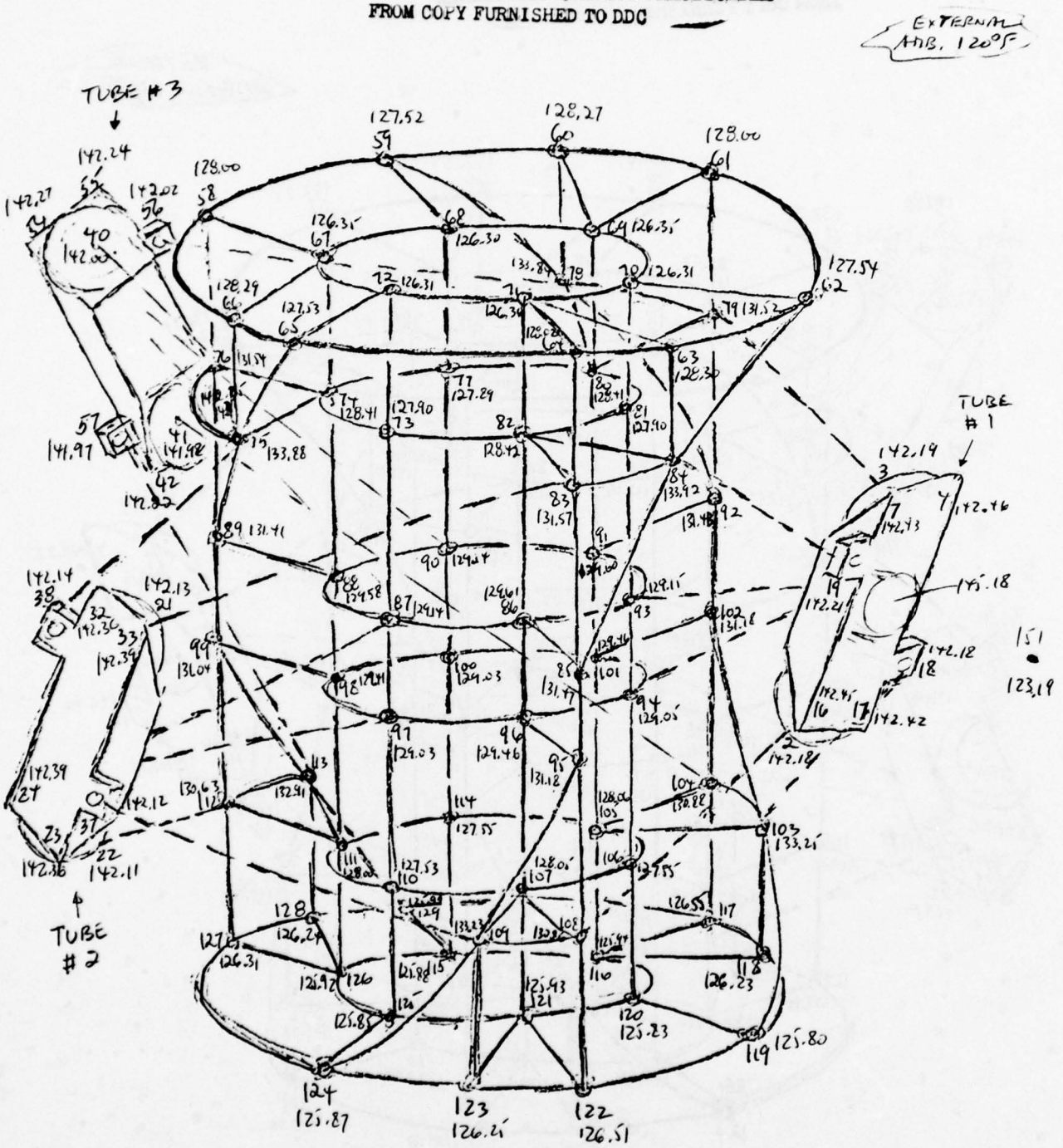

Figure 12. Cervit Block and Laser Tube Temperatures in ^{o}F after 0.86 Hours of Operation

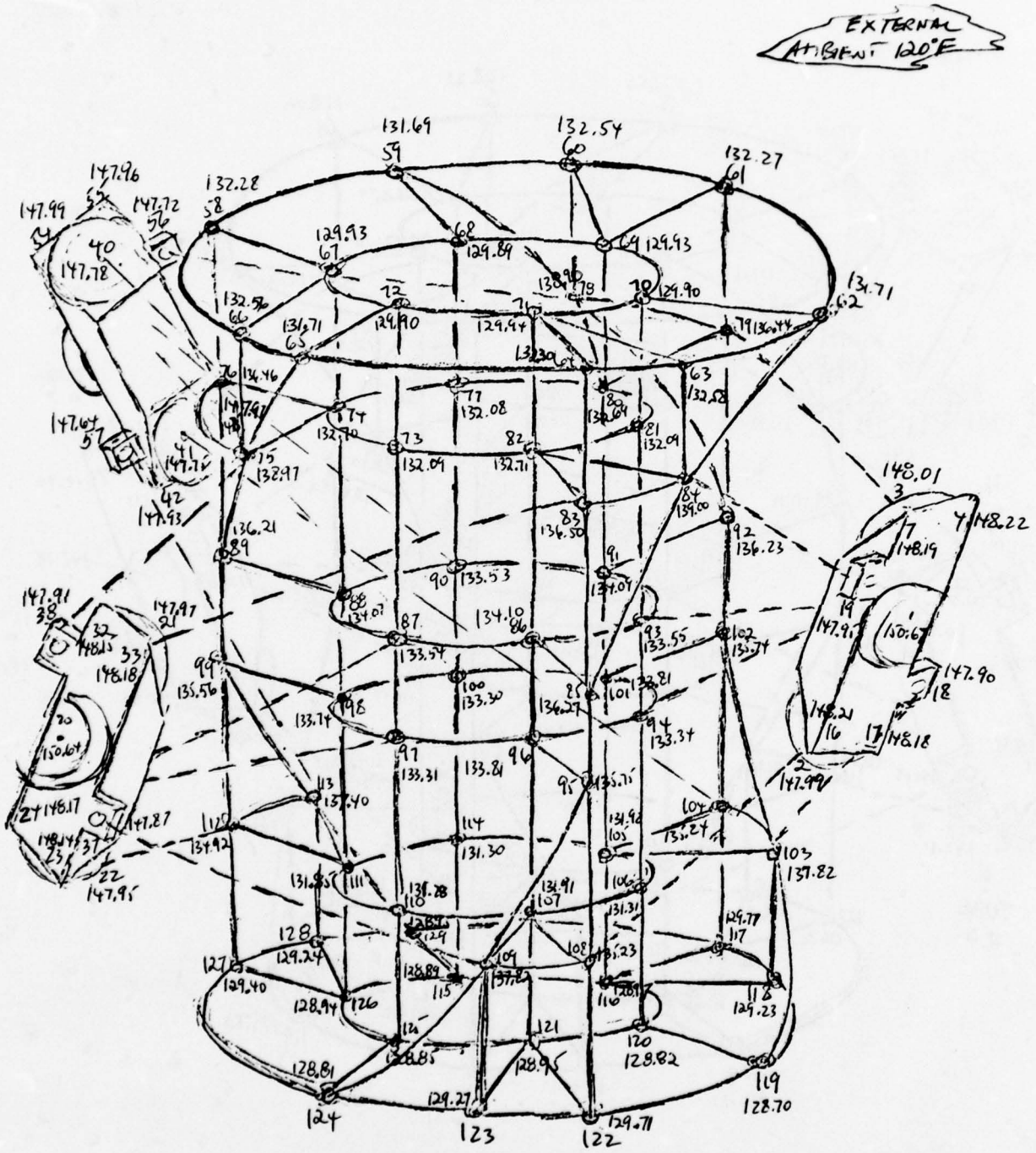

Figure 13. Cervit Block and Laser Tube Temperatures in ^{o}F after 1.5 Hours of Operation

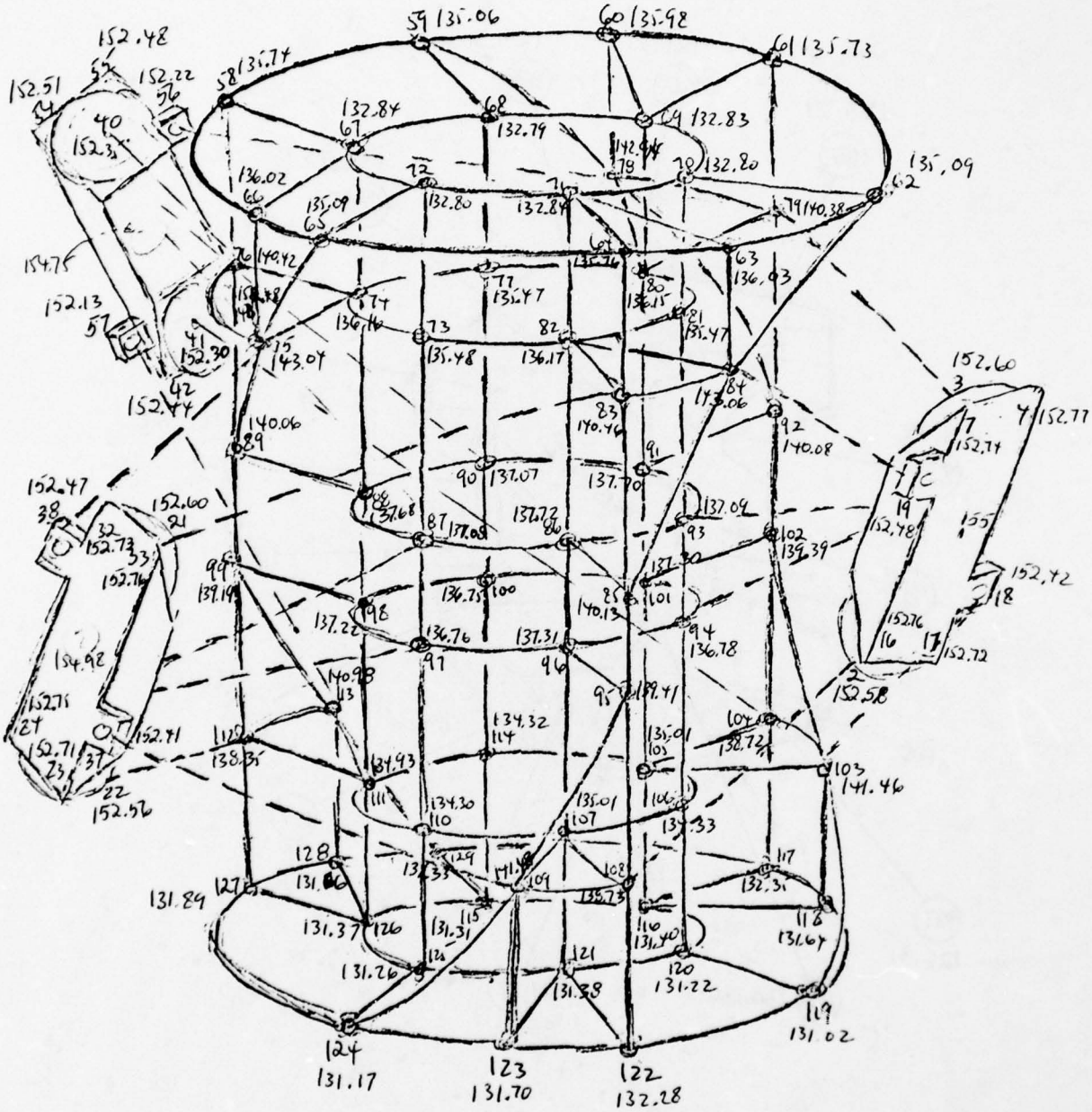

Figure 14. Cervit Block and Laser Tube Temperatures in ^{o}F after 2.78 Hours of Operation

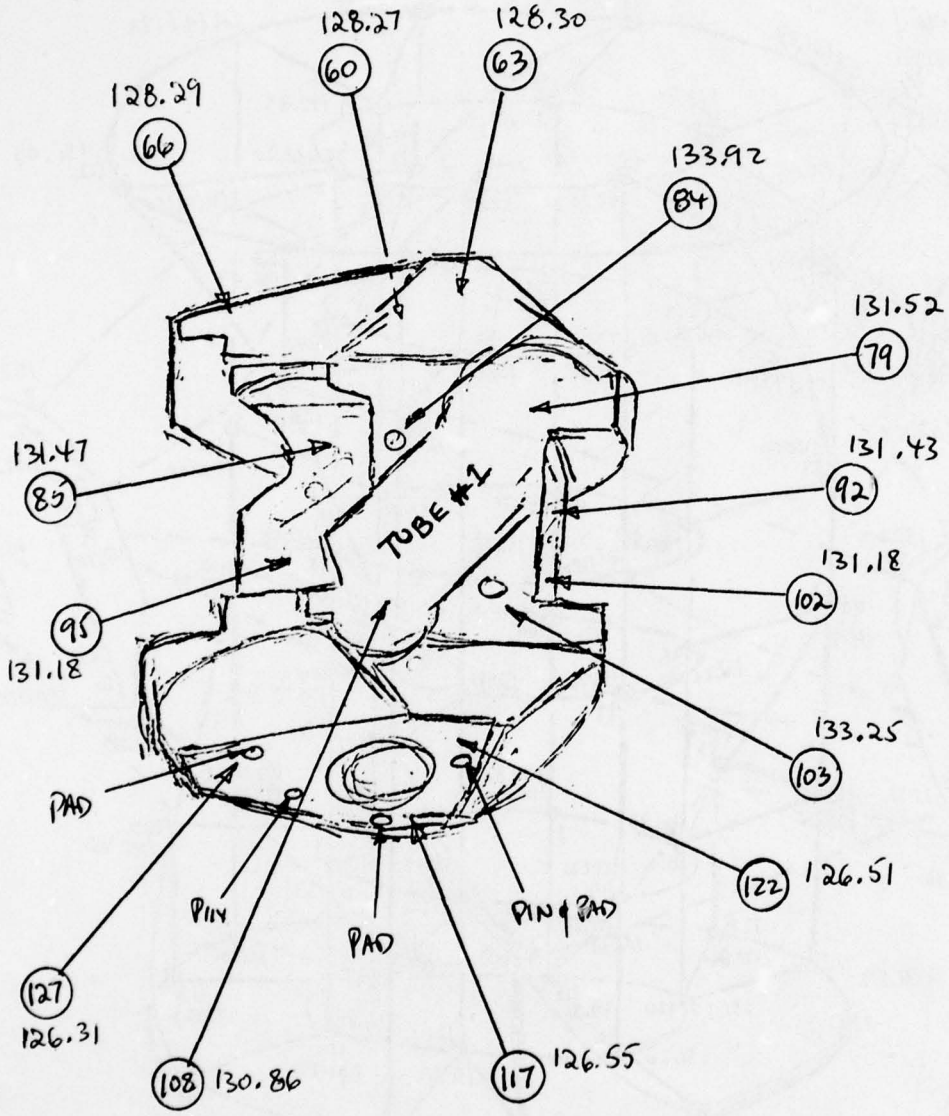

Figure 15. Cervit Block Temperatures in ^{o}F after 0.86 Hours of Operation

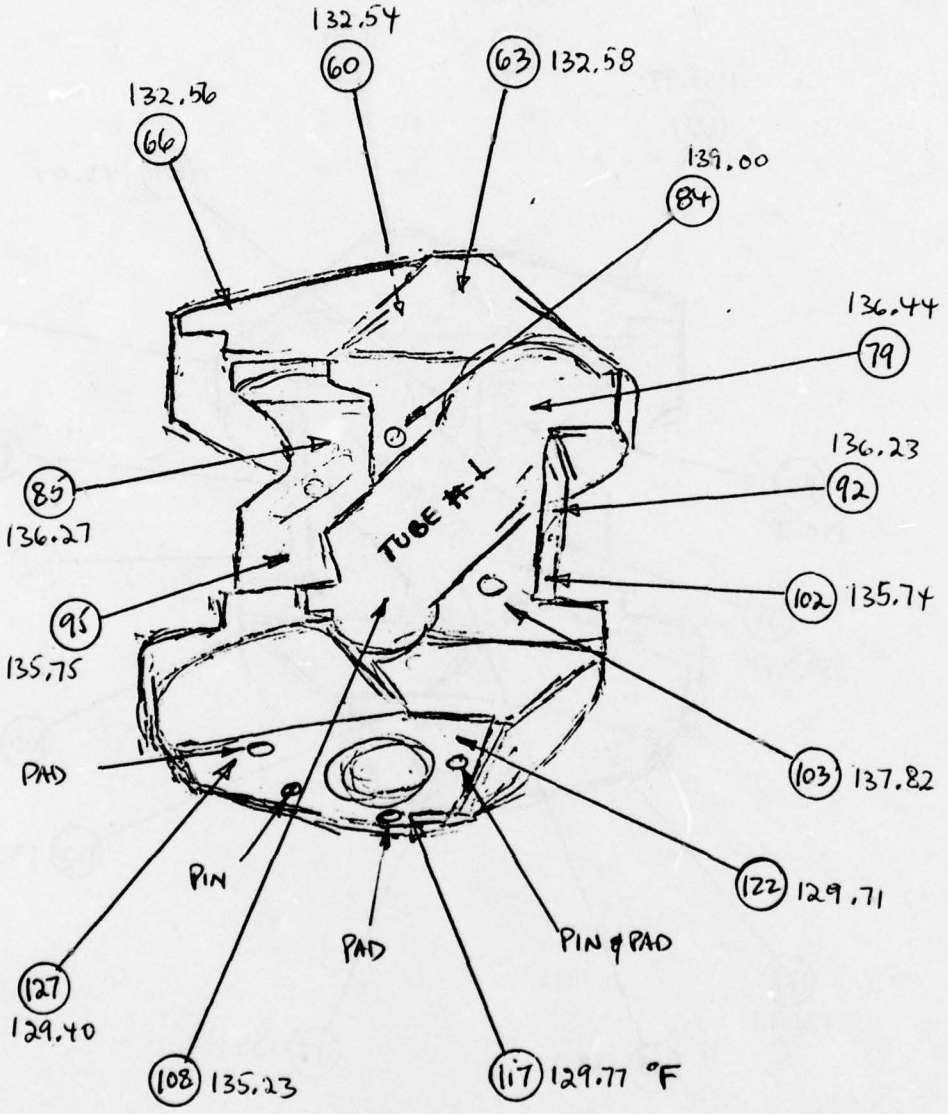

Figure 16. Cervit Block Temperatures in ^{o}F after 1.5 Hours of Operation

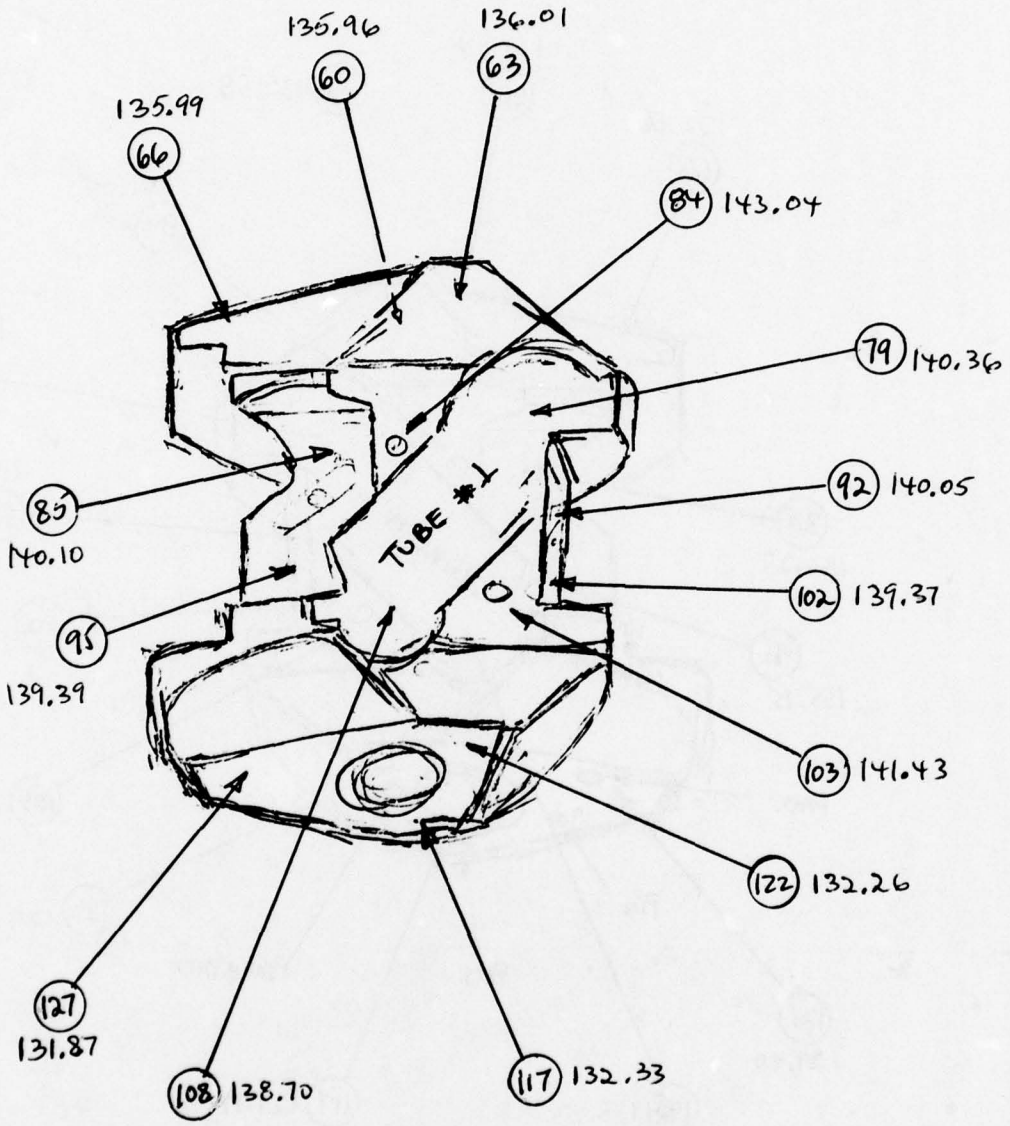

Figure 17. Cervit Block Temperatures in ^{o}F after 2.78 Hours of Operation

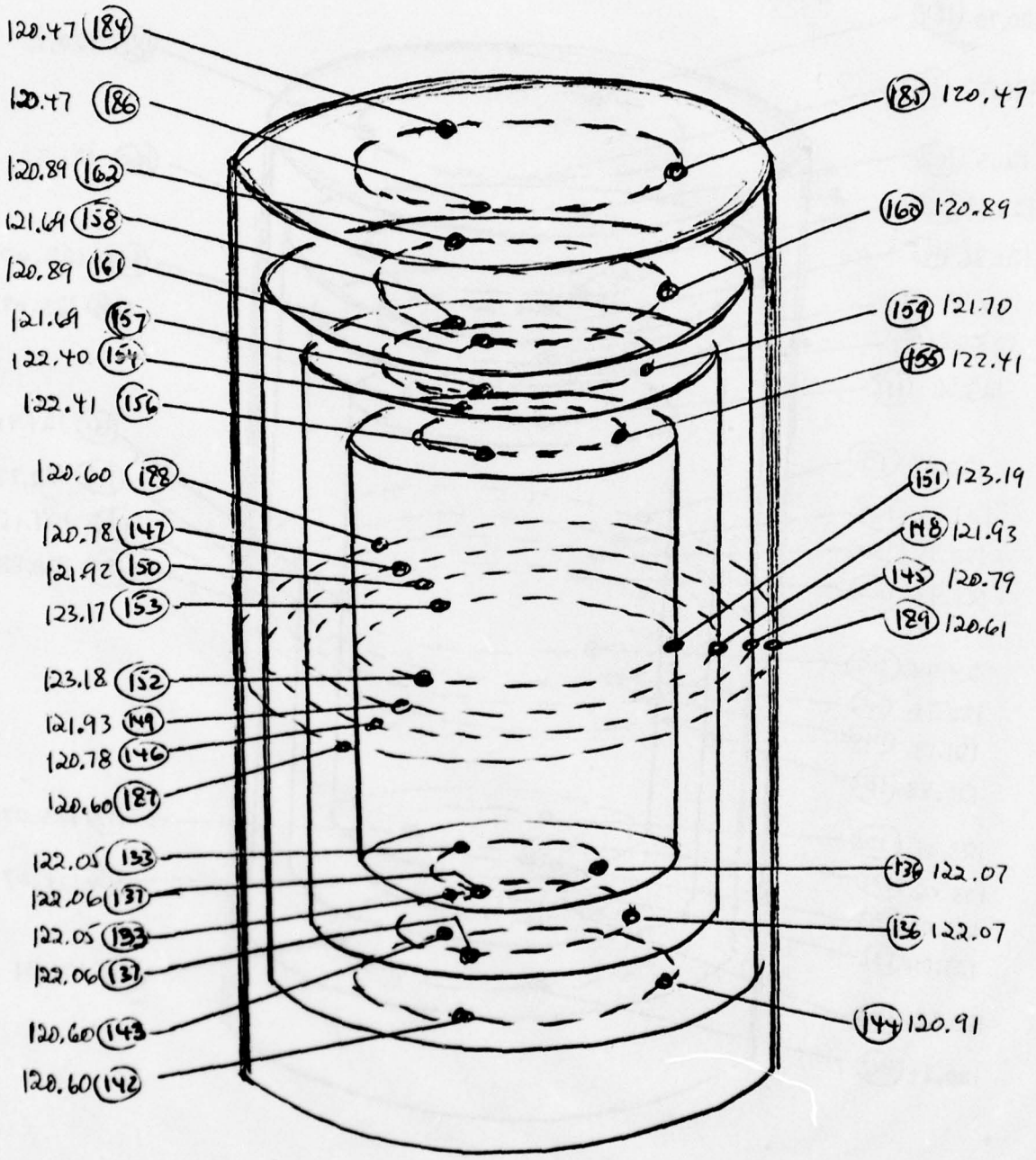

Figure 18. Shield and Case Temperatures in ^{o}F after 0.86 Hours of Operation

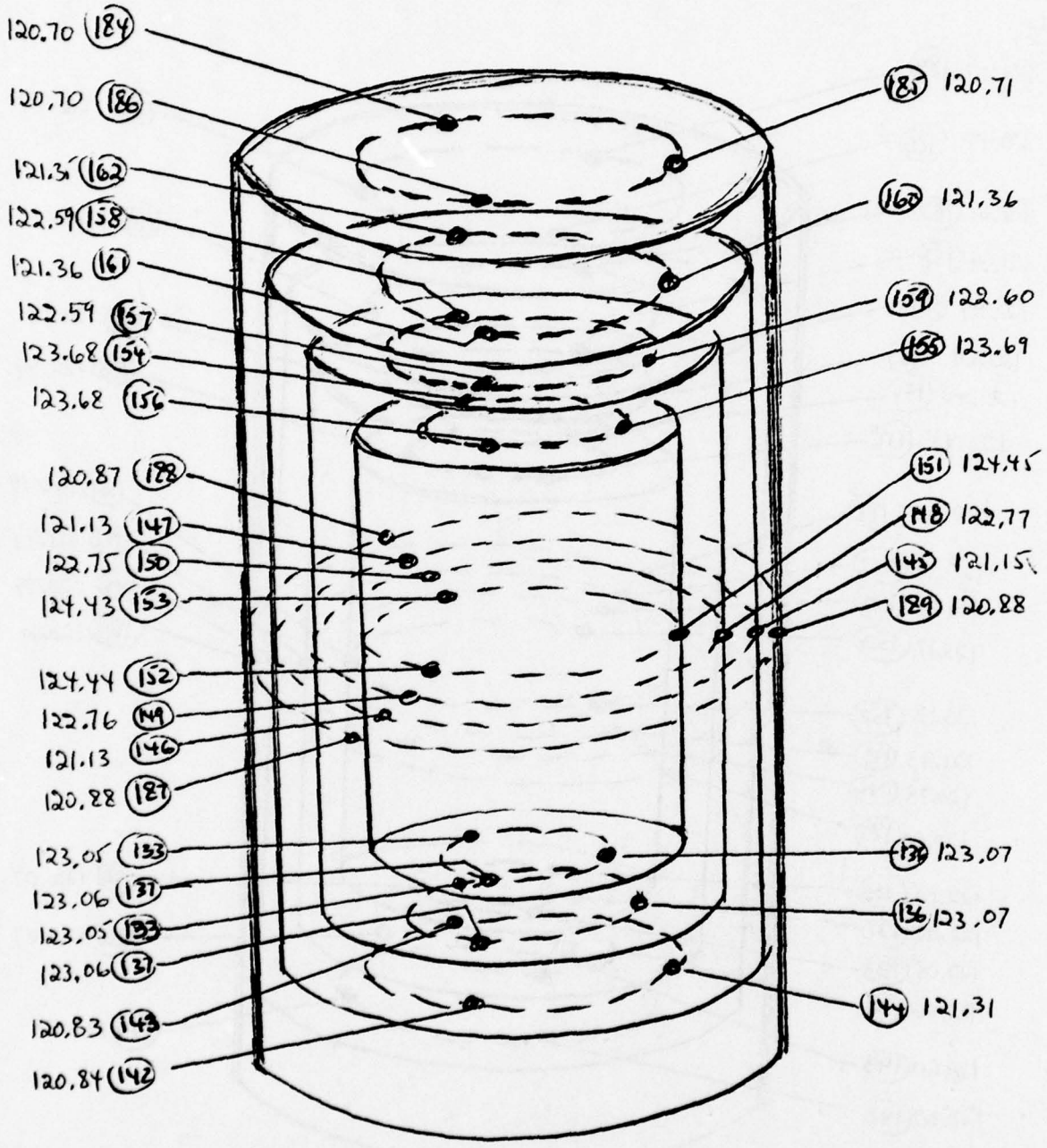

Figure 19. Shield and Case Temperatures in ^{o}F after 1.5 Hours of Operation

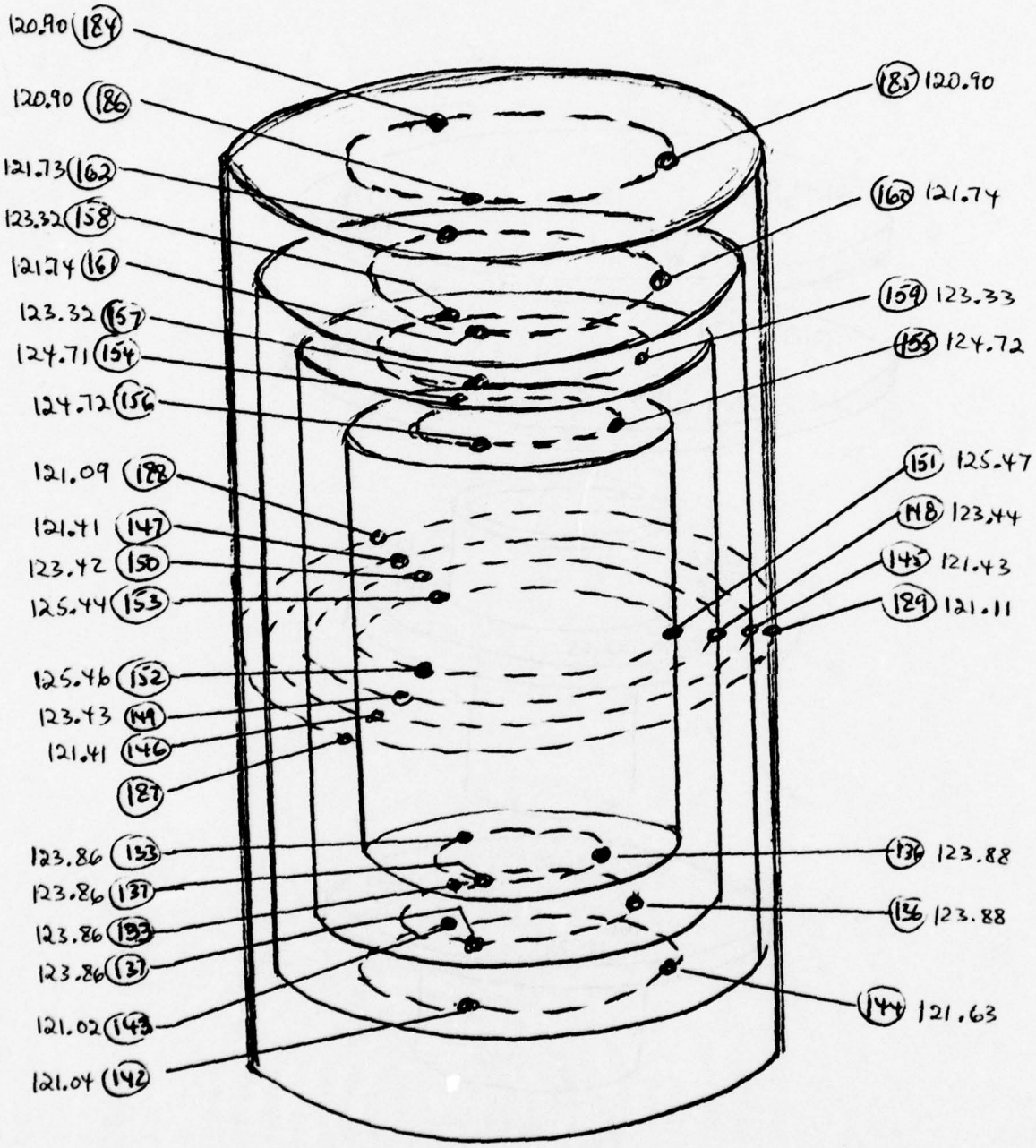

Figure 20. Shield and Case Temperatures in ^{o}F after 2.78 Hours of Operation

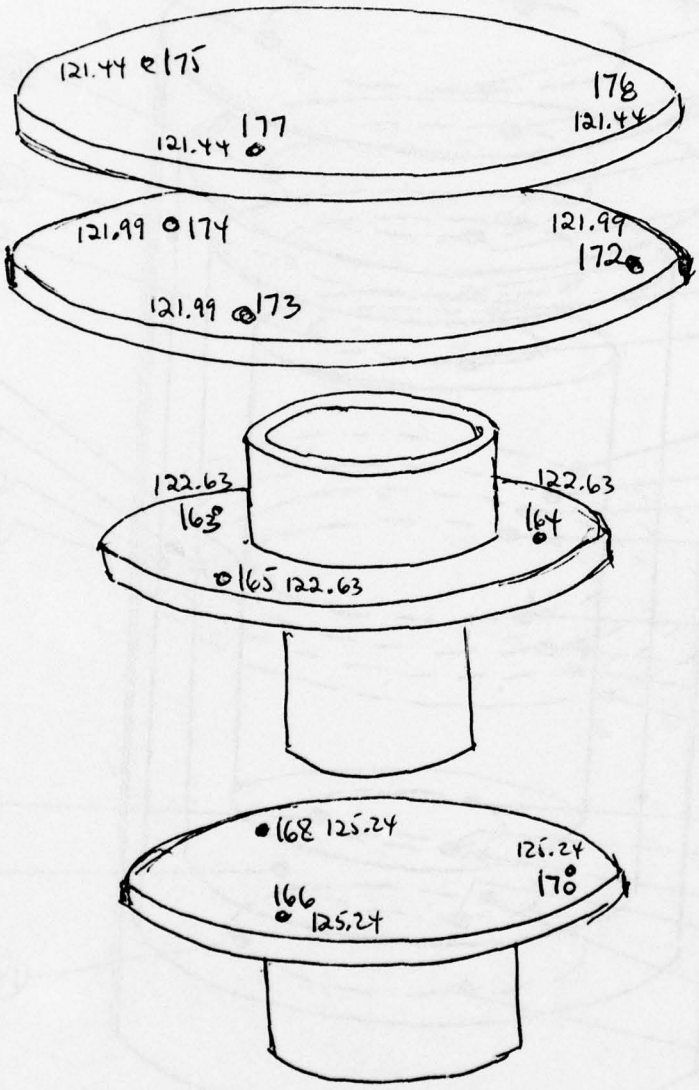

Figure 21. Upper Connecting Hardware Temperatures in ^{o}F after 0.86 Hours of Operation

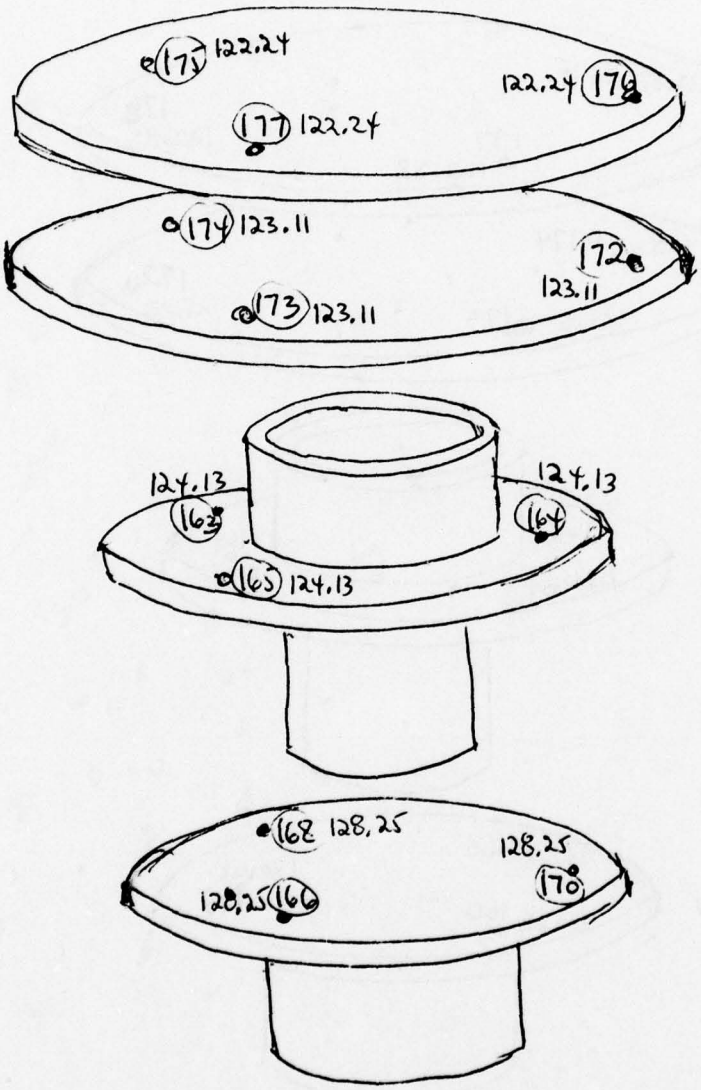

Figure 22. Upper Connecting Hardware Temperatures in ^{o}F after 1.5 Hours of Operation

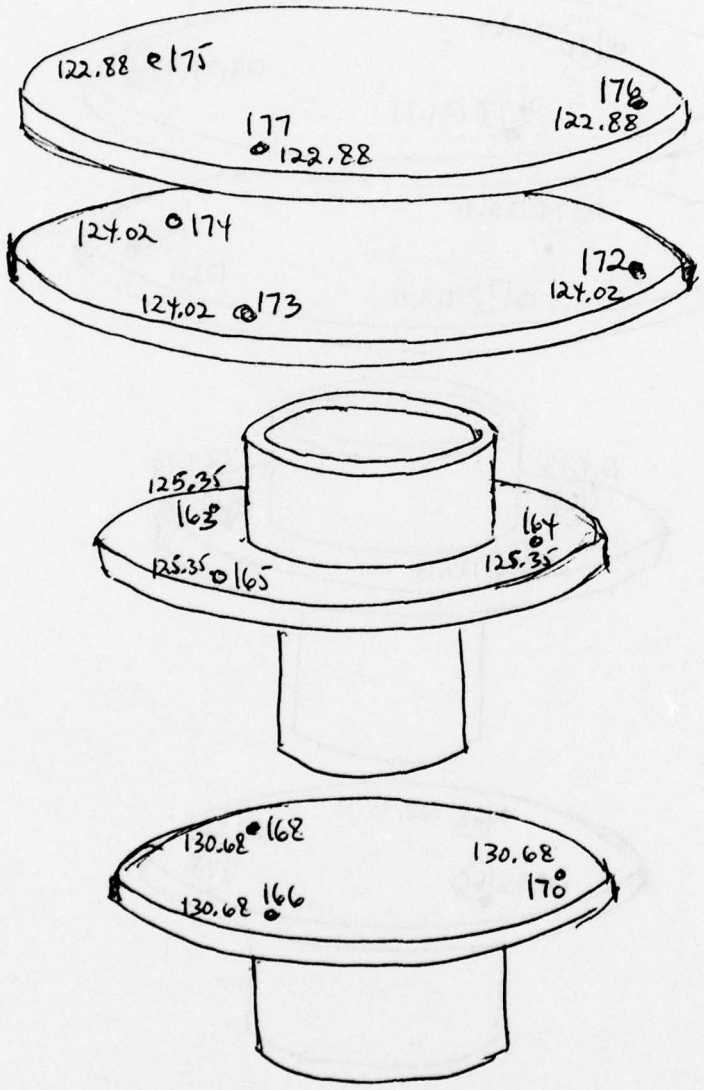

Figure 23. Upper Connecting Hardware Temperatures in ^{o}F after 2.78 Hours of Operation

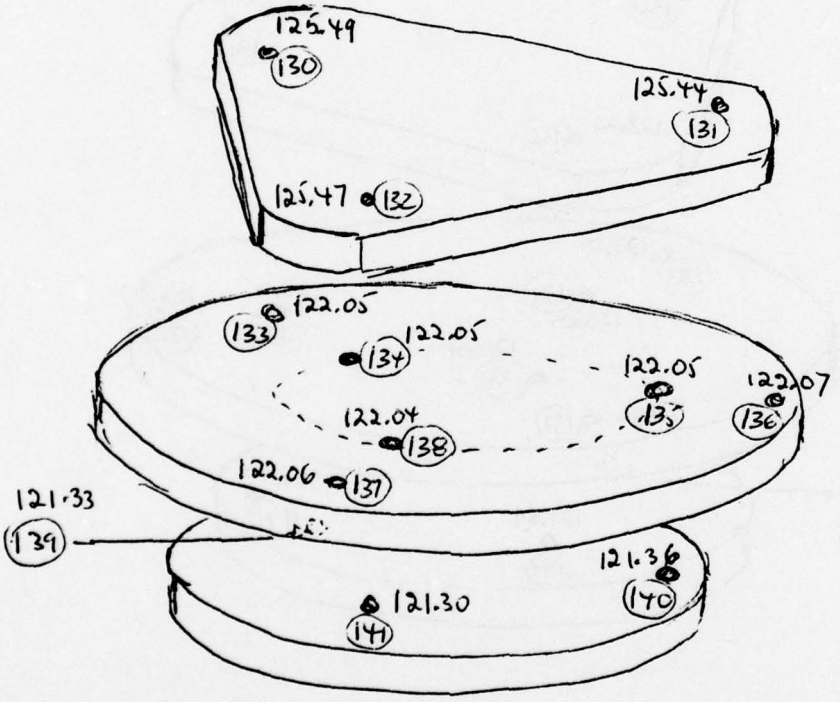

Figure 24. Lower Connecting Hardware Temperatures in ^{o}F after 0.86 Hours of Operation

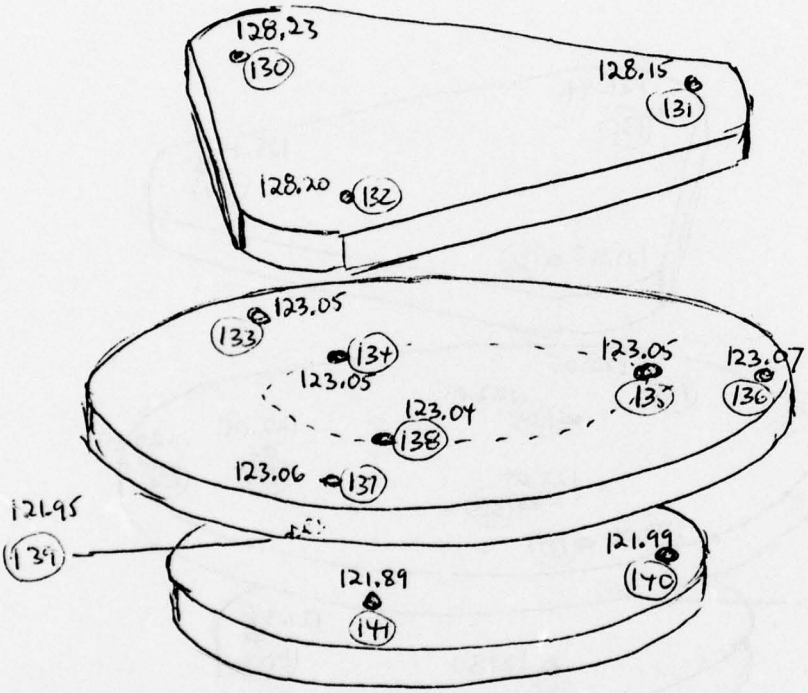

Figure 25. Lower Connecting Hardware Temperatures in ^{o}F after 1.5 Hours of Operation

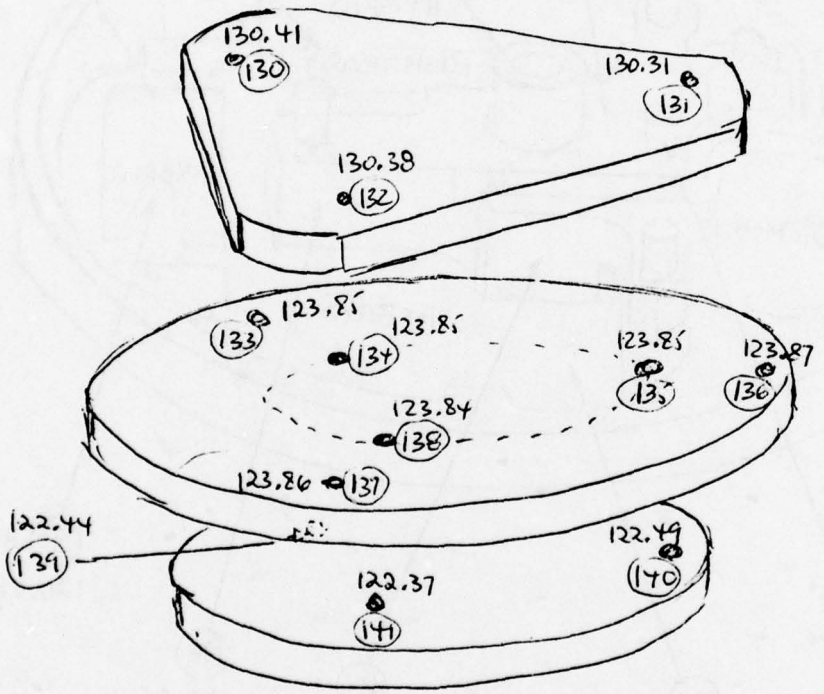

Figure 26. Lower Connecting Hardware Temperatures in ^{O}F after 2.78 Hours of Operation

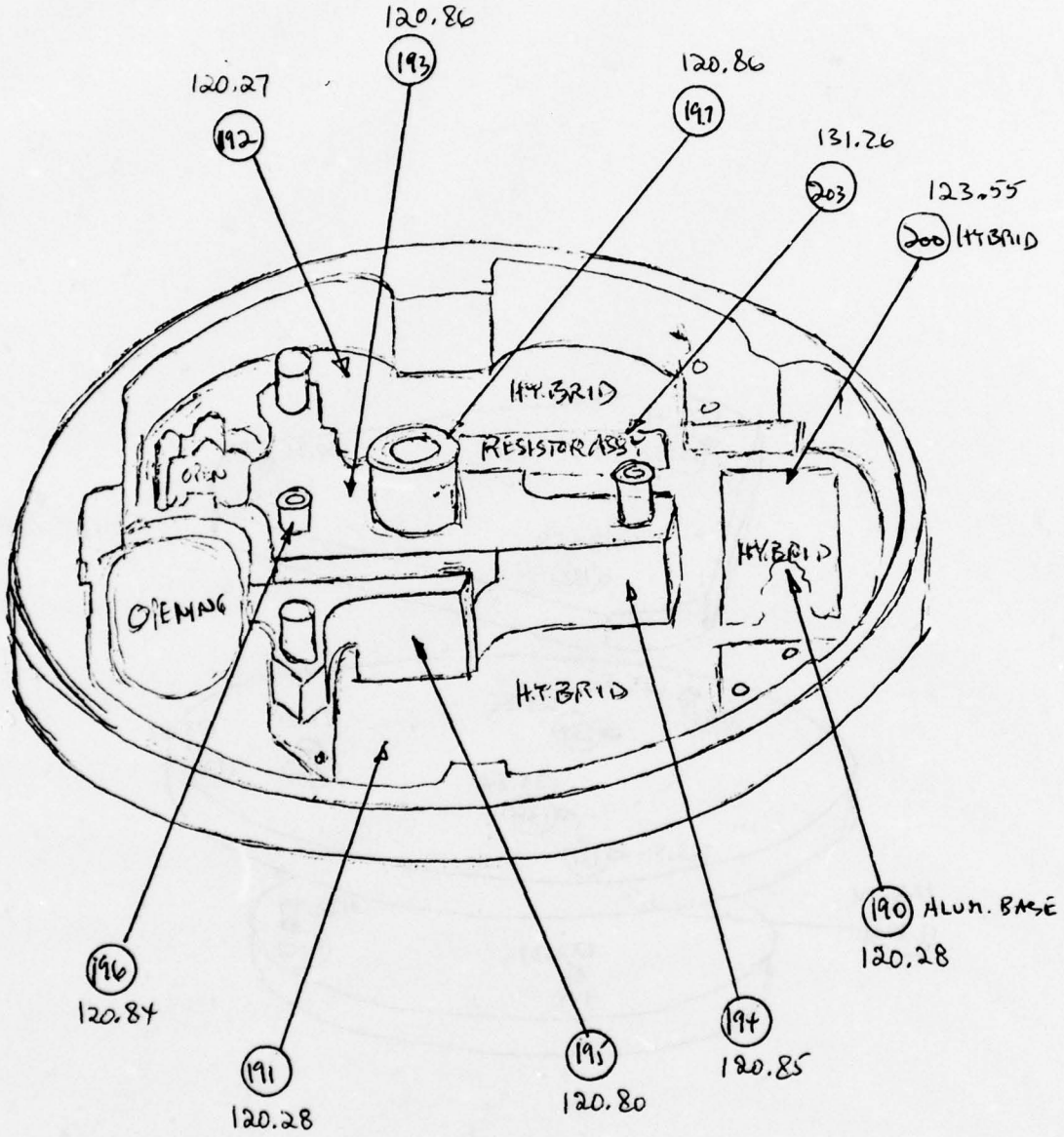

Figure 27. Base Temperature Distribution in ^{o}F after 0.86 Hours of Operation

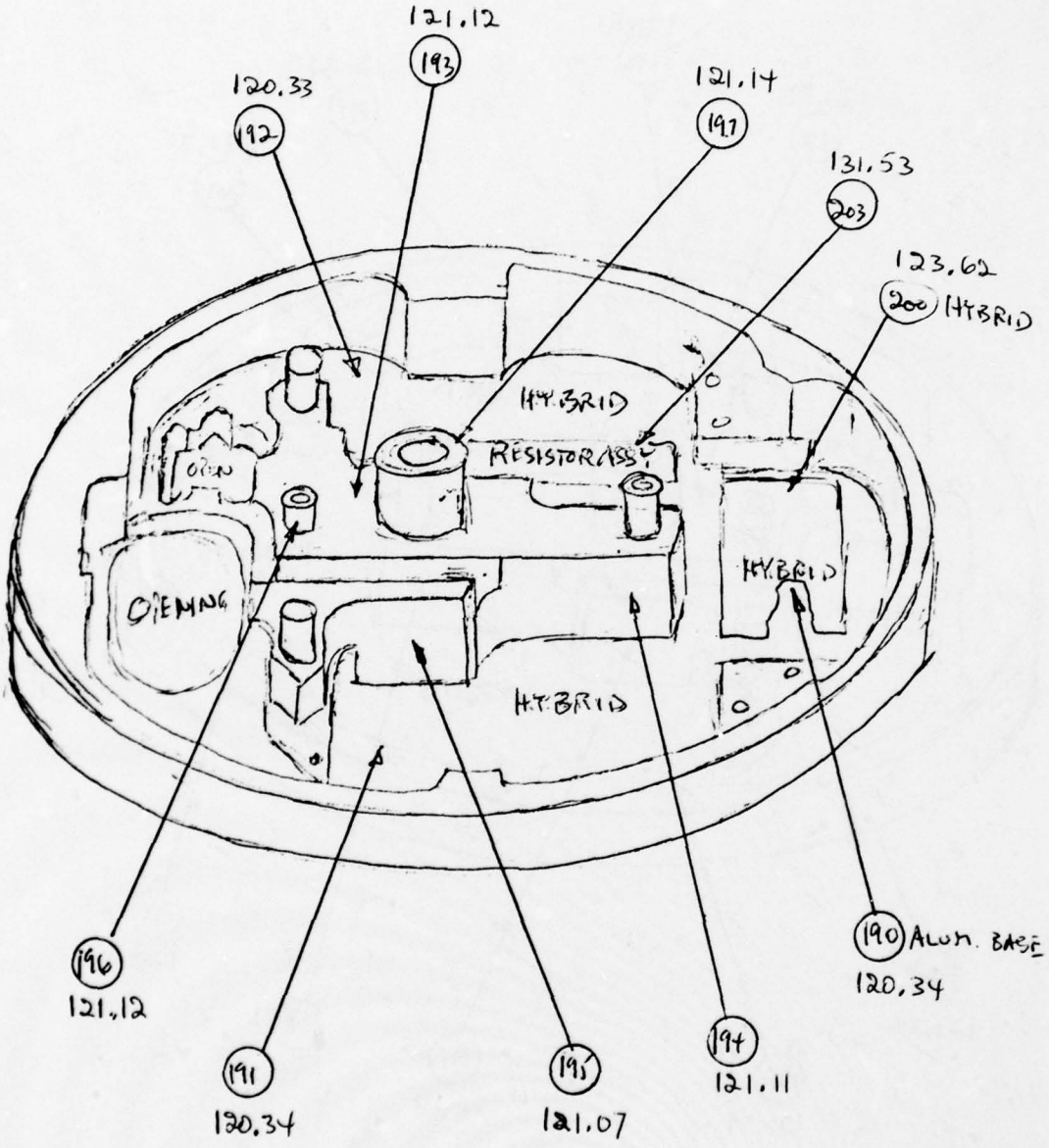

Figure 28. Base Temperature Distribution in ^{O}F after 1.5 Hours of Operation

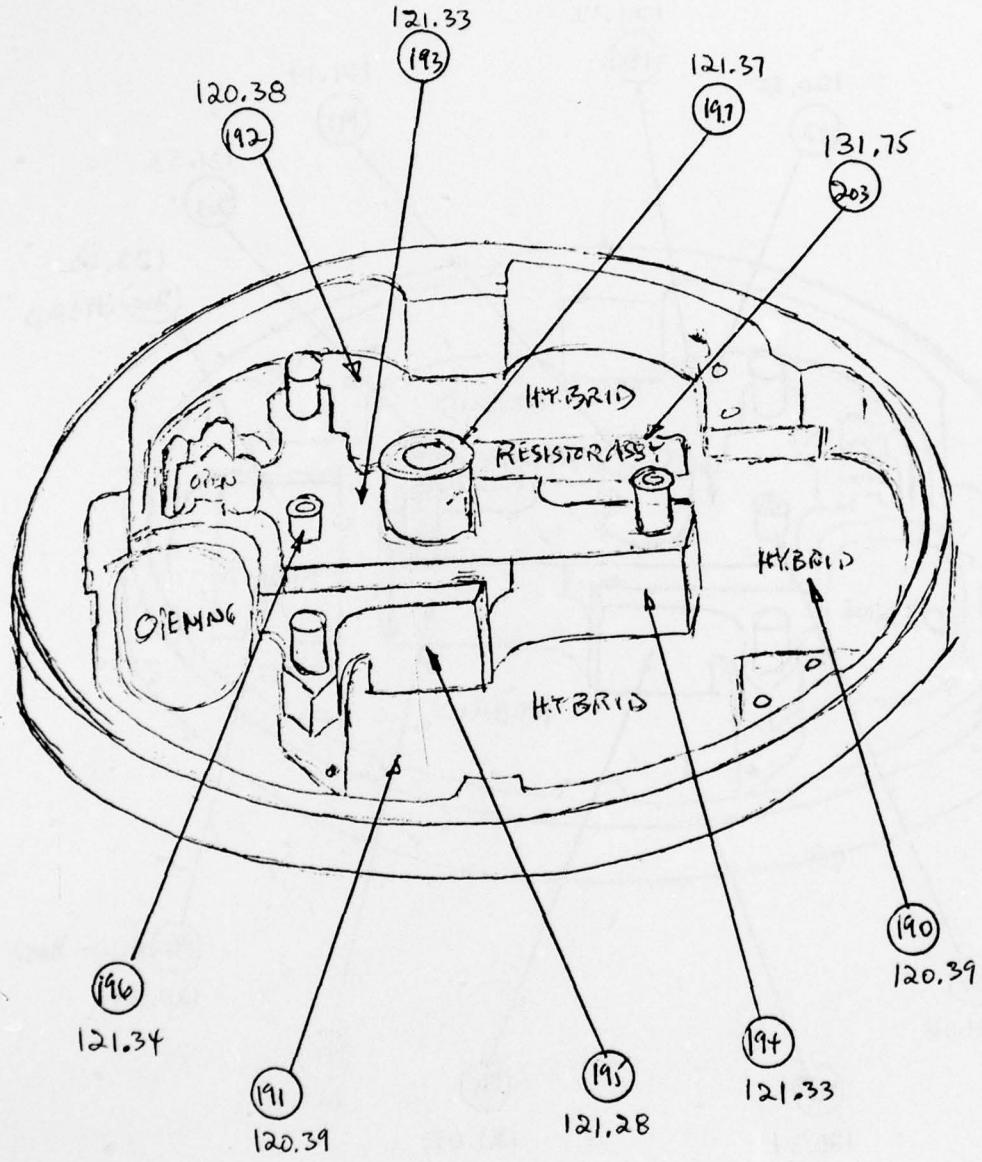

Figure 29. Base Temperature Distribution in ^{o}F after 2.78 Hours of Operation

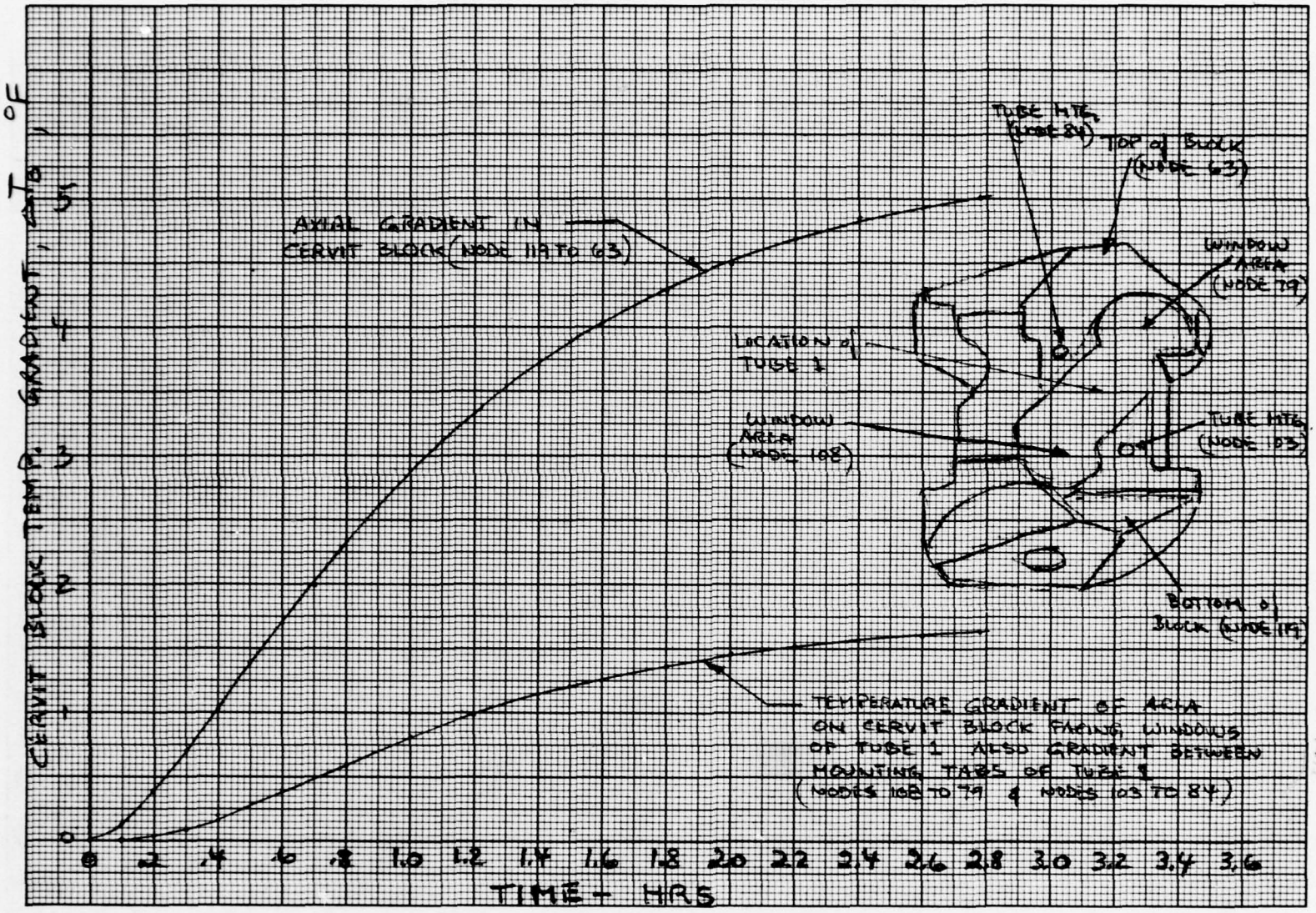

Figure 30. Temperature Gradients in Cervit Block

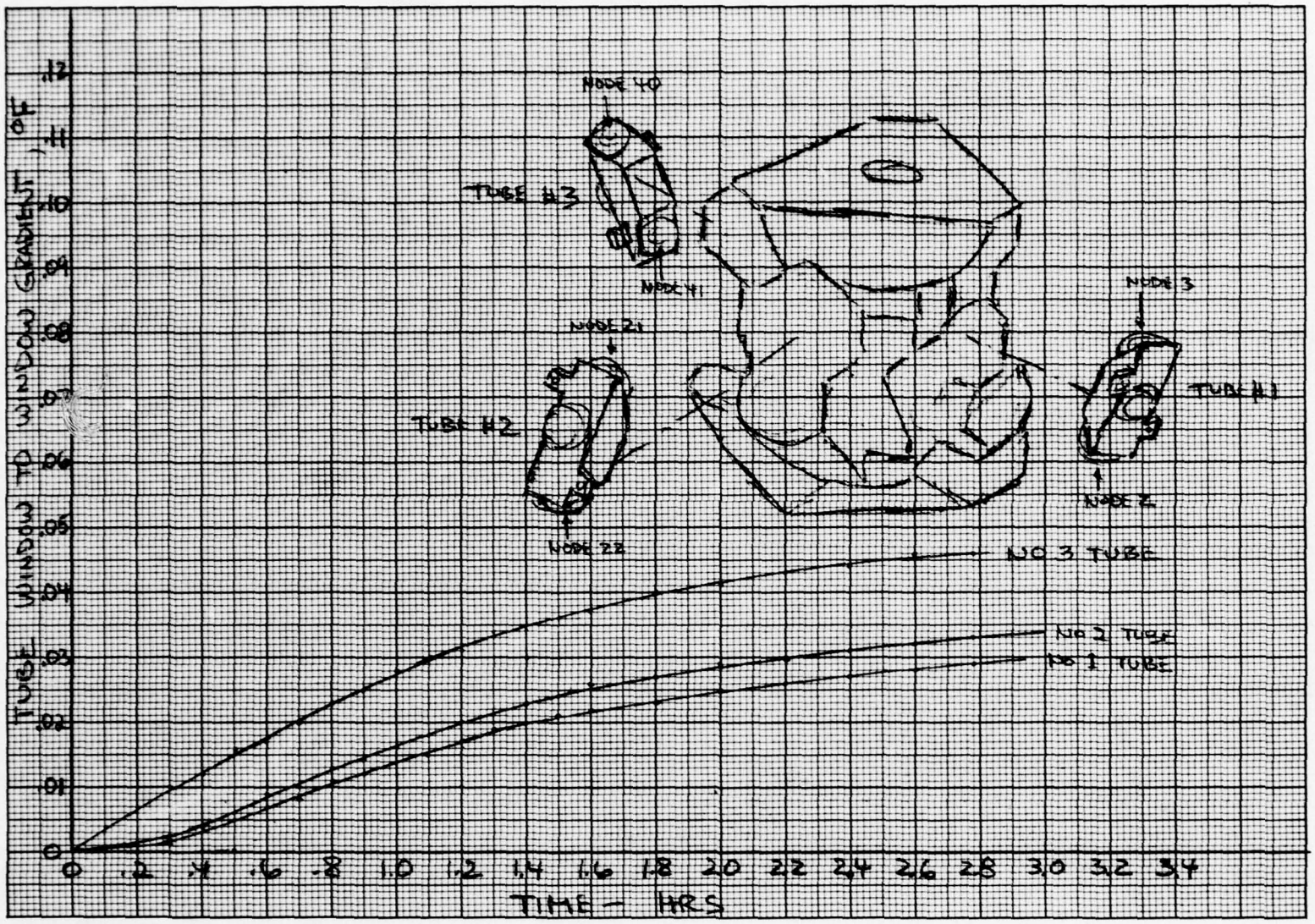

Figure 31. Tube Window Temperature Gradients

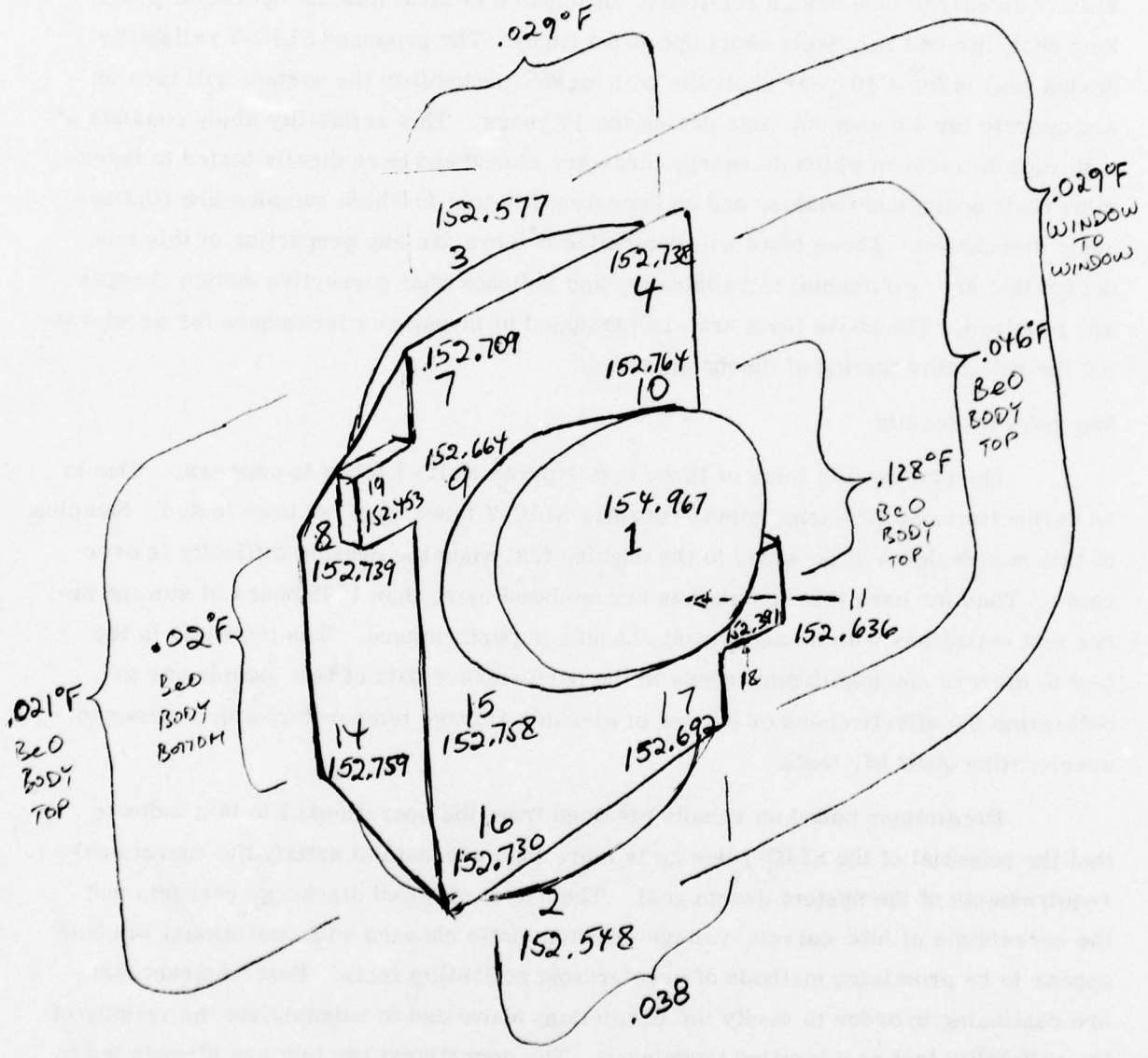

Figure 32. Steady-State Temperature Gradients in Various Parts of Tube No. 1

SLIC-7 DISCHARGE TUBE RELIABILITY INVESTIGATION

Test Objective

The primary objective of this investigation is to assess the reliability of the SLIC-7 discharge tube design relative to anticipated tactical missile operation (i.e., long shelf life and relatively short operating time). The proposed SLIC-7 reliability design goal is for a 10-year shelf life with an 85% probability the system will turn on and operate for 4 hours any time during the 10 years. This reliability study consists of a storage life test in which discharge tubes are stored and periodically tested to determine their operational status, and an operating life test in which samples are continuously discharged. These tests will determine if there are any properties of this tube design that are detrimental to reliability, and indicate what corrective design changes are required. The above tests are also designed to investigate techniques for accelerating the reliability testing of discharge tubes.

Summary of Results

The storage life tests of three metal/pyrex SLIC-7 tubes is underway. Due to an unresolved seal problem, metal/ceramic SLIC-7 tubes have not been tested. Samples of this new design will be added to the ongoing test when the present difficulty is overcome. Thus far each test sample has accumulated more than 1500 hours of storage under test conditions with no significant changes in performance. It is too early in the test to discern any significant trends in the performance data of test samples or to determine the effectiveness of the use of elevated storage temperatures as a means of accelerating shelf life tests.

Predictions based on results obtained from the operational life test indicate that the potential of the SLIC-7 design is more than adequate to satisfy the operational requirements of the system design goal. The use of elevated discharge currents and the correlation of tube current-voltage characteristic changes with operational life both appear to be promising methods of accelerating reliability tests. Post-contract tests are continuing in order to verify the predictions above and to substantiate the validity of the reliability test acceleration techniques. The operational life test has already led to several design improvements in the SLIC-7 tube that enhance reliability.

Acceleration of Reliability Tests

The principle failure mechanisms that limit the useful life of helium-neon discharge tubes are:

- Gas contamination due to outgassing and/or leaks.
- Diffusion of helium out of the tube.
- Cathode failure due to sputtering.

The storage life of a discharge tube is dependent upon only the first two mechanisms, while the operating life depends upon all three. Since the helium diffusion rate and the contaminant outgassing rate increase with temperature, it should be possible to accelerate storage life testing by using elevated temperatures. It may be possible to accelerate operational life testing by discharging samples at higher than normal current levels. The life of a cathode is very sensitive to its discharge current density. In practice cathodes are designed to operate at current densities below 0.5 ma/cm^2; above this level cathode life degrades catastrophically. Two discharge current levels were used but the higher current did not exceed the 0.5 ma/cm^2 design limit. Experiments on cathode life suggest that there may be a correlation between changes observed in tube current-voltage characteristics and operational life. This correlation, if valid, would allow reliable cathode life predictions based on short term observations.

SLIC-7 Storage Life

The storage life test demonstrated reliability consistent with the SLIC-7 design goal as described above. It was originally planned to include samples of the new metal/ceramic SLIC-7 tube in this test program, but due to an unresolved seal problem in this design, only metal/pyrex SLIC-7 tubes have been tested to date. Two metal/pyrex tubes were stored in an enclosure that was temperature controlled to 64^{o} ± 1^{o}C in order to evaluate the use of elevated temperatures as a means of accelerating reliability testing. A third tube, stored at ambient room temperature, served as an experiment control. Measurements of test parameters were made periodically (typically at 1 to 4

week intervals) to determine their operational status. Prior to test parameter measurement, tubes stored at the elevated temperature were allowed to cool to room temperature. Each sample was then tested according to the following sequence:

- Electrical turn-on transient measurement.
- Current-voltage characteristic measurement.
- Lasing threshold measurement.

After the measurements on all samples to be tested were completed, these tubes were discharged at a total current of 1.5 ma to accumulate a total test cycle operating time of 4 hours. The tubes were then returned to their respective storage environments until the next scheduled measurement cycle.

The first parameter measured in the test sequence was the electrical turn-on transient. This measurement involves the monitoring of changes in the anode-cathode voltage of one tube discharge leg with time, when the tube is first turned on after storage and operated at a constant total current of 1.5 ma. Figure 33 describes the test circuit used for this measurement. The network contains sufficient ballast in each tube leg to insure discharge stability and to automatically idle the current down to approximately 1.5 ma when the tube starts. The total discharge current is measured by monitoring the voltage drop across a viewing resistor in the cathode leg. The anode-cathode voltage is measured by using a high impedance voltage divider and a differential voltmeter. The data is taken by igniting the laser tube and manually adjusting the power supply output voltage to maintain a constant 1.5 ma current level. While this is being done, the anode-cathode voltage is monitored as a function of time. This data is summarized in terms of the total percentage change in voltage observed and the duration time of the transient.

The current-voltage characteristic of the tube samples is also measured using the test circuit of figure 33. This test consisted of measuring the anode-cathode voltage of a discharge leg of each tube sample for total discharge currents of 0.750 ma, 1.000 ma and 1.500 ma.

The lasing threshold of samples was measured with the test arrangement of figure 34. This measurement involves the insertion of the tube sample in a linear laser cavity and adjusting the cavity mirrors to obtain the minimum threshold current at which

lasing just begins. The flat laser cavity mirror is dithered at 400 Hz by a piezo actuator to produce an ac optical signal. This signal is monitored by an infrared sensitive photo diode, whose output is amplified and displayed on an oscilloscope. This CRT display is used to detect the presence of lasing. The discharge tube current is measured in terms of a voltage drop across a viewing resistor in the cathode leg of the tube network. The minimum lasing threshold current for each tube sample was recorded.

The test results obtained are summarized in tables 1, 2, and 3 and figures 35, 36, and 37 contain plots of test parameters versus storage time for all the samples. Each sample has accumulated over 1,500 hours of storage time under test conditions. There is no indication of degradation in any test sample and there are no significant differences between tubes stored at room temperature and 64^{o}C. The initial data points are noisy because refinements in test set-ups and procedures were required (refer to footnotes in tables 1, 2, and 3).

Additional testing is required to determine if there are any significant trends in the data, and to evaluate the use of elevated storage temperatures as a means to accelerate shelf life testing.

TABLE 1. SHELF LIFE TEST DATA LOG: SAMPLE 1

SHELF LIFE TEST
SAMPLE. NO. 1 LOG

	DATE	TEST NO.		TURN-ON TRANS. % CHANGE	DURATION		ANODE/CATHODE VOLTAGE @0.75 mA	@1.00 mA	@1.25 mA		LASING THRESH.		OPERATING TIME Δ	TOTAL		STORAGE Δ	TIME TOTAL	STORAGE TEMP.
	9/8/77	0	**	-0.11%	25 min	**	334.8	300.0	288.2	*	.636 mA		1.1 HR	1.1 HR		—	0	25°C
	9/13	1	**	-0.07%	30	**	334.5	299.4	287.3	*	.692		1.6	2.7		112.8	112.8	25°C
	9/20	2	**	-0.13%	30	**	332.0	300.1	287.9		.651		4.3	7.0		91.3	204.1	25°C
	9/27	3		-0.08%	35		326.9	296.7	284.5		.671		5.1	12.1		137.6	341.7	63°C
	10/11	4		-0.08%	30		329.4	296.5	284.8		.637		5.3	17.4		303.8	645.5	64°C
	10/26	5		-0.08%	25		328.5	295.7	283.5		.633		3.3	20.7		328.4	973.9	64°C
	11/21	6		-0.06%	25		326.6	295.8	284.0		.621		3.9	24.6		594.6	1568.5	64°C

* CAVITY MAY NOT HAVE BEEN PROPERLY ALIGNED
** TEST CKT IMPROVED, "NOISY" RESISTOR REPLACED

TABLE 2. SHELF LIFE TEST DATA LOG: SAMPLE 2

SHELF LIFE TEST
SAMPLE. NO. 2 LOG

DATE	TEST NO.		TURN-ON TRIM % CHANGE	DURATION		ANODE/CATHODE VOLTAGE @ 250 μA	@ 1 mA	VOLTAGE @ 5 mA		LASING THRESH	OPERATING TIME Δ	TOTAL	STORAGE Δ	TIME TOTAL	STORAGE TEMP.
9/8/71	0	**	-0.35%	40 min	**	365.4	340.7	331.8	*	.810 mA	1.3 HRS	1.3 HRS	—	0	25°C
9/13	1	**	-0.09%	40	**	364.1	339.5	331.1	*	.756	1.3	2.6	114.9	114.9	25°C
9/20	2	**	+0.25%	40	**	364.0	340.0	331.5		.769	4.2	6.8	94.9	209.8	25°C
9/27	3		+0.27%	45		367.9	336.0	327.7		.752	5.2	12.0	137.6	347.4	25°C
10/11	4		+0.3%	45		359.4	336.3	327.9		.760	5.2	17.2	303.8	651.2	25°C
10/26	5		+0.42%	35		359.1	336.4	328.0		.762	3.2	20.4	328.4	979.6	25°C
10/21	6		+0.27%	40		358.0	336.6	328.2		.753	3.9	24.3	594.6	1574.2	25°C

* CAVITY MAY NOT HAVE BEEN PROPERLY ALIGNED
** TEST CKT IMPROVED, "NOISY" RESISTOR REPLACED

TABLE 3. SHELF LIFE TEST DATA LOG: SAMPLE 3

SHELF LIFE TEST
SAMPLE. NO. 3 LOG

DATE	TEST NO.		TURN-ON % CHANGE	TRANS DURATION		ANODE @0.75	CATHODE @1.00	VOLTAGE @1.50		LASING THRESH.	OPERATING TIME Δ	OPERATING TIME TOTAL		STORAGE TIME Δ	STORAGE TIME TOTAL	STORAGE TEMP
9/8/77	0	**	-0.02%	3 min	**	370.0	340.0	331.8	*	.775 mA	1.2 HRS	1.2 HRS		—	0	25°C
9/13	1	**	-0.3%	35	**	368.3	339.5	331.3	*	.709	1.5	2.7		118.5	118.5	25°C
9/20	2	**	N/A	N/A	**	368.6	340.2	331.9		.713	4.1	6.8		96.9	215.4	25°C
9/27	3		-0.39%	35		367.9	336.2	328.0		.691	4.8	11.6		137.6	353.0	63°C
10/11	4		-0.35%	35		364.9	336.5	328.2		.711	5.2	16.8		303.8	656.8	64°C
10/26	5		-0.29%	35		364.2	336.8	328.6		.688	3.4	20.2		328.4	985.2	64°C
11/21	6		-0.47%	40		365.2	337.2	328.8		.687	3.8	24.0		594.6	1579.8	64°C

* CAVITY MAY NOT HAVE BEEN PROPERLY ALLIGNED
** TEST CKT IMPROVED, "NOISY" RESISTOR REPLACED

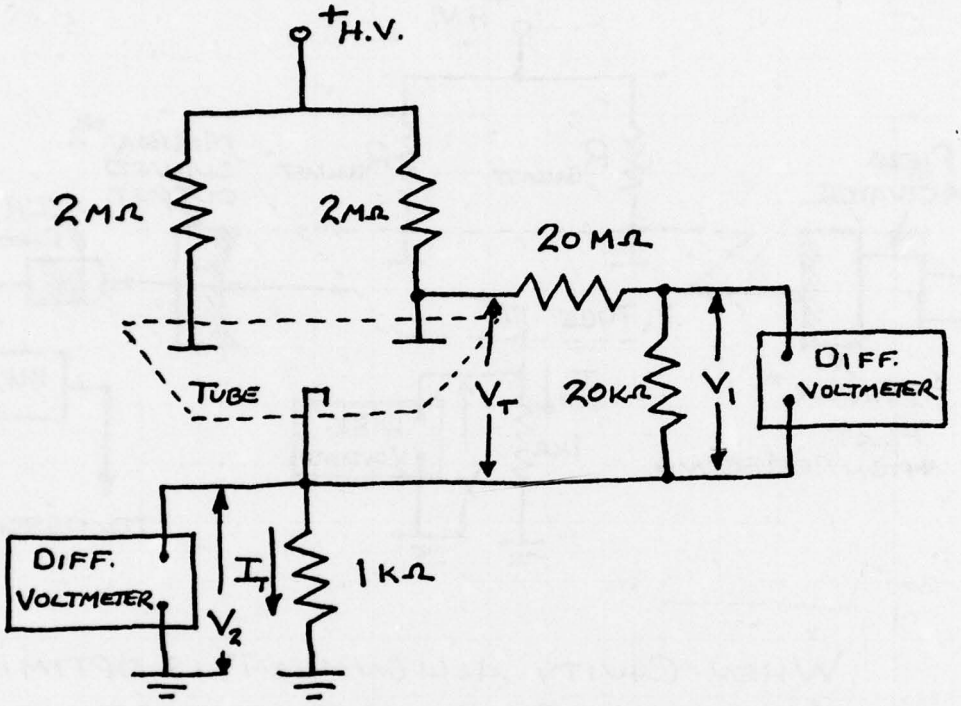

ANODE - CATHODE VOLTAGE; $V_T = \frac{20M\Omega + 20K\Omega}{20K\Omega} V_1$

OR $V_T = 1001\, V_1$

TOTAL TUBE CURRENT $I_T = \frac{V_2}{1K\Omega}$

Figure 33. Turn-on Transient and I-V Characteristic Test Circuit

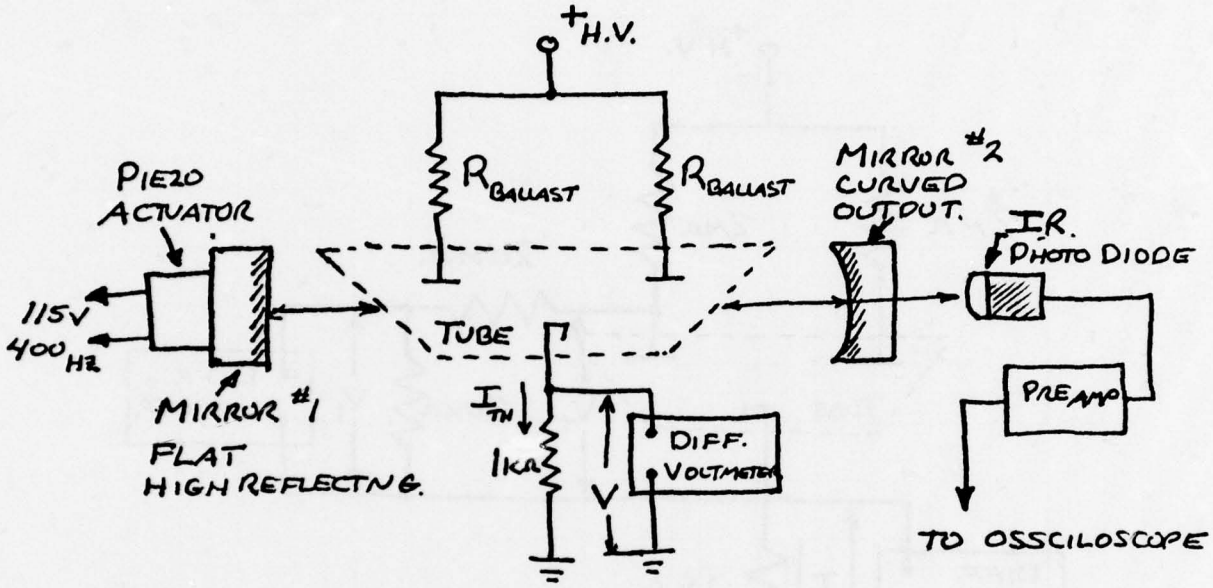

WHEN CAVITY ALLIGNMENT IS OPTIMIZED AND LASING IS ON THE VERGE OF STARTING, THE LASING THRESHOLD CURRENT IS:

$$I_{TH} = V/1K\Omega$$

Figure 34. Lasing Threshold Current Measurement Test Set-up

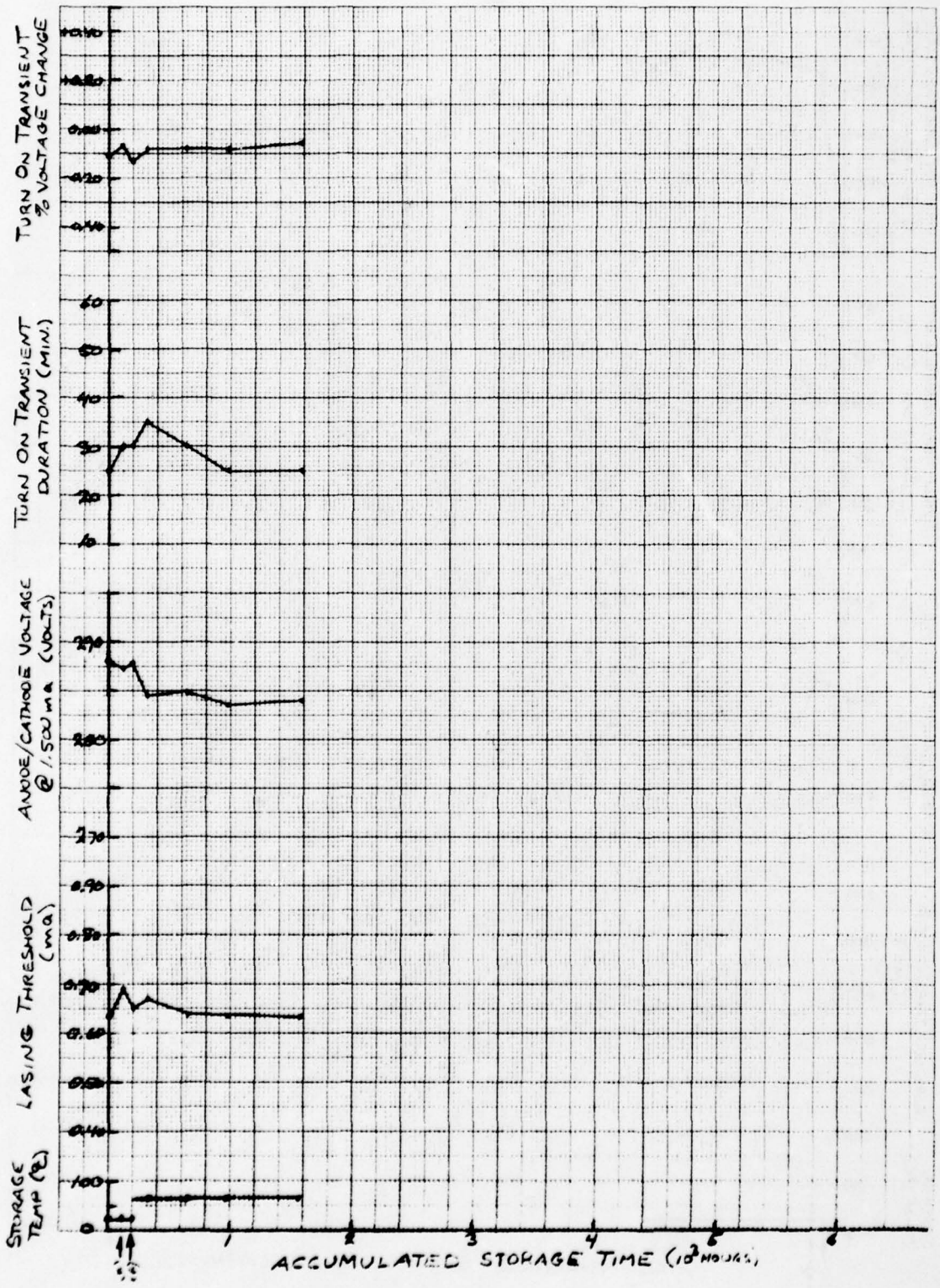

Figure 35. Shelf Life Test Data: Sample 1

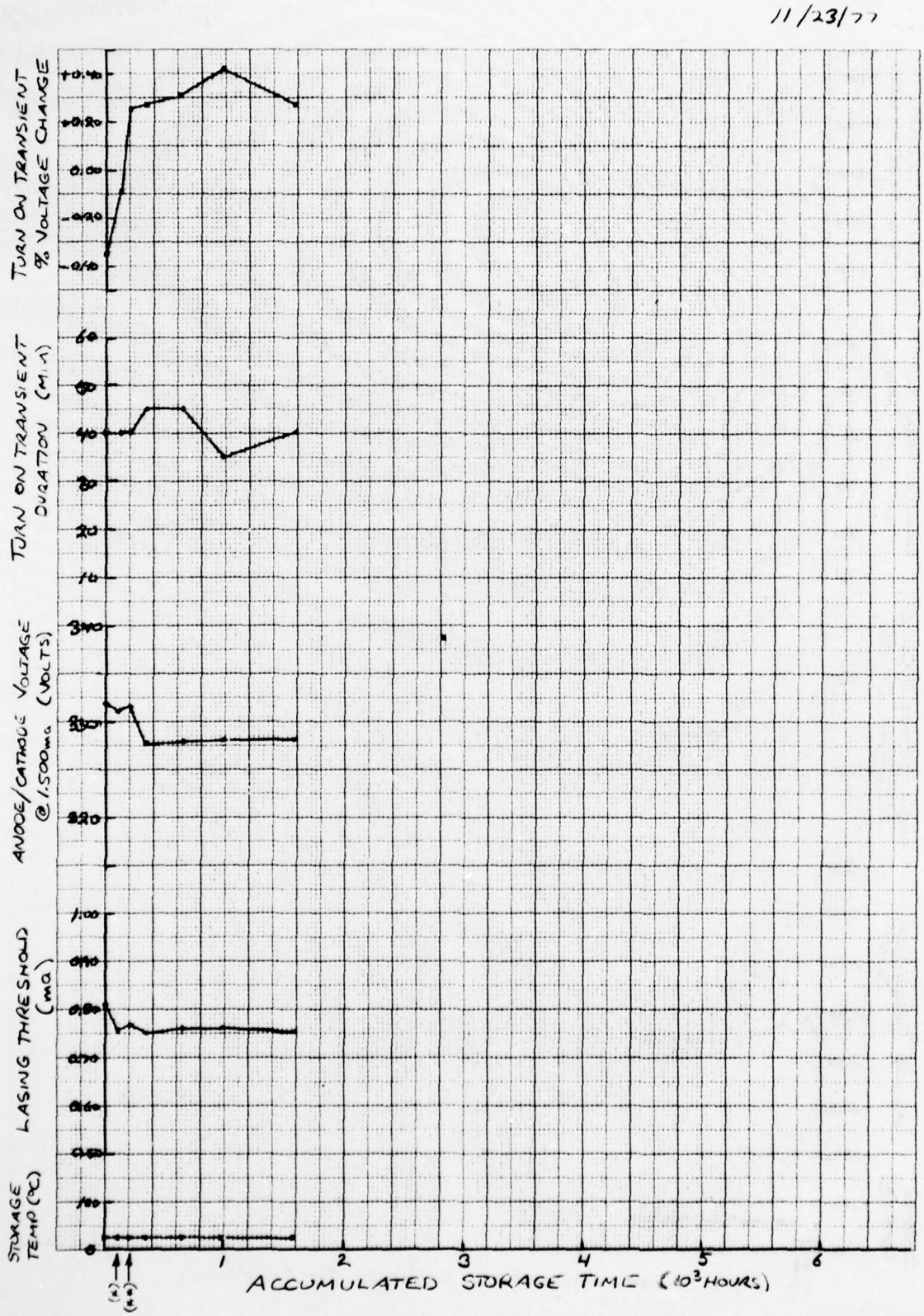

Figure 36. Shelf Life Test Data: Sample 2

11/23/77

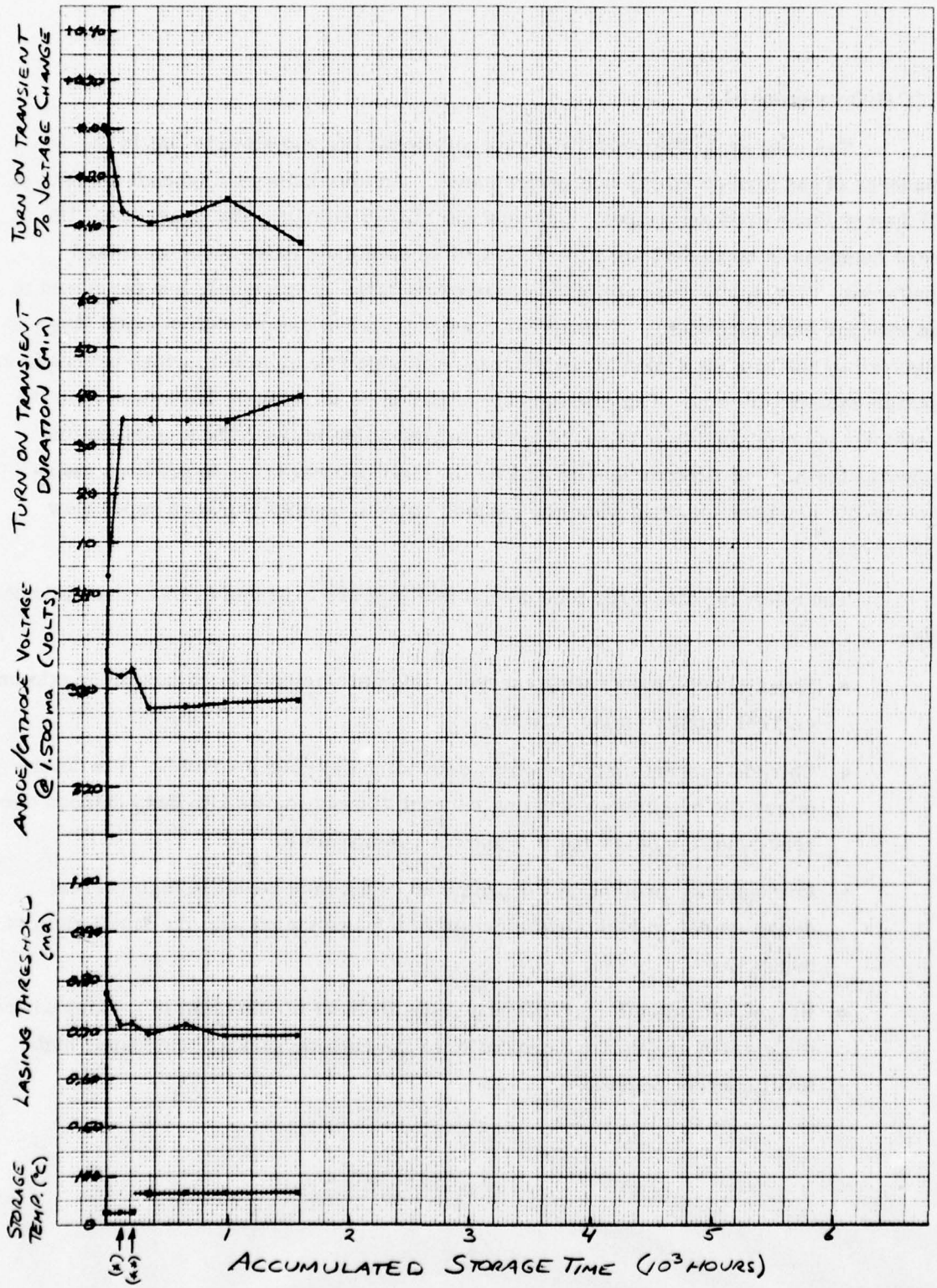

Figure 37. Shelf Life Test Data: Sample 3

SLIC-7 Operational Life

The essential difference between operational life and storage life is the dependence of the former on cathode performance. An aluminum cold cathode is used in all Sperry laser discharge tubes, including the SLIC-7 design. The operational life of these cathodes is dependent upon the ability of an aluminum oxide layer to retard sputtering. The sputtering rate of this hard oxide layer is extremely low compared to the rate for bare aluminum. Cathode failure occurs when the protective oxide layer is ruptured by the eroding action of the plasma, exposing raw aluminum which proceeds to sputter catastrophically. The erosion rate of the oxide is strongly dependent upon the discharge current density it is subjected to and the point on the cathode surface that supports the highest current density will be the first point to fail. In practice satisfactory life has been obtained when the cathode current density has been kept below $0.5\ ma/cm^2$.

The following discharge tube design features are expected to influence cathode life:

- Nominal design operating current: this parameter determines the maximum current density on the cathode.
- Cathode current distribution as determined by tube geometry: this determines the maximum operating current allowed in order to keep cathode current densities below the $0.5\ ma/cm^2$ design limit.
- Cathode edge protection: unprotected edges may result in high current densities due to high local electric fields associated with the small radii of edges.
- Hollow cathode effects: potential enhancement of emission in regions where dielectrics are in close proximity to the cathode surface may cause high local current densitites.

- Gas fill pressure: this parameter may influence the distribution of current on the cathode surface and/or erosive ability of the plasma since it determines the mean free paths of ions.
- Cathode preprocessing: this influences the "quality" of the protective oxide layer.

The relative importance and optimization of the above design features relative to cathode life were studied by means of three types of experiments:

- Cathode operating life tests.
- Segmented cathode measurements.
- Scanning electron microscope studies of cathode surfaces.

These experimental programs and their results are described in detail below.

Cathode Operation Life Test

In this experiment economical test bulbs (see figure 38) that accurately simulate the SLIC-7 cathode configuration were tested. All test bulbs were continuously operated at their prescribed life test currents, except for brief off-on cycles when measurements were made. The current-voltage characteristic (i.e., the anode-cathode voltages for 0.500 ma, 1.000 ma and 1.500 ma) for each sample were monitored and plotted as a function of accumulated operating time in order to assess their progress. The failure of a cathode is indicated by a sudden increase in measured voltages and by the appearance of a sputtered aluminum film on the inside of the test bulb. Figure 39 contains a schematic of the cathode life test arrangement. A high impedance voltage divider and differential voltmeter combination is used to measure anode/cathode voltages and the voltage drop across a viewing resistor is used to determine the discharge current.

A summary of life test sample descriptions and of current sample status is contained in table 4. Samples 1, 2, 8 and 9 are representative of the original SLIC-7 configuration; samples 3, 4, and 10 are of the same configuration as above but with a higher pressure gas fill; samples 5, 6, and 7 probed modifications of the above configuration. Test samples of the original SLIC-7 configuration operated at 1.0 ma, 1.5 ma

and 2.5 ma have respectively maximum local current densities less than, equal to (approximately), and greater than the 0.5 ma/cm^2 design limit (refer to Segmented Cathode Experiments). Figure 40 contains plots of life test data of selected samples. The test results obtained to date indicate the following:

- The reduction of the nominal test current from 2.5 ma to 1.5 ma can increase operational life by as much as a factor of 10 (refer to samples 1 and 2). A further reduction of current to 1.0 ma yields a significant additional increase in life.
- The use of a higher pressure gas fill can enhance operational life at 2.5 ma by as much as a factor of three (refer to samples 1 and 3).
- Test samples 1, 5, 6 and 7 demonstrate poor correlation of life with
  - Bottom edge protection
  - Hollow cathode effects
  - Available cathode area

  Refer to figure 41 for correlation plots.
- Test sample 7 demonstrated a life two times longer than any other test sample with a standard gas fill operated at 2.5 ma. The performance of this sample is due to a geometry change in the cathode protective end cap that has resulted in an improved current distribution on the cathode (this is further substantiated in the segmented cathode experiment section). This improved end cap geometry has been incorporated in the latest SLIC-7 tube design.

The above results can be used to project the life expected from the SLIC-7 cathode configuration with improved end cap design and higher pressure gas fill as follows:

- SLIC-7 configuration with improved end cap, standard gas fill operating at 2.5 ma (test sample 7) - life ~500 hrs.
- Reduction of current to 1.5 ma yields factor of 10 improvement - life ~5000 hrs.
- Use of higher pressure gas fill yields factor of 3 improvement - life ~15,000 hrs.

If the operating current is reduced further to 1.0 ma, tube life should be significantly longer than the 15,000 hours projected above. This projected life is more than adequate to satisfy the intended operational life design goal since the tube can be operated 4 hours a day for 10 years without exceeding 15,000 hours.

The use of elevated test currents appears to be a valid technique to accelerate operational life tests. Data from an accelerated life test was used to make the above life prediction. Additional data is required to fully establish the validity of this method and to provide the information required to project accelerated test results to the entire range of practical discharge tube excitation levels.

Another observation that may lead to a practical method of accelerating life tests involves the initial changes in the current-voltage characteristic of a sample as it is operated for the first time. A re-examination of the life test data of figure 40 will indicate that most samples demonstrate an initial drop in anode/cathode voltage before stabilizing or failing as the case may be. The correlation between this voltage change and life is very good (refer to figure 42); the steeper the slop of the initial voltage drop the shorter the observed life. More testing is required to substantiate this correlation and to determine why a few of the samples tested had voltage increases instead of decreases.

Future life test samples are planned in a post-contract effort to verify the accuracy of the life prediction made above using accelerated test results and also to investigate the effect of perturbations to the present cathode conversion schedule on operational life. Cathode pre-processing has not as yet been systematically studied in the life test program, although it is being studied in a post-contract scanning electron microscope study of cathode surfaces. This additional effort may produce additional life enhancement in this area.

Segmented Cathode Experiments

The samples used in this study were bulbs similar to the ones used in the above test except that the cathode consists of several electrically isolated segments. Figure 43 contains a schematic of a typical segmented cathode experiment. The current distribution for each cathode configuration is determined by measuring the current drawn by each segment and calculating an average current density.

A tabulation of all the configurations tested and their relationships to life test samples of the previous experiment is contained in table 5. The significant results of these experiments are summarized in the three sets of current distribution plots of figures 44, 45, and 46.

Figure 44 contains the data from test 1 which indicates that the current peaks sharply near the center of the cathode while the end farthest from the anode supports very little of the discharge. At 2.5 ma total current, three of the cathode segments have average current densities greater than the 0.5 ma/cm^2 design limit. At 1.5 ma one segment exceeds this limit and at 1.0 ma all segments are below this limit. The region of the cathode farthest from the anode is suspected as being the principle site of hollow cathode effects. Since the segment in this region supports very little of the discharge, it appears that hollow cathode effects are not important in determining SLIC-7 tube operational life.

Figure 45 contains data from tests in which the only difference in configuration was the gas fill pressure. The results indicate that the cathode current distribution is not significantly altered by pressure changes of the same magnitude as used in the life test experiment to enhance cathode life. This implies that the observed life enhancement is not due to improved current distribution but that the ions in a higher pressure fill, with shorter mean free paths, are less effective in eroding the protective cathode oxide layer.

Figure 46 contains data from tests in which different cathode edge protection end cap geometries were studied. The results indicate that changes in end cap design can significantly reduce peaking in the current distribution and improve the utilization of the cathode end farthest from the anode. Test 1 is the same configuration as cathode life test sample 1 and test 4 is similar to the configuration of life test sample 7. The geometries of tests 6 and 9 are not practical for the SLIC-7 tube design because they do not provide adequate space for a getter. The distribution plot obtained in test 4 for 1.5 ma total current is included in this figure to indicate that all segments had an average current density below the 0.5 ma/cm^2 design limit which is an improvement over the configuration of test 1 (refer to figure 44). The configuration of test 4 is representative of the present SLIC-7 cathode design.

Scanning Electron Microscope Study of Cathode Surfaces

In this program samples of SLIC-7 and SLG-15 cathodes were studied using a scanning electron microscope. The objective of the study is to observe and measure cathode oxide layers, and to determine a pre-processing schedule that will make the oxide coating on the SLIC-7 design equivalent to the one on the long life SLG-15 cathode. Preliminary observations of SLIC-7 cathodes that have failed reveal a very rough textured surface and a surface layer that was originally interpreted as an oxide layer, but is now believed to be a deposited aluminum film due to sputtering. At the present time, a post-contract study is underway in which SLIC-7 cathode samples that have only been preprocessed are to be examined. A listing of these samples is included in table 6. The samples are designed to probe the influence of each pre-processing step and perturbations to the standard process schedule on the cathode oxide coating. A standard pre-processed SLG-15 cathode is included to serve as a reference. Thus far efforts to observe oxide layers on these samples have been unsuccessful. Work is continuing in this area. Other surface analysis techniques are being investigated as methods of measuring cathode oxide coatings such as Auger electron spectroscopy and secondary ion mass spectroscopy.

TABLE 4. CATHODE LIFE TEST SAMPLE SUMMARY

TEST BULB	CATHODE TYPE	CONVERSION SCHED	CONVERSION CONFIG.	CATHODE AREA AVAIL.	CATHODE AREA EFFECT.*	EDGE PROTECTION BOTTOM	EDGE PROTECTION TOP	HOLLOW CATHODE EFFECT BOTTOM	HOLLOW CATHODE EFFECT TOP	GAS PRESSURE	TEST CURRENT	TEST STATUS	OPERATING LIFE (HOURS) AS OF 1/3/75
1	STD CYLINDER	STD.	STD	.116 in²	.075 in²	NONE	.032 in	NONE	YES	STD	2.45 mA	FAILED	230
2	"	"	"	.116 in²	.075 in²	NONE	.032 in	NONE	YES	"	1.52 mA	FAILED	2315
3	"	"	"	.116 in²	.075 in²	NONE	.032 in	NONE	YES	HIGH	2.43 mA	FAILED	47
4	"	"	"	.116 in²	.075 in²	NONE	.032 in	NONE	YES	HIGH	1.50 mA	OPERATING	(5353)
5	"	"	MOD #1	.104 in²	.101 in²	.032 in	.032 in	NONE	NONE	STD	2.44 mA	FAILED	136
6	"	"	"	.093 in²	.061 in²	.063 in	.032 in	YES	YES	"	2.45 mA	FAILED	139
7	"	"	"	.093 in²	.050 in²	.063 in	.032 in	NONE	SOME	"	2.44 mA	FAILED	517
8	"	"	"	.116 in²	.075 in²	NONE	.032 in	NONE	YES	"	1.65 mA	OPERATING	(4771)
9	"	"	"	.116 in²	.075 in²	NONE	.032 in	NONE	YES	STD	0.99 mA	OPERATING	(791)
10	"	"	"	.116 in²	.075 in²	NONE	.032 in	NONE	YES	HIGH	1.00 mA	OPERATING	(791)

* EFFECTIVE CATHODE AREA: BASED ON MEASUREMENTS MADE ON SPUTTERED CATHODES. ASSUME THAT AREA WILL BE THE SAME FOR ALL SAMPLES OF A GIVEN TEST CONFIGURATION.

TABLE 5. SEGMENTED CATHODE TESTS

DATE	TEST #	CATH. TYPE	EDGE TOP	PROTECT. BOTTOM	END CAP	GAS PRESS.	LIFE TEST COUNTER PART
7/12/77	1	CYLINDER	.032	NONE	TRUNCATED CONE	STD	SAMPLES #1, #2 + #8
"	2	"	"	"	"	HIGH	SAMPLES #3 + #4
"	3	"	"	"	"	LOW	NONE
7/13/77	4	"	"	"	SECTIONED TRUNCATED CONE	STD	SAMPLE #7 (APPROX.)
7/14/77	5	"	"	"	"	HIGH*	NONE
7/15/77	6	"	"	"	FLAT	STD	SAMPLE #5 (APPROX.)
"	7	"	"	"	"	HIGH	NONE
"	8	"	"	"	"	HIGH*	NONE
8/4/77	9	"	"	"	FLAT WITH CYLINDER	STD	NONE

*DIFFERENT He/Ne RATIO

TABLE 6. CATHOD PREPROCESSING VS OXIDE LAYER, TEST SAMPLE DESCRIPTIONS

SAMPLE		SURFACE PREP		PREPROCESSING		SCHED.
No.	TYPE	SAND-BLAST	ETCH	GAS	CURRENT	TIME
1	MINI	✓	NO	—	NONE	—
2	MINI	✓	✓	—	NONE	—
3	MINI	✓	✓	AIR	STD	STD
4	MINI	✓	✓	AIR	<STD	STD
5	MINI	✓	✓	AIR	>STD	STD
6	MINI	✓	✓	AIR	STD	<STD
7	MINI	✓	✓	AIR	STD	>STD
8	MINI	✓	✓	O_2	<STD	STD
9	STD.	✓	✓	AIR	STD	STD

SCHEMATIC: AREAS TO BE INSPECTED ON EACH CATHODE SAMPLE

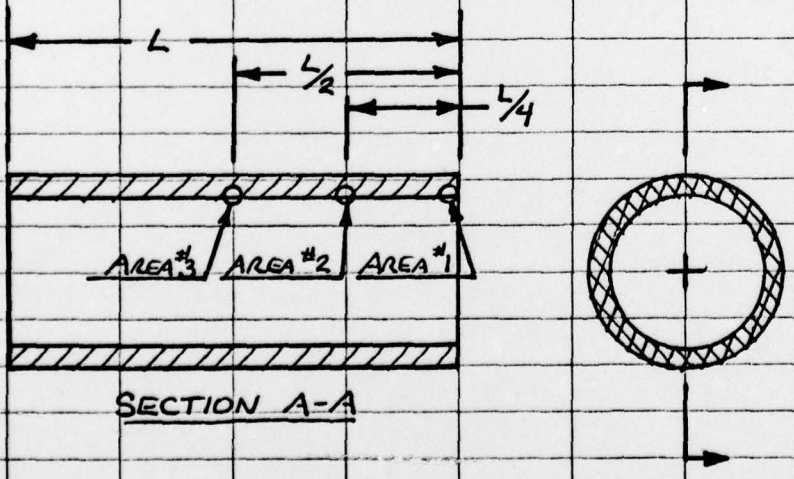

SECTION A-A

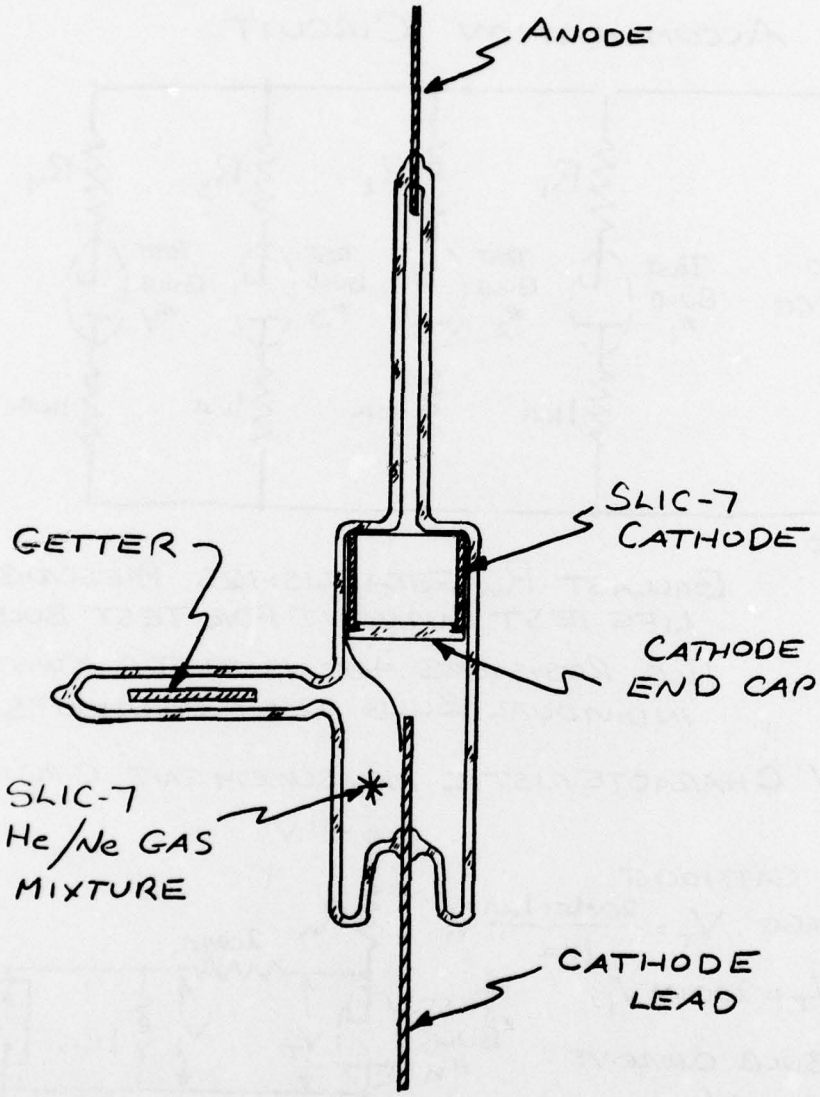

Figure 38. Cathode Life Test Bulb

A. LIFE ACCUMULATION CIRCUIT.

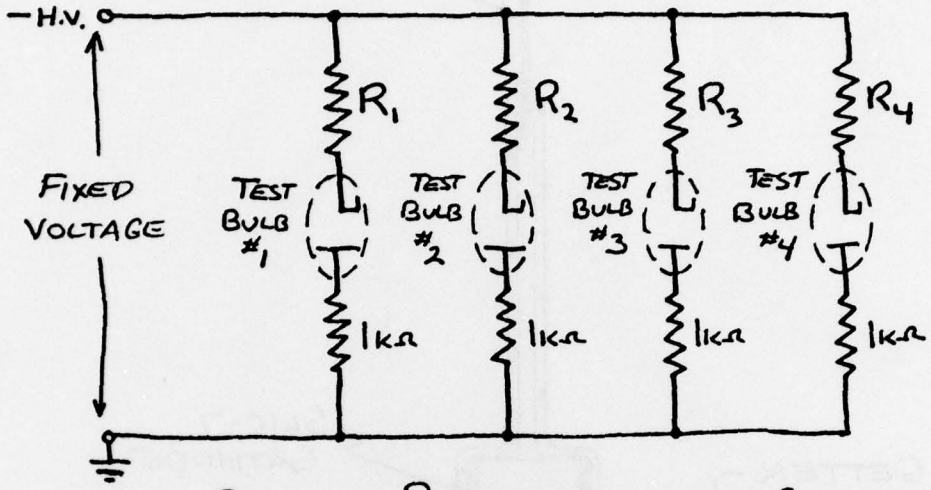

BALLAST R_n ESTABLISHES PRESCRIBED LIFE TEST CURRENT FOR TEST BULB #n

1KΩ RESISTORS ARE USED FOR MONITORING INDIVIDUAL BULB TEST CURRENTS.

B. I-V CHARACTERISTIC MEASUREMENT CIRCUIT.

ANODE CATHODE VOLTAGE $V_T = \frac{20M\Omega + 1K\Omega}{1K\Omega} V_1$

OR $V_T = 2000 V_1$

TEST BULB CURRENT $I_T = \frac{V_2}{1K\Omega}$

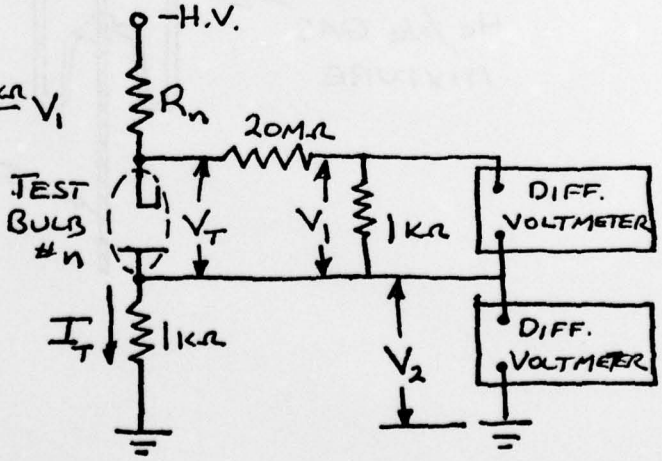

Figure 39. Operational Life Test Circuit

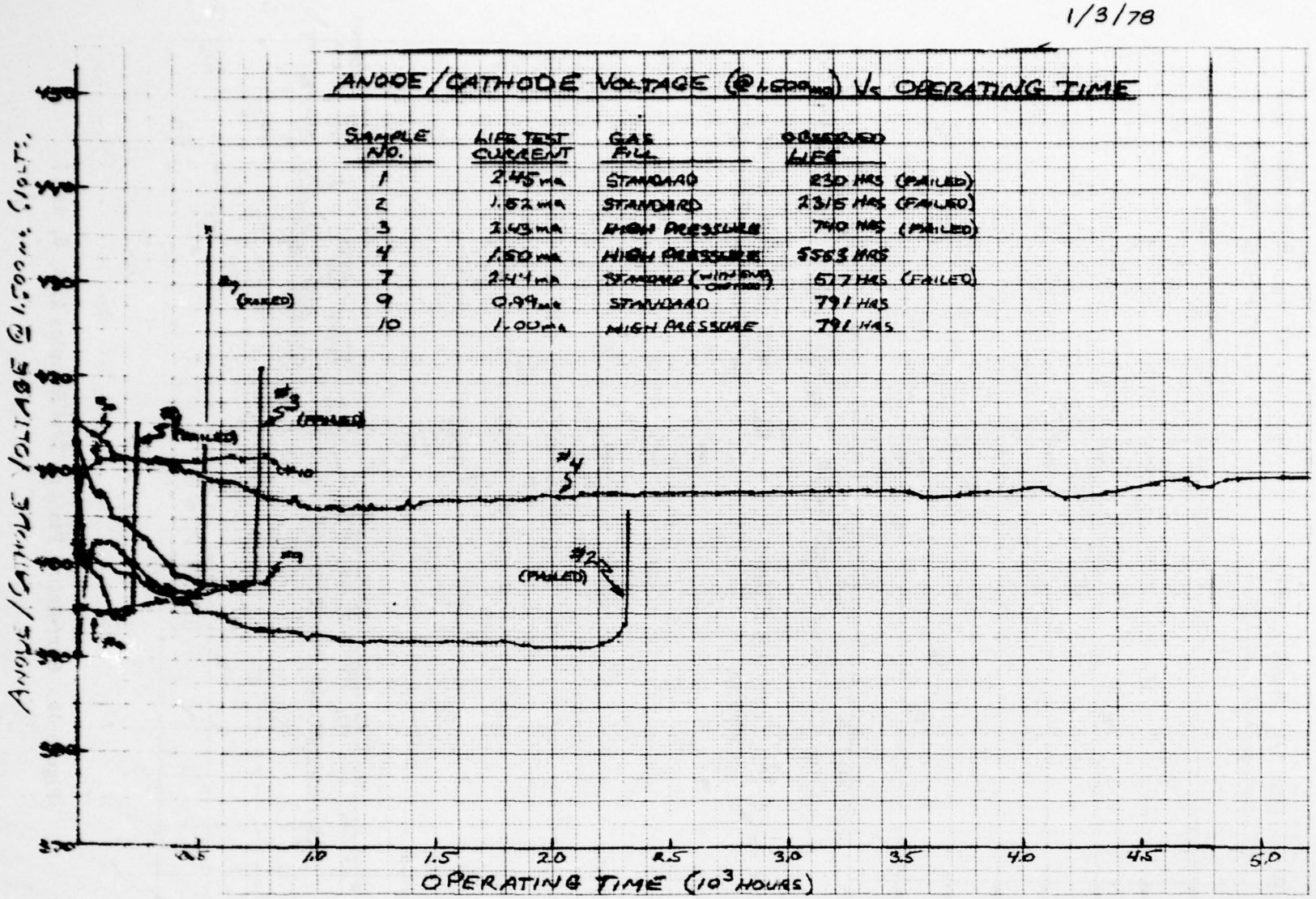

Figure 40. Cathode Life Test Sample Plots

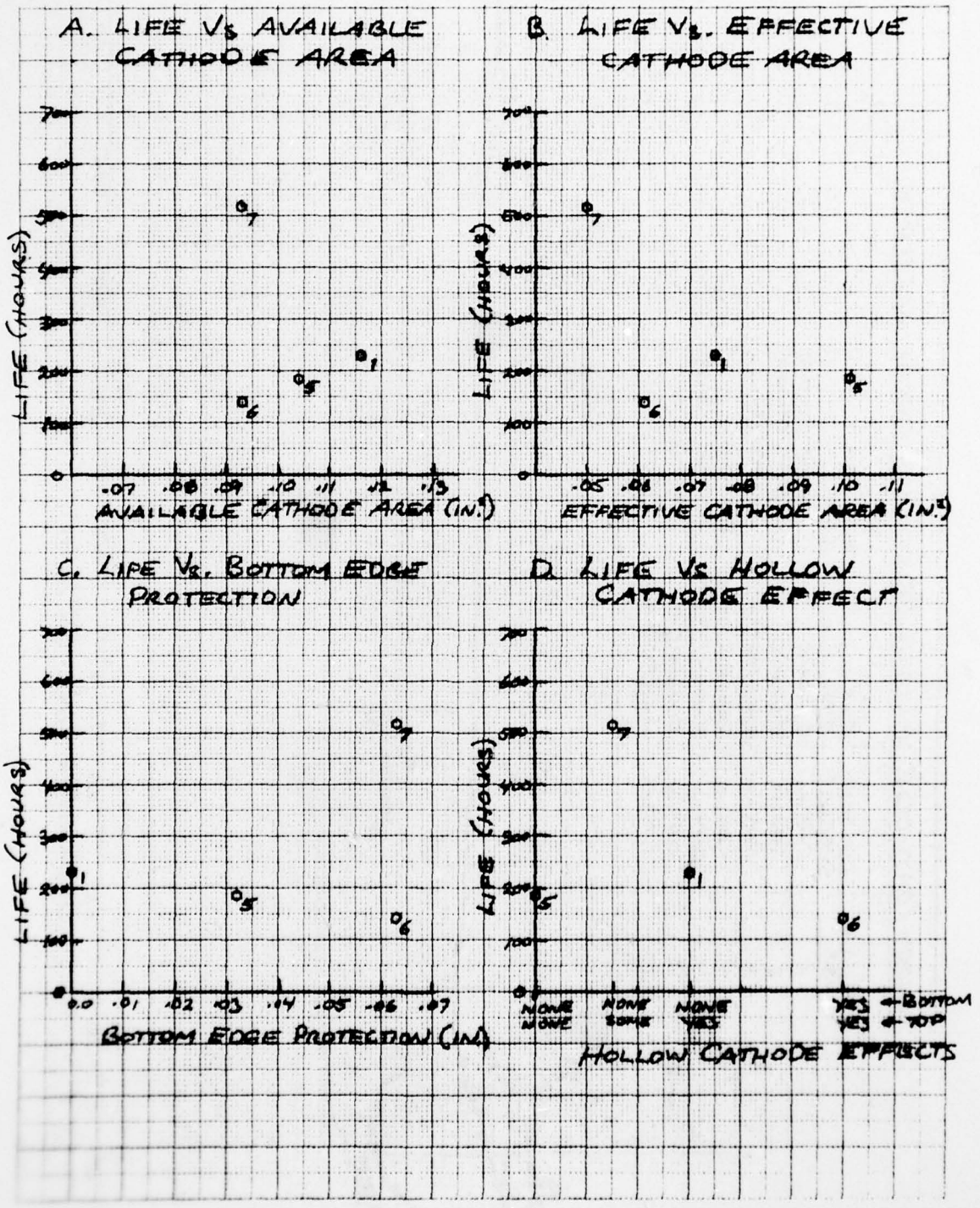

Figure 41. Correlation Plots of Test Samples 1, 5, 6, and 7

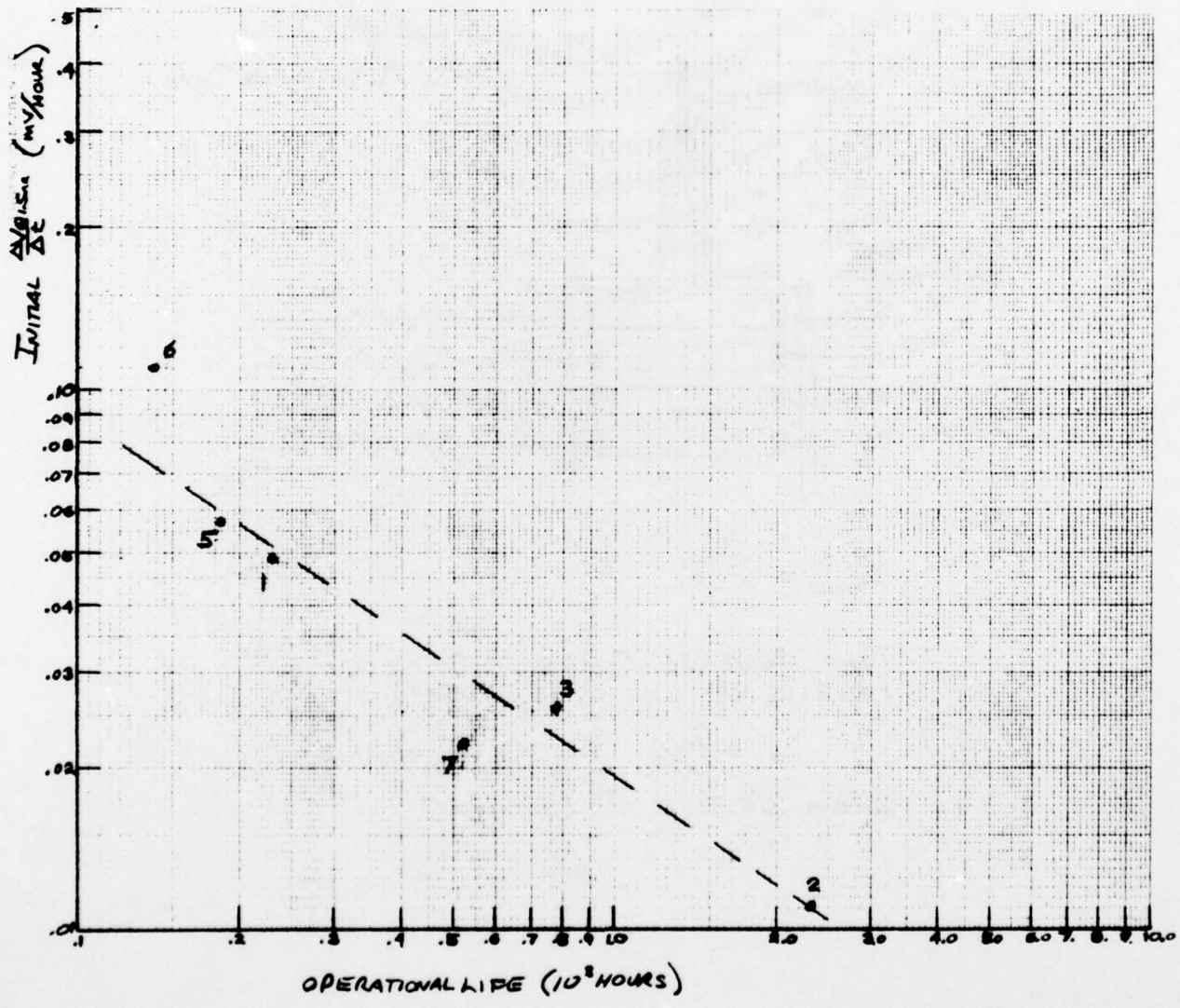

Figure 42. Correlation Plot of Initial Life Test Sample $\frac{\Delta V}{\Delta t}$ Vs Life

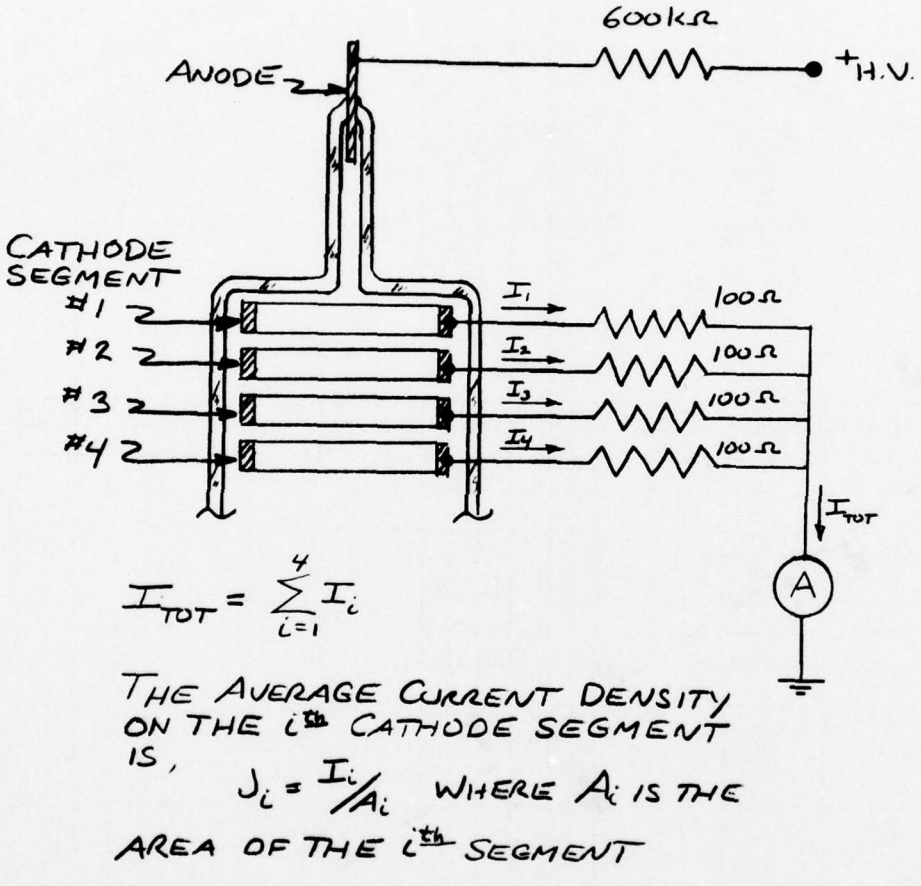

Figure 43. Segmented Cathode Test Schematic

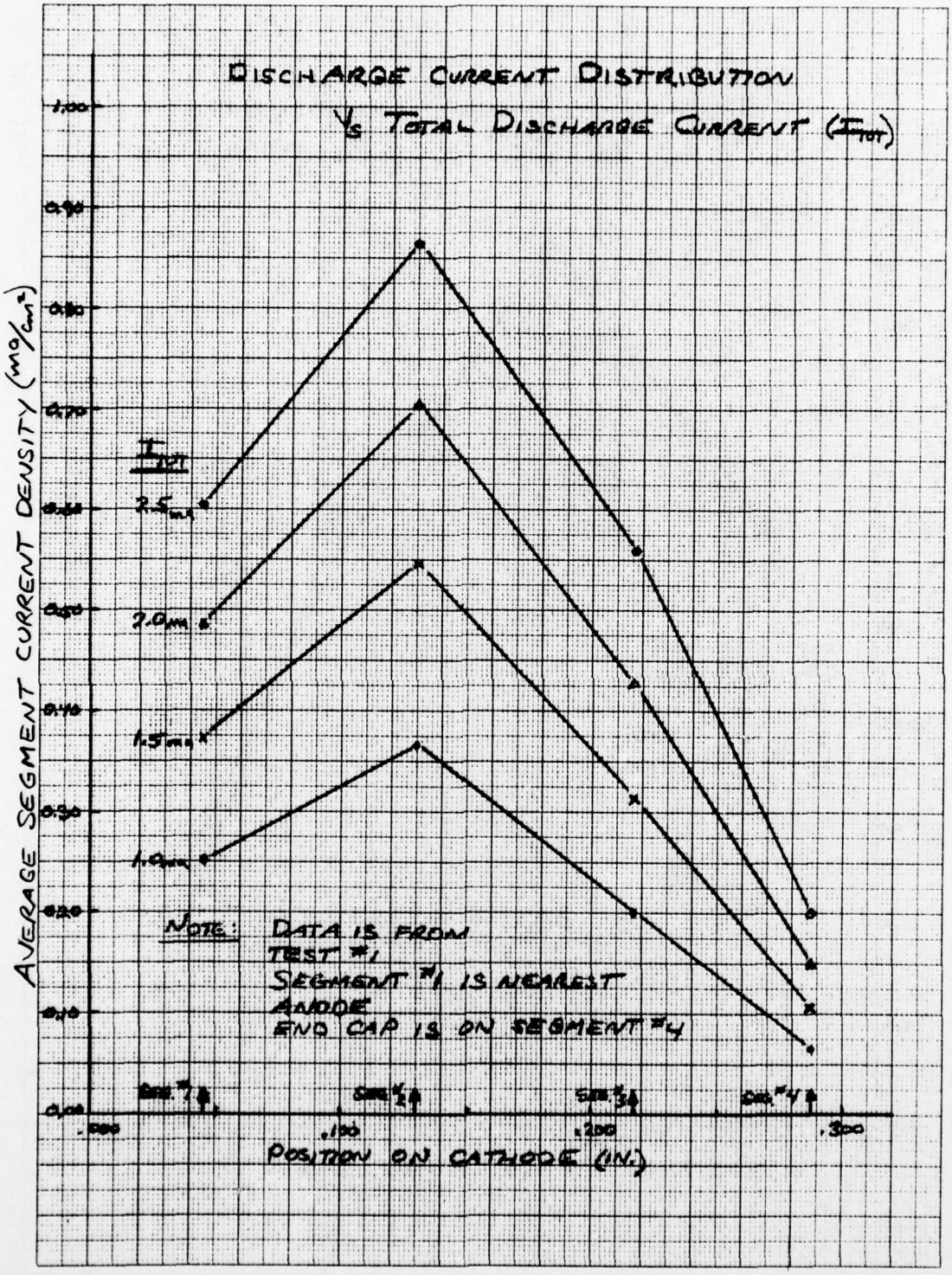

Figure 44. Discharge Current Distribution Vs Total Discharge Current

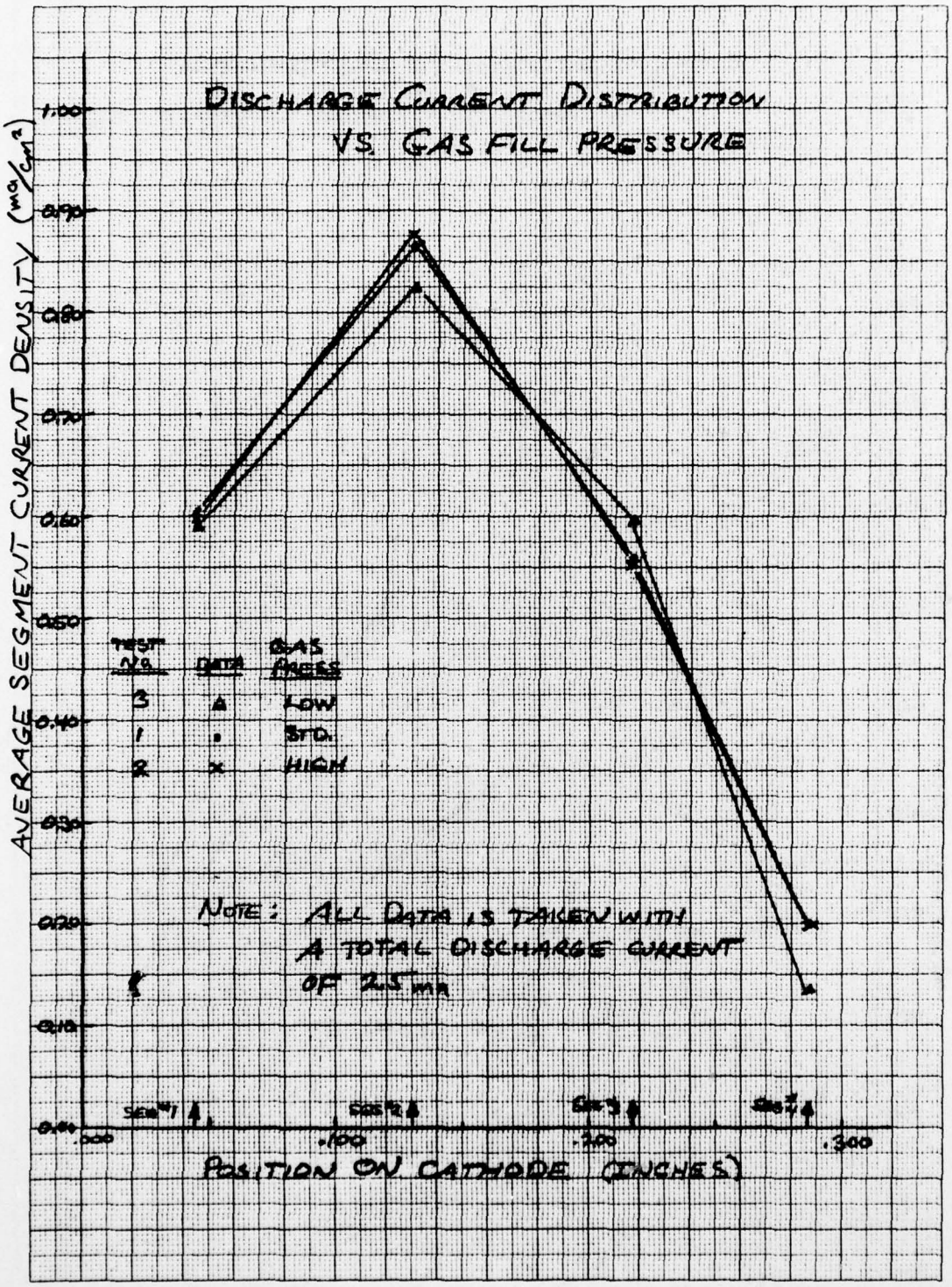

Figure 45. Discharge Current Distribution Vs Gas Fill Pressure

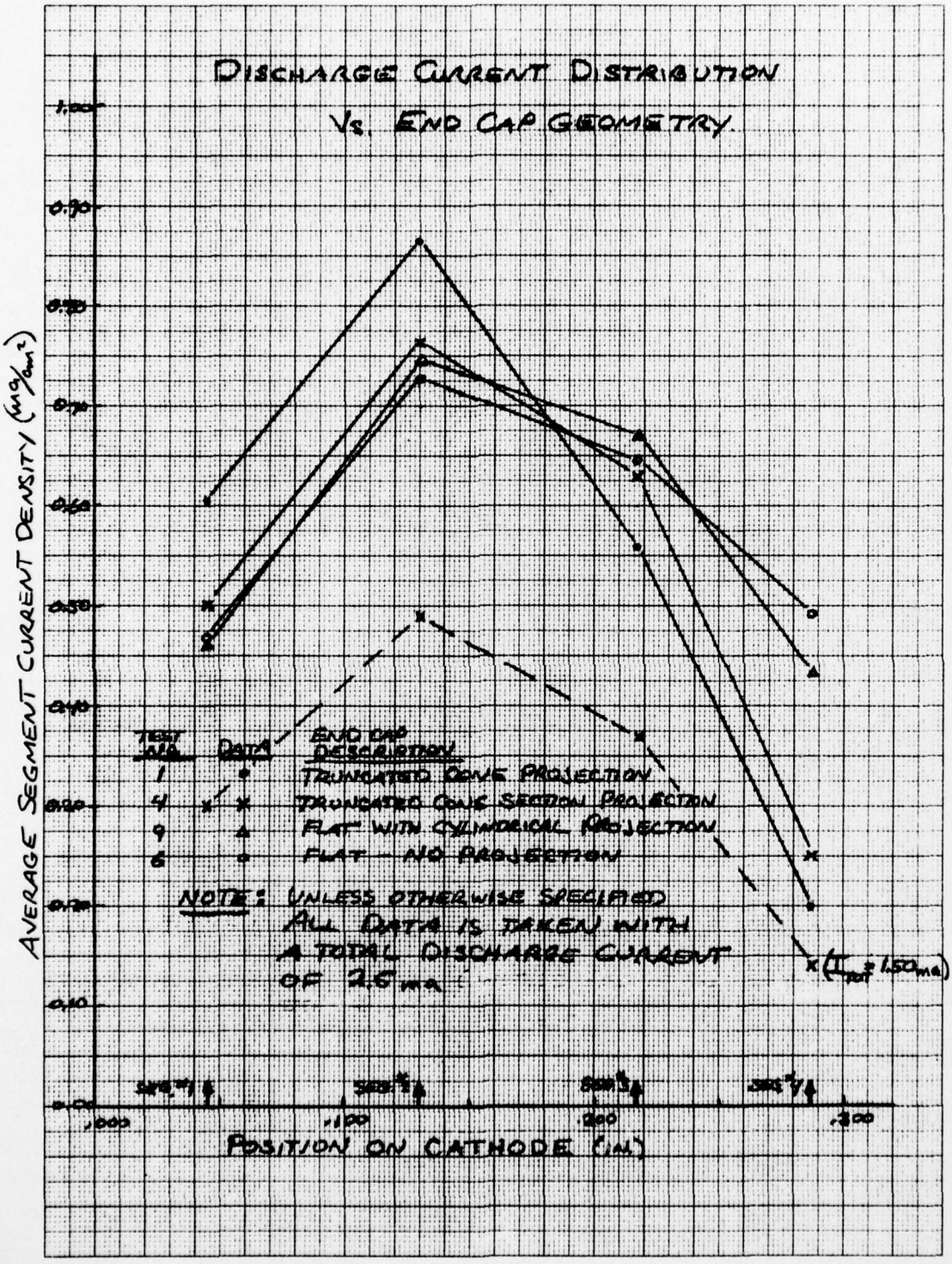

Figure 46. Discharge Current Distribution Vs End Cap Geometry

☆U.S.Government Printing Office: 1978 — 757-080/760